ポルフィリン・クロリン共集合体の構築と光照射による
酸素配位能復活に関する研究

（課題番号：１３６５０９３８）

平成１３年度～１４年度　科学研究費補助金（基盤研究(C)）

研究成果報告書

平成１５年３月

研究代表者：小　松　晃　之

（早稲田大学・理工学総合研究センター・講師）

目　次

研究組織

研究代表者： 小松　晃之（早稲田大学・理工学総合研究センター・講師）

研究協力者： 宗　慶太郎（早稲田大学・理工学総合研究センター・助手）

土田　英俊（早稲田大学・理工学総合研究センター・顧問研究員）

研究経費

平成１３年度	３，０００	千円
平成１４年度	７００	千円
計	３，７００	千円

1）はじめに

　本報告書は、日本学術振興会　科学研究費補助金（基盤研究（C）、課題番号：13650938、平成13年度～14年度（2年間））の助成のもとに実施された研究課題「ポルフィリン・クロリン共集合体の構築と光照射による酸素配位能復活に関する研究」のまとめである。研究代表者は、得られた新知見が単なる学術的な貢献に留まることなく、近い将来何らかの形で社会に還元できる革新技術へと繋がることを強く願っている。

　本研究の発端は、ポルフィリン鉄錯体に両親媒性構造を付与すると、それがリン脂質小胞体の分子二層膜中へ均一に包埋され、錯体部の電子移動が抑制される結果、従来不可能とされていた生理条件下（水中、pH 7.4、37℃）における可逆的な酸素配位錯体の生成が可能となったことに遡る（1983年）。この発見を契機として、一群の両親媒性ポルフィリン誘導体（リピドポルフィリン類）を設計・合成し、それらが単独でも水中で自己集合して様々な形態のナノ組織体（小胞体、紐状繊維、平板など）を形成することを見出した。さらに、自己組織化したリピドポルフィリン鉄(II)組織体がヘモグロビンと同様に酸素を吸脱着できることを実証、その高濃度水溶液が生体内で酸素輸送のできる全合成系酸素運搬体として機能することを明らかにした。水相系における可逆的酸素配位錯体系が確立した後に残る唯一の未解決課題は、酸素分子の脱着により徐々に自動酸化される中心鉄(III)の再還元過程の実現にある。

　本研究では、この点に焦点を絞り、自己組織化能を有するリピドポルフィリン鉄とクロリンまたはポルフィリン誘導体のハイブリッド組織体を創製し、光照射による励起条件を解明、これをリピドポルフィリン鉄(III)の還元反応に利用して、自動酸化しても光照射のみで酸素配位能を復活できる系として具現化することを目的とした。初年度は、水中で自己組織化できるリピドポルフィリン鉄の精密合成、その集合組織のナノ構造解明、酸素配位平衡、配位酸素の電荷分極構造の解析に集約した。第二年次は、系内に共存させたプロトポルフィリン誘導体の励起状態から、ポルフィリン鉄(III)への電子移動経路を構築、還元過程の詳細を検討すると共に、電子供与体（犠牲試薬）を共存させることでFe(II)体の蓄積を可能とし、これをFe(III)錯体の光還元法として確立した。

　二年間の期限内に予想を上回る進展が見られ、例えば、電子供与体となるポルフィリン誘導体を探索している際、リピドポルフィリンとその Zn(II)錯体からなる小胞体を調製すると、二分子膜内部で、Zn(II)ポルフィリン一重項励起状態からフリーベースポルフィリンへ効率高いエネルギー移動が生起することを見出した。これは水相系における新しい光捕集システムのモデルにもなり得ると考えられる。

　成果の多くは既に報文として印刷済みであるが、未発表知見もいくつか残されおり、今後も継続展開の成果を合わせながら、続報としてまとめていきたい。日本学

2) 研 究 発 表

2-1) 研究報文リスト

1. "Effect of Heme Structure on O_2-Binding Properties of Human Serum Albumin–Heme Hybrids: Intramolecular Histidine Coordination Provides a Stable O_2-Adduct Complex", T. Komatsu, Y. Matsukawa, E. Tsuchida, *Bioconjugate Chem.* **2002**, *13*, 397–402.

2. "Human Serum Albumin Incorporating Synthetic Hemes as an O_2-Carrying Hemoprotein: Control of O_2-Binding Ability by Heme Structure", E. Tsuchida, T. Komatsu, Y. Matsukawa, T. Okada, *Macromol. Symp.* **2002**, *186*, 1–6.

3. "Self-organized Lipid-porphyrin Bilayer Membranes in Vesicular Form: Nanostructure, Photophysical Properties and Dioxygen Coordination", T. Komatsu, M. Moritake, A. Nakagawa, E. Tsuchida, *Chem. Eur. J.* **2002**, *8*, 5469–5480.

4. "自己組織化リピドヘム小胞体のナノ構造と酸素結合能", 小松晃之, 森武美保, 土田英俊, *人工血液* **2002**, *10*, 120–125.

5. "*meso*-Tetrakis[*o*-(*N*-methyl)pyridinium]porphyrin Ensemble with Axially Coordinated Cyclodextrin-penetrating Phenethylimidazole: Reversible Dioxygen-binding in Aqueous DMF Solution", T. Komatsu, S. Hayakawa, E. Tsuchida, H. Nishide, *Chem. Commun.* **2003**, *2003*, 50–51.

6. "Synthetic Dioxygen-carrying Hemoprotein: Human Serum Albumin Including Iron(II) Complex of Protoporphyrin IX with an Axially Coordinated Histidylglycyl-propionate", A. Nakagawa, T. Komatsu, N. Ohmichi, E. Tsuchida, *Chem. Lett.* **2003**, *32*, 504–505.

7. "Molecular Energy and Electron Transfer Assemblies Made of Self-organized Lipid-porphyrin Bilayer Vesicles", T. Komatsu, M. Moritake, E. Tsuchida, *Chem. Eur. J.* **2003**, *9*, 4626–4633.

2-2) 学会発表

(招待講演)

1. T. Komatsu, E. Tsuchida, "Human Serum Albumin Incorporating Lipidhemes as an Oxygen-Infusion", The 6th International Symposium on Polymers for Advanced Technologies, Eilat (Israel), 2–6 Sept. 2001. (Key Note Lecture)

2. 小松晃之、土田英俊／全合成系酸素輸液：アルブミン-ヘム複合体－ヘム構造が酸素配位能に与える効果-(招待講演)／第 8 回日本血液代替物学会年次大会、東京、2001 年 9 月

3. 小松晃之／酸素輸液を目指したポルフィリン組織体の構築と機能(依頼講演)／2001-02 高分子錯体研究会、横浜、2002 年 1 月

4. T. Komatsu, E. Tsuchida, "Serum Albumin Included Iron-porphyrins as a Novel Synthetic O_2-Carrying Hemoprotein", 2nd International Conference on Porphyrins and Phthalocyanines, Kyoto, 30 June–5 July 2002. (<u>Invited Lecture</u>)

5. T. Komatsu, E. Tsuchida, "Serum Albumin Including Synthetic Hemes as an Oxygen-Carrying Hemoprotein", 9th International Symposium on Blood Substitutes, Tokyo, 3–5 March 2003. (<u>Invited Lecture</u>)

6. 小松晃之、土田英俊／酸素輸送合成ヘム蛋白質"アルブミン-ヘム"の構築と生体への応用（<u>依頼講演</u>）／第 52 回高分子討論会、山口、2003 年 9 月

7. 小松晃之、土田英俊／人工酸素運搬体"アルブミン-ヘム"の特徴と酸素輸送能（<u>招待講演</u>）／第 18 回日本薬物動態学会年会、札幌、2003 年 10 月

（国内学会）

1. 小松晃之、森武美保、土田英俊／リピドポルフィリンが自己組織化して形成する二分子膜小胞体の特徴と酸素配位／第 50 回高分子討論会、東京、2001 年 9 月

2. 中川晶人、森武美保、小松晃之、小林 修、土田英俊／リピドポルフィリンとイミダゾール誘導体が自己組織化して形成する組織体の特徴と酸素配位／第 50 回高分子討論会、東京、2001 年 9 月

3. 小松晃之、森武美保、土田英俊／ポルフィリンが自己組織化して構成する二分子膜小胞体の特徴と酸素配位能／第 51 回錯体化学討論会、松江、2001 年 9 月

4. 森武美保、小松晃之、西出宏之、土田英俊／リピドポルフィリンが自己組織化して形成する小胞体の微細構造と酸素配位／第 81 日本化学会春季年会、東京、2002 年 3 月

5. 小松晃之、森武美保、西出宏之、土田英俊／2 種のリピドポルフィリンが共組織化して形成する二分子膜小胞体の光電子移動反応／第 81 日本化学会春季年会、東京、2002 年 3 月

6. 石原星児、小松晃之、西出宏之、土田英俊／イミダゾリル基を有するリン脂質の合成とプロトポルフィリン共組織体の特徴／第 81 日本化学会春季年会、東京、2002 年 3 月

7. 小松晃之、森武美保、西出宏之、土田英俊／両親媒性テトラフェニルポルフィリン－プロトポルフィリンからなる二分子膜小胞体の光電子移動反応／第 51 回高分子学会年次大会、横浜、2002 年 5 月

8. 森武美保、小松晃之、西出宏之、土田英俊／リピドポルフィリン二分子膜小胞体の微細構造と光誘起エネルギー移動／第 51 回高分子討論会、北九州、2002 年 10 月

9. 小松晃之、森武美保、土田英俊／ポルフィリン二分子膜小胞体における光誘起エネルギー移動／第52回高分子学会年次大会、名古屋、2003年5月

（国際会議）

1. T. Komatsu, M. Moritake, E. Tsuchida, "Self-assembled Bilayer Vesicle Made of Tetraphenylporphyrin with Dialkylphosphocholine Groups: Nano-structure and O_2-Coordination", IUPAC 9th International Symposium on Macromolecule-Metal Complexes, New York (USA), 19–23 Aug. 2001.

2. T. Komatsu, M. Moritake, E. Tsuchida, "Self-assembled Bilayer Vesicle Made of Amphiphilic Porphyrin: Nano-structure and O_2-Coordination", The 6th International Symposium on Polymers for Advanced Technologies, Eilat (Israel), 2–6 Sept. 2001.

3. Akito Nakagawa, T. Komatsu, E. Tsuchida, "Coordination Structure ans Geminate Recombination of Albuin-heme with O_2 and CO", 2nd International Conference on Porphyrins and Phthalocyanines, Kyoto, 30 June–5 July 2002.

4. M. Moritake, T. Komatsu, H. Nishide, E. Tsuchida, "Self-organized Lipid-porphyrin Bilayer Membranes in Vesicular Form: Nano-structure and O_2-Coordination", 2nd International Conference on Porphyrins and Phthalocyanines, Kyoto, 30 June–5 July 2002.

5. T. Komatsu, E. Tsuchida, "Molecular Energy and Electron Transfer Assemblies Made of Self-organized Lipid-porphyrins", IUPAC 10th International Symposium on Macromolecule-Metal Complexes, Moscow (Russia), 19–23 May 2003.

6. T. Komatsu, E. Tsuchida, "Energy and Electron Transfer Assemblies Made of Self-organized Lipid-porphyrins in Water", 7th International Symposium on Polymers for Advanced Technologies, Fort Landerdale (USA), 21–24 Sept. 2003.

3）研究目的

リピドポルフィリン鉄(II)錯体が水中で自己集合して形成するナノ組織体を利用して、ヘモグロビンに匹敵する酸素配位錯体系を構築した後に残る重要課題は、酸素分子の脱着に伴い徐々に酸化した中心鉄(III)の再還元過程の実現にある。いわゆるメトヘムの化学還元は従来報告例も多いが、本研究では組織体の内部に共存させたクロリンまたはポルフィリン誘導体の光励起状態からリピドポルフィリン鉄(III)錯体への電子移動を利用して、リピドポルフィリン鉄(III)組織体の酸素配位能を復活させる方法の確立を目指した。

具体的には、自己組織化能を有する新規なリピドポルフィリン鉄(III)を精密合成し、それが水中で構成する集合体の微細構造と酸素結合能を解析、さらにプロトポルフィリン誘導体を共存させたハイブリッド組織体を創製し、光照射による励起条件を解明、外水相に共存させた電子供与体（犠牲試薬）からリピドポルフィリン鉄(III)への電子移動経路を構築し、これを酸素配位能を失った Fe(III)錯体の光還元法として確立する。

4）研究成果
4-1）新しいリピドポルフィリンが自己組織化して形成する小胞体のナノ構造

ジアルキルホスホコリン基をポルフィリン面上に導入したリピドポルフィリンの一群が、水中で自発的に組織化してヘム鉄のみからなる二分子膜小胞体を形成することを明らかにしてきている。アルキレン側鎖が規則配列して構築する疎水場の中央にヘムが二次元配列するため、結果としてμ-oxo 二量体形成とプロトン酸化の二つの酸化過程が同時に抑制され、安定な酸素錯体が得られる。リピドポルフィリン鉄小胞体の酸素親和性はヒト赤血球と同程度で、酸素結合解離速度もヘモグロビンと同等、所望の濃度（[ヘム]=5-10 mM）に調整したリピドポルフィリン鉄(II)小胞体水分散液は、赤血球の酸素輸送能を十分に代替できる完全合成型の人工酸素運搬体となり得る。しかし、リピドポルフィリンの合成工程は多段階からなり、総収率も低いため、簡便に効率良く得られる誘導体の設計・開発が望まれていた。

そこで本研究においては、まずジアルキルホスホコリン基の骨格部位であるグリセロールを同じ三価アルコールであるトリメチロールエタンに変換し、合成工程の簡略化と収率高いジアシル鎖構造の構築を試みた。即ち、リン脂質置換基のジアシル鎖結合部位としてトリメチロールエタンを有する新規リピドポルフィリン (1) を精密合成し、それが水相系で自己集合して形成する二分子膜小胞体のナノ構造と酸素結合能について検討した。
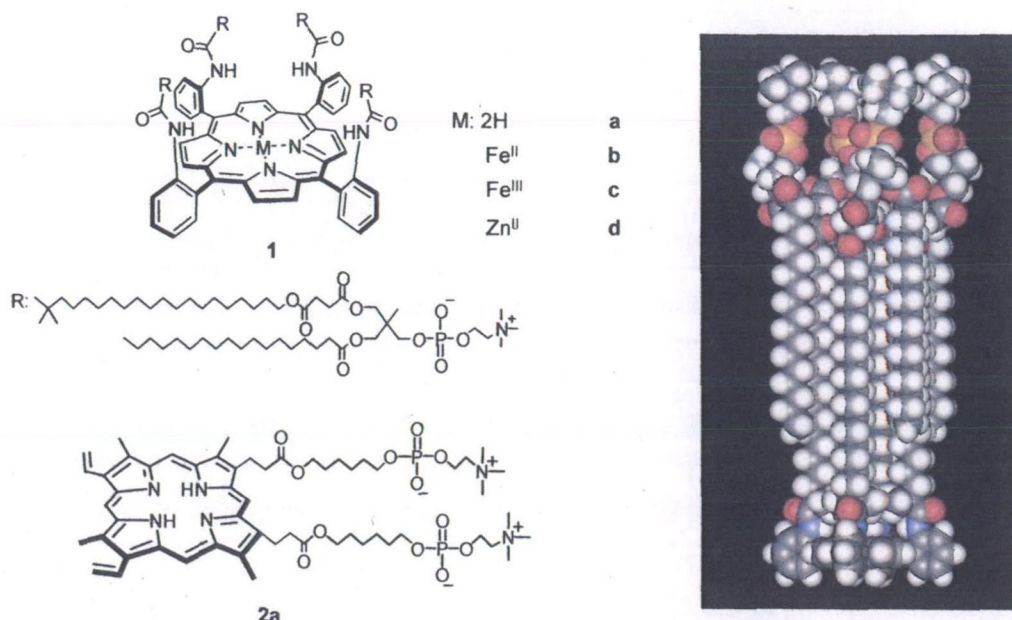
Lipid-porphyrin complexes and full-spacing model of **1a**.

　フリーベースのリピドポルフィリン（**1a**）を水中に分散させ、得られた組織体の形態観察と構造解析を行った。**1a** 水分散液（10 μM–10 mM）はきわめて安定で、調製 6 ヶ月後でも沈殿凝集を認めない。この水溶液の透過型電子顕微鏡（TEM）観察から **1a** が粒径約 100 nm の一枚膜小胞体を形成することを明らかにした（Fig. 1 (a)）。膜厚（10 nm）がリピドポルフィリン分子長（4.6 nm）の二倍に相当したことから、小胞体はリピドポルフィリンの分子二層膜からなると考えられる（Fig. 1 (b)）。ジアシル鎖の結合部位がグリセロールである従来型のリピドポルフィリンと同様の小胞体を構成できることから、グリセロールをトリメチロールエタンに置換しても、小胞体形成能に変化はないと考えられる。実際に、二つのパルミトイル鎖をトリメチロールエタンで連結したリン脂質も、DPPC と同様に水相系で自己集合し、二分子膜小胞体を与えた。グリセロールより対称性の高いトリメチロールエタンを含む分子構造のほうが、二分子膜形成時の分子充填率は高い可能性もある。動的光散乱法により測定した小胞体の粒径は 100±36 nm で、TEM 観察の結果と一致した。

　1a 小胞体水分散液の UV-vis. スペクトルにおいては、Soret 帯の λ_{max}（434 nm）が、有機溶媒（ベンゼン／MeOH=4／1）中の **1a** 単量体の λ_{max}（422 nm）に比べ 12 nm 赤方シフトした（Fig. 2）。両者の可視部吸収帯には大きな変化が見られなかったことから、Soret 帯における λ_{max} の相違は、ポルフィリン環どうしの励起子相互作用に基づくものであり、ポルフィリン平面は edge-to-edge に配列していると推察された。これらの挙動はリピドポルフィリン亜鉛錯体（**1d**）でも同様に観測された。
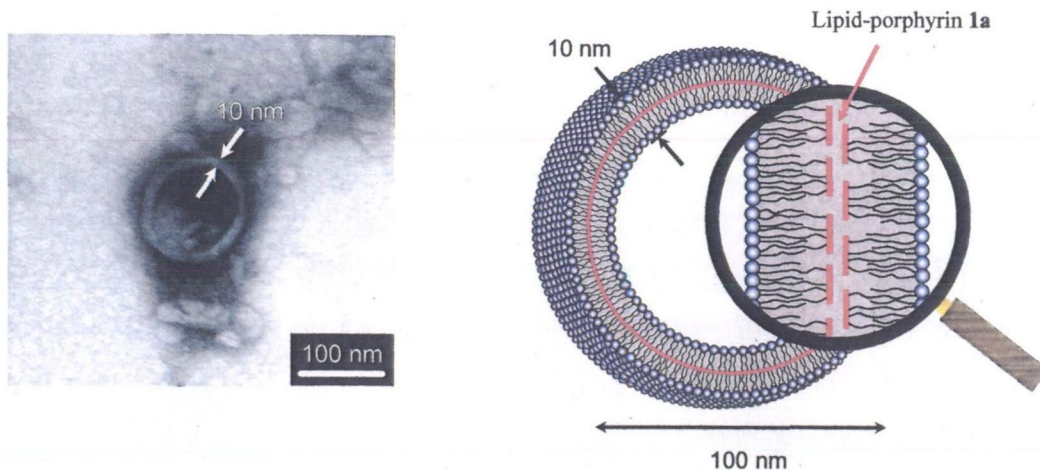
Fig. 1 (a) Transmission electron micrograph of the negatively stained sample of the free-base lipid-porphyrin (**1a**) vesicle with uranyl acetate, and (b) its schematic representation composed of the bilayer membrane.

　次に、リピドポルフィリン（**1a**）のΠ-A 曲線から、その分子占有面積を決定した。表面圧の減少に伴い、液体膨張膜が形成され、液体凝縮膜から固体膜へと移行する過程は、脂肪酸の典型的なΠ-A 相関と類似し、崩壊圧も 43 mN m^{-1} と高い（Fig. 3）。リピドポルフィリンが水面上で充填状態の良い単分子膜を形成できることが示された。分子占有面積は 2.2 nm^2/molecule であり、テトラフェニルポルフィリン環の面積を 2.5 nm^2 とすると、リピドポルフィリンは配向膜中でシリンダー状分子構造をとる。また、この値から、粒径 100 nm の二分子膜小胞体の構成分子数は外層内層合わせて約 23,000 分子と見積もられた。
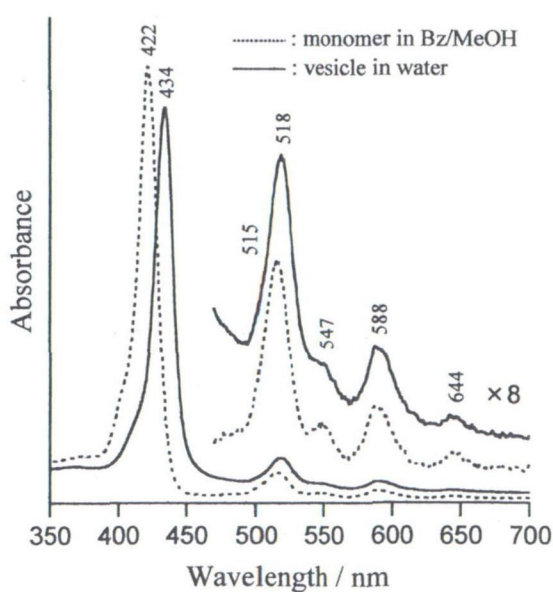

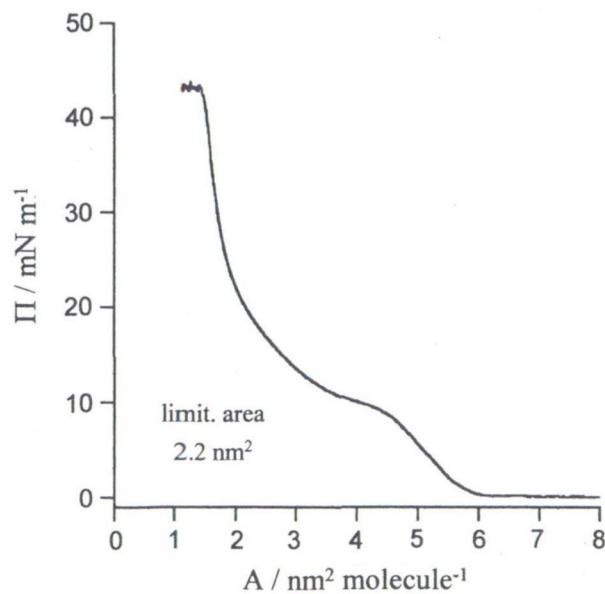**Fig. 2** UV-vis. absorption spectra of lipid-porphyrin (**1a**) at 25°C.

Fig. 3 The Π-A isotherm of lipid-porphyrin (**1a**). The subphace was pure water. The film was compressed at the rate of 10 mN min^{-1}.

1a 及び**1d** 小胞体の Soret 帯に見られる赤方シフトは励起子相互作用によるものと考えられるので、二分子膜小胞体内におけるポルフィリン環の配列モデルを作り、Kasha の式を用いた励起子計算から、Soret 帯のλ_{max}を見積もった。仮定では、(i) 内外層におけるポルフィリン部の二次元配向状態はテトラフェニルポルフィリン単結晶（三斜晶系）と同等、(ii) ポルフィリン環は二つの遷移モーメント（S_x, S_y）を有し、(iii) ΔE は x, y 方向成分の和として表されるものとした（Fig. 4）。内外層間距離（d）を 6.0 Å とすると、**1a** 二分子膜のλ_{max}は 431 nm と計算され、これに van der Waals シフトを加えると、実測値とよく一致した。

　1d 小胞体の場合、λ_{max}: 431, 438 nm の二つのピークが得られた。実測スペクトルが非対称であったため、これを二成分に分割してみると、λ_{max}: 433, 441 nm に吸収が存在し、計算値とよく一致した。つまり、**1a**、**1d** いずれの場合も、二分子膜小胞体におけるポルフィリン部の配列はテトラフェニルポルフィリン単結晶の最密充填状態に類似していると考えられる。
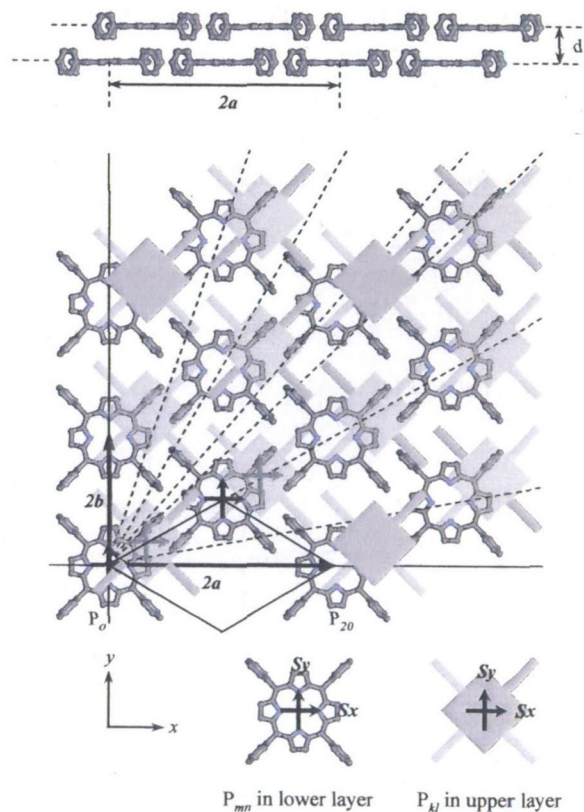
$$\Delta E = (M^2/r_{mn}^3 h)(1 - 3\cos^2\theta)$$

$$r_{mn} = [(ma)^2 + (nb)^2]^{1/2}$$

Fig. 4 Predicted arrangements of the porphyrin planes as a model for the bilayer membranes of lipid-porphyrin (**1a**). The porphyrin P_o locates on the origin of the coordinate axes.

4-2) リピドポルフィリン鉄小胞体の酸素結合反応

リピドポルフィリン鉄の水分散液（**1c**/1-ドデシルイミダゾール（DIm）、1/3 mol/mol、[ヘム]=10 μM–10 mM）も安定で、調製6ヶ月後でも沈殿凝集は認めなかった。この水溶液の透過型電子顕微鏡（TEM）観察から **1c** と DIm が水中で均一分散して、粒径約 100 nm の一枚膜小胞体を形成することを明らかにした（Fig. 5 (a)）。膜厚（10 nm）は **1a** 小胞体の場合と同じく分子長（4.6 nm）の二倍に相当したことから、この小胞体もリピドポルフィリン鉄の分子二層膜からなると考えられる。動的光散乱法から測定した小胞体の粒径は 97±73 nm で、TEM 観察の結果と一致した。

また、**1c**/DIm 水分散液をグラファイト基板上で乾燥させ原子間力顕微鏡（AFM）観察を行うと、小胞体が潰れて変形した円盤状組織像が認められた（Fig. 5 (b)）。これは DPPC などのリン脂質からなる小胞体に見られる現象と類似しており、内水相を有する小胞組織の AFM 観察では一般的である。円盤の高さは均一で 19.5 nm。この高さがリピドポルフィリン鉄二分子膜の厚みの二倍と一致したことからも、分子二層膜構造が裏付けられた。
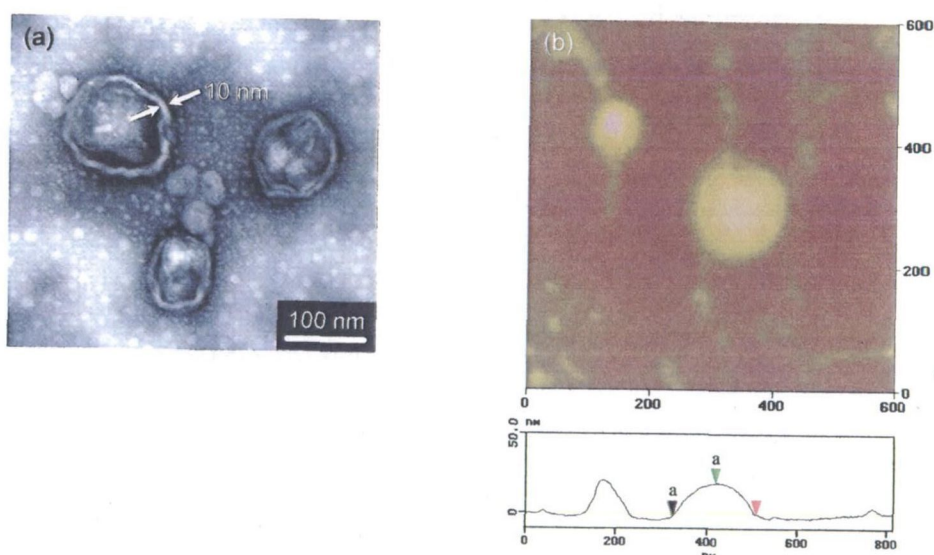

Fig. 5 (a) Transmission electron micrograph of the negatively stained sample of the lipid-porphyrinatoiron(III) **1c**/DIm vesicles with uranyl acetate. (b) SFM images (tapping mode) of the evaporated sample of the **1c**/DIm vesicles on HOPG. Image size is 600×600 nm (z-range: 50 nm) and its cursor profile (vertical distances: a-a 19.5 nm).

1b/DIm 小胞体の UV-vis.スペクトルは、窒素雰囲気下で λ_{max} : 436, 538, 568 nm を示し、**1b** の両軸配位座に DIm が結合した6配位鉄(II)低スピン錯体の形成を示した．そこへ酸素を通気するとスペクトルパターンは速やかに酸素錯体型（λ_{max} : 435, 543 nm）へ移行し、この酸素結合解離は 酸素／窒素の吹き込みに伴い可逆的に変化した（Fig. 6）。また、一酸化炭素を吹き込むときわめて安定なカルボニル錯体（λ_{max} : 433, 545 nm）が得られた。異なる酸素分圧に対する UV-vis.スペクトル変化から算出した

酸素親和性（$P_{1/2}$）は 30 Torr（37 ℃）でヒト赤血球の値（27 Torr）に近く、酸素錯体の半減期も 17 hr（37 ℃）と長い。酸素結合サイトであるヘム部が小胞体表面から約 4.0 nm 内側の疎水場に規則正しく配列して固定されているため、μ-oxo 二量体形成とプロトン酸化が同時に抑制されるのである。ヘモグロビンの酸素結合過程に見られる協同現象（いわゆるアロステリック効果）は観測されないが、例えば肺（Po_2: 110 Torr）～末梢組織（Po_2: 40 Torr）間におけるリピドポルフィリン鉄(II)小胞体の酸素運搬効率（22%）は、赤血球の値（22%）に匹敵することから、人工酸素運搬体として十分な酸素輸送能力を有しているといってよい（Fig. 7）。
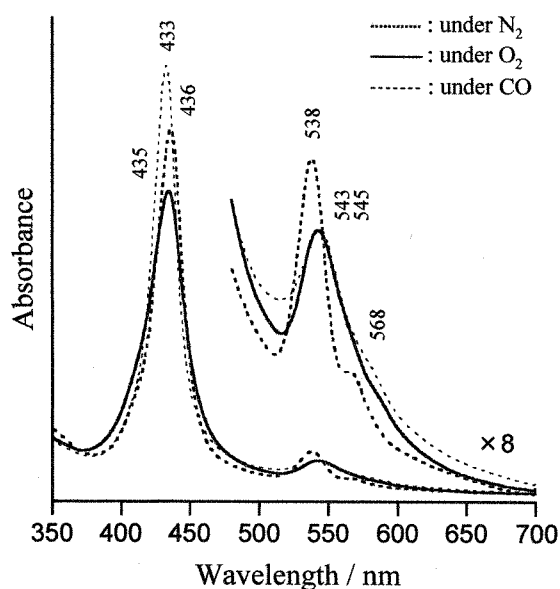

Fig. 6 Visible absorption spectral changes of the lipid-porphyrinatoiron(II) 1b/DIm vesicles in phosphate buffered solution (pH 7.4) at 25°C.
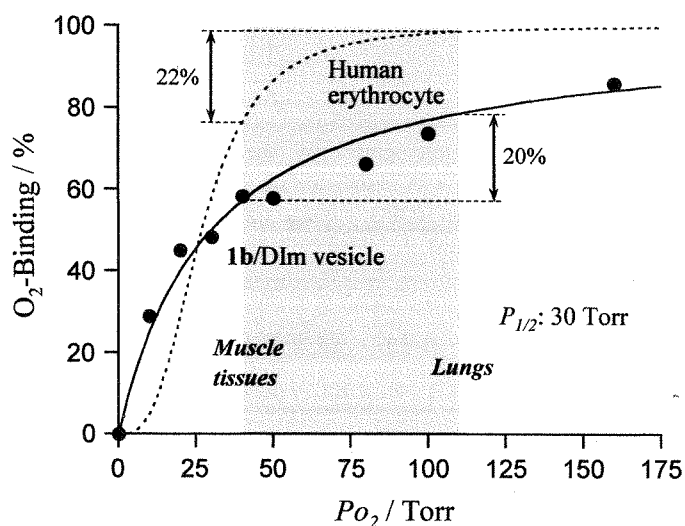

Fig. 7 O₂–Equiblium curve of the lipid-porphyrinato-iron(II) 1b/DIm vesicles in phosphate buffered solution (pH 7.4) at 37°C.

1b/DIm(CO)小胞体水分散液にレーザーフラッシュを照射すると、配位 CO の解離と再結合が観測される。この瞬時に起こる非平衡状態から平衡状態への UV-vis.スペクトル変化から、配位気体分子の結合解離速度定数（k_{on}，k_{off}）が算出できる。レーザー照射 10 μs 後における過渡吸収スペクトルは、窒素、一酸化炭素雰囲気下における吸収帯の差スペクトルとは異なるパターンを示した。つまりこの実験条件下では、レーザー照射により一酸化炭素が解離した後、近傍に存在する DIm が第 6 配位座に配位することなく、一酸化炭素の再結合が先行して生起する。レーザフラッシュホトリシス法により決定したリピドポルフィリン鉄(II)小胞体の k_{on}、k_{off} はヘモグロビンの値と同等値を示し（Table 1）、これは赤血球と比較した場合、酸素吸脱着の速度が 1,500 倍速いことを意味する。

Table 1 O_2- and CO-binding rate constants of lipid-porphyrinato-iron(II) **1b/DIm** vesicle in phosphate buffer solution (pH 7.3) at 25 °C.

	O_2		CO
	k_{on} [$M^{-1}s^{-1}$]	k_{off} [s^{-1}]	k_{on} [$M^{-1}s^{-1}$]
1b/DIm vesicle	1.6×10^7	2.5×10^2	1.2×10^7
Hb(T-state)α[a]	2.9×10^6	1.8×10^2	2.2×10^5
Red blood cell[b]	1.1×10^4	1.6×10^{-1}	1.4×10^4

[a] pH 7.0-7.4, 20 °C.　[b] pH 7.4.

4-3) リピドポルフィリン鉄小胞体の酸素配位構造

　ヘムやヘム蛋白質の磁気円偏向二色性（MCD）スペクトル測定からは、その酸化状態、スピン状態、配位構造に関する重要な知見が得られる。**1b/DIm** 小胞体の窒素、酸素、一酸化炭素雰囲気下における MCD スペクトルは、それぞれ異なるパターンを示した（Fig. 8）。これらは Collman らが報告しているテトラフェニルポルフィリン鉄(II)−ビス(N-メチルイミダゾール) [FeTPP(N-MeIm)$_2$]錯体、FeTPP(N-MeIm)(CO)錯体、および近位結合型置換 FeTPP(O_2)錯体のパターンとよく一致した。つまり、窒素雰囲気下では、2 つの DIm が両軸配位座に結合した鉄(II)6 配位低スピン錯体構造をとるが、そこへ酸素、一酸化炭素を通気すると、DIm の 1 つが O_2、CO に置換され、Soret 帯領域に対称性の高い大きな MCD が出現する。この結果は、従来 UV-vis.スペクトルから考察していた **1b/DIm** 小胞体の軸配位構造変化が正しいことを示す。

　また、ヘム錯体における配位酸素の伸縮振動（v_{O_2}）は、IR スペクトルにより直接観測することができる。**1b/DIm($^{16}O_2$)**錯体から **1b/DIm(CO)**錯体の IR スペクトルを差し引くと、1155 cm^{-1} に配位酸素の伸縮振動（$v^{16}O_2$）が観測された（Table 2）。この
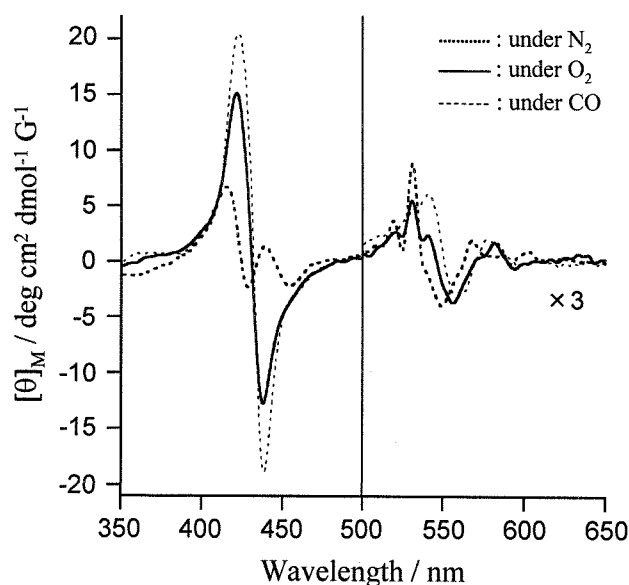
Fig. 8 MCD spectra of the lipid-porphyrinatoiron(II) 1b/DIm vesicles in phosphate buffered solution (pH 7.4) at 25°C.

値がスーパーオキサイド（1145 cm^{-1}）に近いことから、FeTPP 誘導体と同様、リピドポルフィリン鉄の酸素配位構造は bent end-on 型と考えられる。さらに、1b/DIm($^{18}O_2$)錯体－1b/DIm(CO)錯体の差スペクトルには $\nu^{18}o_2$（1081 cm^{-1}）が出現し、$\nu^{16}o_2 - \nu^{18}o_2$ 間 同位体シフト値（74 cm^{-1}）は、計算値（74 cm^{-1}）とよく一致した。これらの事実は間違いなく分子状酸素がリピドポルフィリン鉄(II)小胞体のヘム鉄に配位していることを示している。

また、配位一酸化炭素の伸縮振動（ν_{CO}=1969 cm^{-1}）も FeTPP 誘導体の値と一致した。自己組織化した 1b/DIm 小胞体の中でも、軸塩基である DIm の中心鉄への配位に歪みはないと考えられる。

Table 2 IR spectral data of lipid-porphyrinatoiron(II) 1b/DIm vesicle in phosphate buffer solution (pH 7.3) at 25 °C.

	O_2		CO
	$\nu^{16}O^{-16}O$ [cm^{-1}]	$\nu^{18}O^{-18}O$ [cm^{-1}]	$\nu^{12}C^{-16}O$ [cm^{-1}]
1b/DIm vesicle	1155	1081	1969
FeTpivPP(MIm)[a]	1159	1075	1969
O_2 or CO (gas)	1556	-	2143
O_2^-	1145	-	-

[a]FeTpivPP(MIm): Picket-fence Fe(II)porphyrin(1-methyl-imidazole) complex (Nujol).

4-4）リピドポルフィリン鉄とプロトポルフィリンが共集合して形成する組織体のナノ構造

　1c/DIm小胞体の二分子層間に両親媒性クロリンまたはポルフィリン誘導体を配置し、光照射により誘起される**1c**錯体への電子移動経路の構築を検討した。クロリン誘導体は高波長側に吸収を持つ特徴を有するが、不安定であったため、プロトポルフィリン誘導体（**2a**）を用いた。まず、**1a**/**2a**（10/1 mol/mol）混合水分散液を調製、そのTEM観察から粒径約100 nmの小胞体の形成を観測した（Fig. 9 (b)）。**2a**は単独で水中に分散して繊維状組織を構成すること（Fig. 9 (a)）、**2a**の割合を増加させると小胞体数が減少することから、**2a**は**1a**小胞体内に取り込まれていると推測された。

　また、その水分散液のUV-vis.スペクトルと**1a**単独小胞体水分散液との差スペクトルが、**2a**をDPPC小胞体に包埋させた溶液のスペクトルとほぼ一致したことから、**2a**は**1a**二分子膜中で会合体を形成することなく均一に包埋されているものと考えられた（Fig. 9 (c)）。**2a**のポルフィリン部が、**1a**分子層（46 Å）面に対して垂直に配向しているとすると、その中心は膜表面から23 Åのところ（膜の中央）に位置することになる。
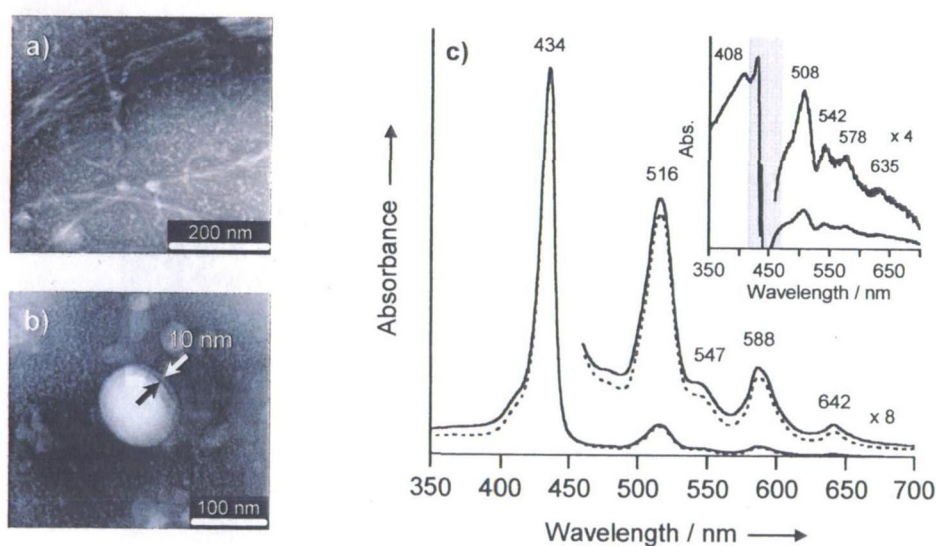
Fig. 9 Transmission electron micrographs of the evaporated aqueous solutions of a) **2a** and b) the **1a**/**2a** ensemble (molar ratio: **1a**/**2a** = 10). c) UV-Vis. absorption spectra of **1a** vesicles (dotted line) and **1a**/**2a** ensemble vesicles (solid line) in water at 25 °C. The inset shows a different spectrum for both solutions, in which the absorption maxima coincided with those of the DPPC vesicles incorporating **2a** (molar ratio: DPPC/**2a** = 40/1) in water.

4-5）プロトポルフィリンの光励起を利用したリピドポルフィリン鉄（III）の光還元反応

　同様の方法で調製したリピドポルフィリン鉄（III）錯体（**1c**）/DIm/**2a**（1/3/0.1 mol）小胞体の外水層へ犠牲試薬（トリエタノールアミン（TEOA））を添加し、窒素雰囲気下で光照射（λ_{ex}: 390 nm）すると、中心鉄の還元が進行した（Fig. 10）。**2a**を包埋させない場合やTEOAが共存しない場合の還元率は低いことから、光励起された**2a**が

1c を還元し、TEOA が酸化された 2a を還元するため、鉄(II)錯体が効率よく蓄積されると考えられる（Fig. 11）。得られたリピドポルフィリン鉄(II)小胞体は、酸素の通気により安定な酸素錯体を形成した。

$$Fe^{3+}LP / LPP \xrightarrow{h\nu} Fe^{3+}LP / LPP^*$$

$$\rightleftharpoons Fe^{2+}LP / LPP^+ \xrightarrow{e^-}$$

$$Fe^{2+}LP / LPP$$

$$Fe^{2+}LP + O_2 \rightleftharpoons Fe^{2+}LP(O_2)$$
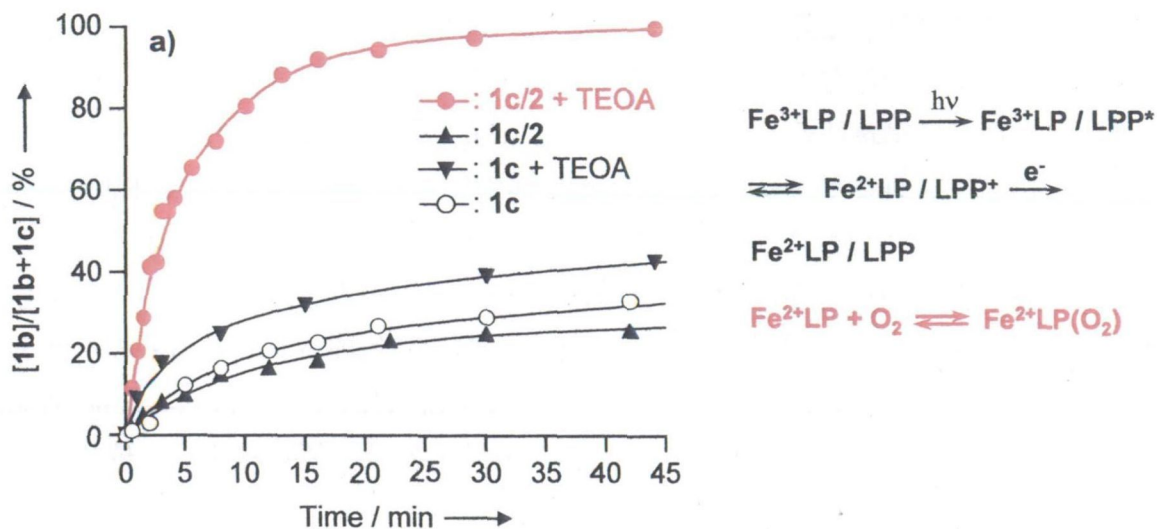
Fig. 10　Photoreduction of Fe³⁺TPP moieties of **1c/2**/DIm vesicles in aqueous phosphate buffer (pH 7.3) at 25 °C.
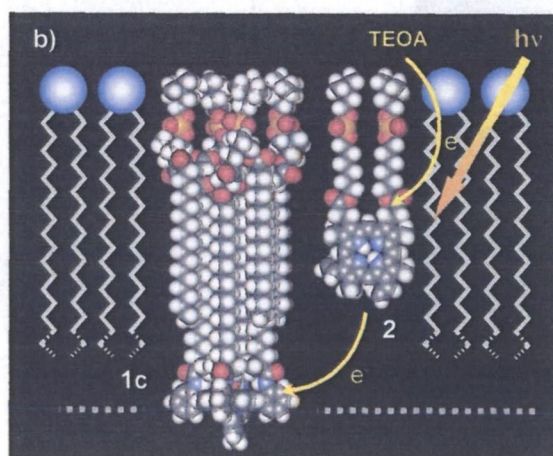
Fig. 11　The schematic representation of the **1c/2a**/DIm monolayer membrane interior using the space-filling model for the each compound (DIm is replaced by 1-methylimidazole for clarification).

4-6）リピドポルフィリン／リピドポルフィリン亜鉛錯体からなる小胞体の光エネルギー移動

　電子供与体となるポルフィリン誘導体を探索している際、リピドポルフィリン（1a）とその Zn(II)錯体（1d）からなるハイブリッド小胞体を調製すると、その内部で、1d の一重項励起状態からフリーベース 1a への効率高いエネルギー移動が生起することを見出した。1a と 1d 小胞体は共に強い蛍光発光を示すことから、光励起エネルギー・電子移動系の構築が可能である。1a/1d 混合水分散液の TEM 観察から、

粒径約 100 nm の一枚膜小胞体の形成を観測。この小胞体水分散液の UV-vis. スペクトルは、各成分の和と一致した。**1a** と **1d** が共集合して相溶性高く組織体を構成し、さらに **1a** と **1d** 間に基底状態での相互作用はないことが明らかとなった（Fig. 12）。
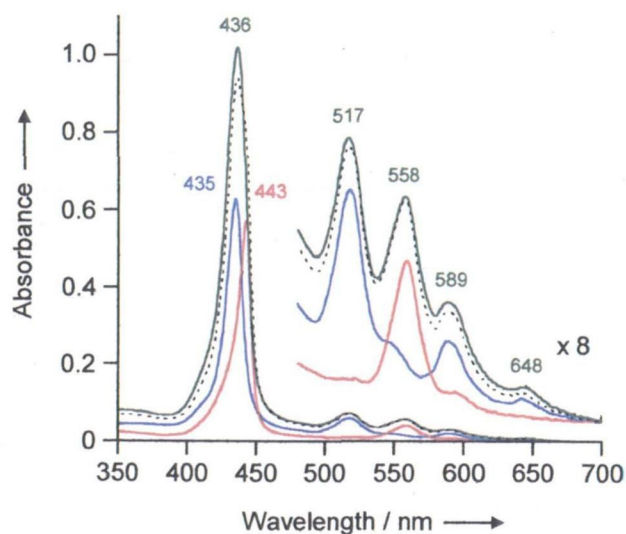
Fig. 12 UV-Vis. absorption spectra of **1a** vesicles (blue line), **1d** vesicles (red line), and **1a/1d** ensemble vesicles (molar ratio: 1/1, green line) in water at 25 °C. Black dotted lines represent the superposition of the spectra for **1a** and **1d**.

亜鉛錯体の吸収波長（λ_{ex}: 558 nm）で光励起し、蛍光スペクトルを測定すると、フリーベース体の大きな蛍光（λ_{em}: 650, 712 nm）が観測された（Fig. 13）。**1d** から **1a** へのエネルギー移動が生起しているものと考えられる。
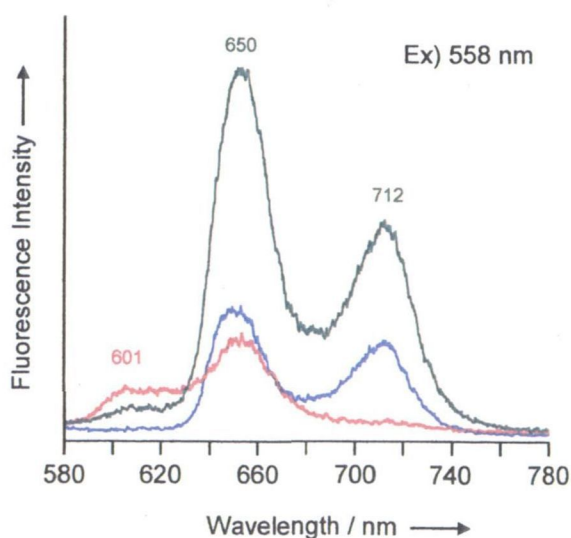
Fig. 13 Steady-state fluorescence emission spectra of **1a** vesicles (blue line), **1d** vesicles (red line), and **1a/1d** ensemble vesicles (molar ratio: 1/1, green line) in water at 25 °C (Ex. 558 nm).

また、蛍光寿命測定からエネルギー移動速度定数、エネルギー移動収率を算出した。

$$k_{ET} = 1/\tau_{1a/1d} - 1/\tau_{1d} = 3.1 \times 10^9 \, (s^{-1})$$
$$\phi_{ET} = k_{ET}/(k_{ET} + 1/\tau_{1d}) = 0.81$$

　これらの値は、従来報告されている Zn－フリーベースポルフィリン共有結合型光エネルギー移動モデルにおける値と同等であった。リピドポルフィリン **1a/1d** 小胞体では、亜鉛錯体が光捕集アンテナとして機能することが実証された。

5）まとめ

　自己組織化能を有するリピドポルフィリン鉄とクロリンまたはポルフィリン誘導体のハイブリッド組織体を創製し、光照射による励起条件を解明すると共に、これをリピドポルフィリン鉄(III)の還元反応に利用して、光照射のみで鉄(II)錯体へ再還元できる分子構成、すなわち自動酸化しても酸素配位能を復活できる系として具現化することを研究目的とした。

　先ず、水中で自己組織化できる新規リピドポルフィリン鉄を設計・精密合成した。リン脂質置換基のジアシル鎖結合部位としてトリメチロールエタンを導入、このリピドポルフィリンが粒径 100 nm の二分子膜小胞体を形成できたことから、グリセロールをトリメチロールエタンに置換しても、小胞体形成能に変化はないことを明らかにした。その組織体の微細構造、酸素配位平衡、配位酸素の電荷分極構造を各種物理化学的測定から詳細に解析。酸素親和性は 30 Torr でヒト赤血球に近く、酸素錯体半減期は 17 hr と長かった。

　続いてリピドポルフィリン(III)小胞体内に共存させたプロトポルフィリン誘導体の励起状態から、ポルフィリン鉄(III)への電子移動経路を構築、還元過程を検討すると共に、電子供与体（犠牲試薬）を共存させることで Fe(II)体の蓄積を可能とし、これを Fe(III)錯体の光還元法として確立した。

　さらに、リピドポルフィリンとその Zn(II)錯体からなるハイブリッド二分子膜小胞体では、組織内部で Zn(II)ポルフィリン一重項励起状態からフリーベースポルフィリンへの効率高いエネルギー移動が生起することも見出した。エネルギー移動速度と収率は、共有結合型ポルフィリン二量体モデルに匹敵する。このリピドポルフィリン組織体は水相系における新しい光捕集システムのモデルにもなり得ると考えられる。

ARTICLES

Effect of Heme Structure on O₂-Binding Properties of Human Serum Albumin−Heme Hybrids: Intramolecular Histidine Coordination Provides a Stable O₂−Adduct Complex

Teruyuki Komatsu, Yasuko Matsukawa, and Eishun Tsuchida*,†

Department of Polymer Chemistry, Advanced Research Institute for Science and Engineering, Waseda University, Tokyo 169-8555, Japan. Received July 3, 2001; Revised Manuscript Received October 8, 2001

5,10,15,20-Tetrakis[(α,α,α,α-*o*-pivaloylamino)phenyl]porphinatoiron(II) and 5,10,15,20-tetrakis-{[α,α,α,α-*o*-(1-methylcyclohexanoylamino)]phenyl}porphinatoiron(II) complexes bearing a covalently bound 8-(2-methyl-1-imidazolyl)octanoyloxymethyl or 4-(methyl-L-histidinamido)butanoyloxymethyl side-chain [**FeRP(B)** series: R = piv or cyc, B = Im or His] have been synthesized. The histidine-bound derivatives [**FepivP(His)**, **FecycP(His)**] formed five N-coordinated high-spin iron(II) complexes in organic solvents under an N₂ atmosphere and showed large O₂-binding affinities in comparison to those of the 2-methylimidazole-bound analogues [**FepivP(Im)**, **FecycP(Im)**] due to the low O₂-dissociation rate constants. On the contrary, the difference in the fence groups around the O₂-coordination site (pivaloyl or 1-methylhexanoyl) did not significantly influence to the O₂-binding parameters. These four porphinatoiron(II)s were efficiently incorporated into recombinant human serum albumin (rHSA), thus providing the synthetic hemoprotein, the albumin−heme hybrid [rHSA−**FeRP(B)**]. An rHSA host absorbs a maximum of eight **FeRP(B)** molecules in each case. The obtained rHSA−**FeRP(B)** can reversibly bind and release O₂ under physiological conditions (in aqueous media, pH 7.3, 37 °C) like hemoglobin and myoglobin. As in organic solutions, the difference in the fence groups did not affect their O₂-binding parameters, but the axial histidine coordination significantly increased the O₂-binding affinity, which is again ascribed to the low O₂-dissociation rates. The most remarkable effect of the heme structure appeared in the half-life (τ₁/₂) of the O₂−adduct complex. The dioxygenated rHSA−**FecycP(His)** showed an unusually long lifetime (τ₁/₂: 25 h at 37 °C) which is ca. 13-fold longer than that of rHSA−**FepivP(Im)**.

INTRODUCTION

A recombinant human serum albumin (rHSA) incorporating 2-[8-(2-methyl-1-imidazolyl)octanoyloxymethyl]-5,10,15,20-tetrakis[(α,α,α,α-*o*-pivaloylamino)phenyl]porphinatoiron(II) [**FepivP(Im)**¹] [albumin−heme; rHSA−**FepivP(Im)**] is an entirely synthetic hemoprotein which can reversibly bind and release O₂ under physiological conditions like that of hemoglobin (Hb) and myoglobin (Mb) (Tsuchida et al., 1999). The exchange transfusion with this rHSA−**FepivP(Im)** solution into anesthetized rats has shown that it becomes an O₂-carrying fluid as a red blood cell substitute (Tsuchida et al., 2000). The

albumin−heme hybrid is now recognized to be one of the most promising materials not only as a blood replacement composition, but also as an O₂-carrying medicine which will be adopted for use in several clinical applications, such as myocardial infraction, anemia, and tracheal blockade, etc. Only one limitation of this material is the relatively short lifetime of the O₂−adduct complex; the half-life of the dioxygenated rHSA−**FepivP(Im)** at 37 °C (pH 7.3 under 100% O₂ atmosphere) was 2 h. We believe that it should be improved by the optimizing of the chemical structure of the incorporated heme. Actually, the relationship between the heme structure and the O₂-binding parameters has been elucidated, but its effect to the O₂−adduct stability is still controversial (Collman et al., 1983; Traylor et al., 1985). We have employed **FepivP(Im)** as an active site of the albumin−heme, in which the sterically hindered 2-methylimidazole coordination plays a crucial role to realize the similar O₂-binding affinity with red blood cells. On the other hand, the low-binding constant of the 2-methylimidazolyl N atom to the central iron(II) has also been postulated to lead the short lifetime of the dioxygenated species. Other factors that regulate the O₂-binding ability of the heme are the basicity of the imidazole ligand and the hydrophobicity of the cavity around the coordinated O₂. The pK_a of the histidine, which is found in nature, is 6.0. This

* To whom the correspondence should be addressed. Phone: +81 3−5286−3120; Fax: +81 3−3205−4740. e-mail: eishun@mn.waseda.ac.jp.
† CREST investigator, JST.

value is significantly low compared to those of the *N*-alkylimidazole derivatives and may provide both a suitable O_2-binding affinity and a long lifetime. To increase the stability of the O_2-adduct complex of the albumin—heme hybrid, new porphinatoiron(II) derivatives with different substituents on the *distal* and *proximal* sides of the porphine planes [5,10,15,20-tetrakis[(α,α,α,α-*o*-pivaloylamino)phenyl]porphinatoiron(II) bearing a covalently bound 4-methyl-L-histidinamido-butanoyl-oxymethyl chains [**FepivP(His)**], and 5,10,15,20-tetrakis{[α,α,α,α-*o*-(1-methylcyclohexanoylamino)]-phenyl}porphinatoiron(II) with a 8-(2-methyl-1-imidazolyl)octanoyloxymethyl or the histidine side-chain [**FecycP(Im)** or **FecycP(His)**] have been synthesized. This paper describes the O_2-binding equilibria and kinetics of these newly synthesized **FeRP(B)** complexes in organic solvents and their rHSA hybrids in aqueous media. This is the first reported evaluation of the effect of the heme structure on the O_2-binding property of the albumin—heme hybrid.

FepivP(Im): R=

FecycP(Im): R=

FepivP(His): R=

FecycP(His): R=
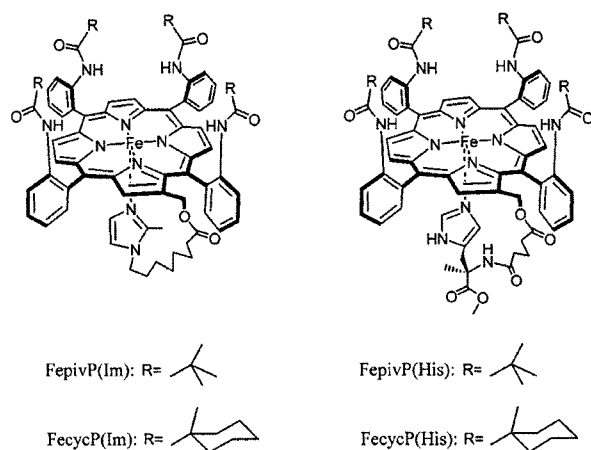
EXPERIMENTAL PROCEDURES

Materials and Apparatus. Thin-layer chromatography was carried out on 0.2 mm precoated plates of silica gel 60 F_{254} (Merck). Purification was performed by silica gel 60 (Merck) column chromatography. Infrared spectra were measured with a JASCO FT/IR-410 spectrometer. ^{1}H NMR spectra were recorded using a JEOL Lambda 500 spectrometer. Chemical shifts were expressed in parts per million downfield from Me_4Si as an internal standard. FAB-MS spectra were obtained from a JEOL JMS—SX102A spectrometer. UV—vis absorption spectra were recorded on a JASCO V-570 spectrophotometer. 2-Hydroxymethyl-5,10,15,20-tetrakis[(α,α,α,α-*o*-pivaloylamino)phenyl]porphine (**3-piv**), 8-(2-methyl-1-imidazolyl)-octanoic acid, and 2-[8-(2-methyl-1-imidazolyl)octanoyl-oxymethyl]-5,10,15,20-tetrakis[(α,α,α,α-*o*-pivaloylamino)-phenyl]porphinatoiron(III) bromide [**FepivP(Im)Br⁻**] were prepared according to our previously reported literature (Tsuchida et al., 1995). All solvents were purified by distillation before use. Other chemicals were commercial high-purity grades. The water used was deionized using a ADVANTEC GS-200 system. An rHSA (25 wt %) was provided from WelFide Corporation (Sumi et al., 1993).

Reduction of Ferric Complex to Ferrous Complex in Organic Solvent. Reduction to the porphinato-iron(II) complex was carried out using toluene (or benzene)—aq $Na_2S_2O_4$ in a heterogeneous two-phase system under aerobic conditions as previously reported (Tsuchida

et a., 1995). After separation of the two phases, the organic layer containing the reduced compound was transferred into 1-cm quartz cuvette under an Ar atmosphre.

Resonance Raman Spectroscopy. RR spectra were obtained on a JASCO NRS-2000 laser Raman spectrometer equipped with a CCD multichannel detector. Excitation was carried out by the 457.9-nm line of an NEC GLG2162 Ar⁺ ion laser at 25 °C. The details of the measurements were reported elsewhere (Komatsu et al., 1999; Wu et al., 1998).

Preparation of rHSA—FeRP(B) Hybrid. Aqueous ascorbic acid (15 mM, 20 μL) was added to an EtOH solution of **FeRP(B)** derivative (75 μM, 4 mL) under carbon monoxide (CO). After complete reduction of the central ferric ion, the UV—vis absorption spectrum showed a formation of the six-coordinated carbonyl complex. This EtOH solution was slowly injected into the phosphate buffer solution (33 mM, pH 7.3, 8 mL) of rHSA (4.69 μM) via the narrow tube under a CO atmosphere, and the mixture was dialyzed with cellulose membrane against phosphate buffer (pH 7.3) for 2 h and 15 h at 4 °C. We confirmed that the EtOH concentration in the solution reduced to less that 100 ppm. Finally, the total volume was adjusted to 15 mL, giving carbonyl rHSA—**FeRP(B)** solution (**FeRP(B)**/rHSA = 8 (mol/mol), [Fe] = 20 μM).

Binding Numbers of FeRP(B) into rHSA. Based on the absorbance intensity of the UV—vis absorption spectra of the rHSA—**FeRP(B)** hybrid with different **FeRP(B)**/rHSA mixing ratios, the binding numbers of **FeRP(B)** in the albumin host were assayed as previously reported (Komatsu et al., 1999). Furthermore, in the course of preparation of the hybrid, the remaining carbonyl **FeRP(B)** at the bottom of the round flask was extracted with $CHCl_3$ and its concentration was determined by the absorption spectra.

O_2-Coordination Equilibria and Kinetics. O_2-coordinations to **FeRP(B)** derivative are expressed by

$$\text{FeRP(B)} + O_2 \underset{k_{off}}{\overset{k_{on}}{\rightleftharpoons}} \text{FeRP(B)}{-}O_2 \qquad (1)$$

$$(K = k_{on}/k_{off})$$

The O_2-binding affinity ($P_{1/2} = 1/K$) of **FeRP(B)**s in organic solvents or their rHSA hybrids in aqueous media were determined by spectral changes at various partial pressure of O_2 as in previous literatures (Komatsu et al., 1999; Tsuchida et al., 1995). **FeRP(B)**s concentrations of 20 μM were normally used for UV—vis. absorption spectroscopy. The spectra were recorded within the range of 350—700 nm. The O_2-association and -dissociation rate constants (k_{on}, k_{off}) were measured by a competitive rebinding technique using a Unisoku TSP-600 laser flash photolysis apparatus (Collman et al., 1983; Tsuchida et al., 1995; Traylor et al., 1985). The absorption decays accompanied O_2-rebinding to **FeRP(B)**s in organic solvents obeyed single exponential, so that we applied a first-order kinetics to calculate the rates. On the other hand, rHSA—**FeRP(B)** in aqueous solution showed triphases. We used triple-exponential kinetics described elsewhere to analyze the absorption decays (Komatsu et al., 2000).

RESULTS AND DISCUSSION

Synthesis of FeRP(B) Complexes. We first report the synthesis of tetrakis[(α,α,α,α-*o*-amino)phenyl]porphinatoiron(II) derivatives with bulky fences around the

Scheme 1

M=2H **1(H)**
M=Cu(II) **1(Cu)**

POCl₃/DMF
CH₂Cl₂

M=2H **2(H)**
M=Cu(II) **2(Cu)**

NaBH₄
CH₂Cl₂/MeOH

3

3-cyc

DMF, DCC, DMAP

4-cyc

FeBr₂
THF, 2,6-lutidine

FecycP(Im) Br⁻

R= ∠ piv

R= ∠ cyc

3

THF, DMAP

5

L-HisOMe
DMF, BOP

6

FeBr₂
THF, 2,6-lutidine

FepivP(His) Br⁻
FecycP(His) Br⁻
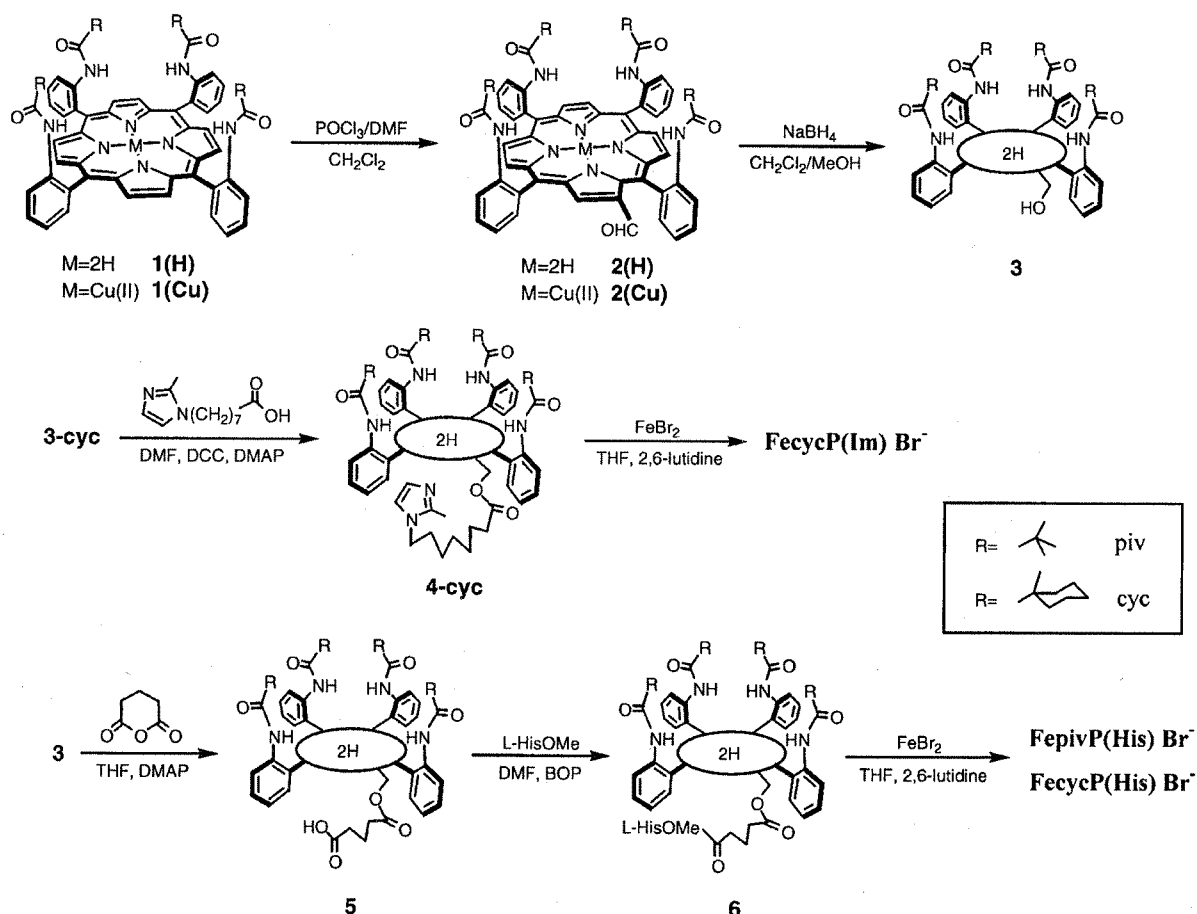
O_2-coordination site (pivaloyl or 1-methylcyclohexanoyl) and a proximal base [2-methylimidazole or methyl-L-histidine (L-HisOMe)] at the β-pyrrolic position (Scheme 1, see Supporting Information). The parent porphines, namely 2-hydroxymethyl-5,10,15,20-tetrakis[(α,α,α,α-*o*-pivaloylamino)phenyl]porphine (**3-piv**) and 2-hydroxy-methyl-5,10,15,20-tetrakis{[α,α,α,α-*o*-(1-methylcyclohex-anoylamino)]phenyl}porphine (**3-cyc**) were prepared using the Vilsmeir reaction. The hydroxyl group was converted into a carboxylic acid chain by glutaric anhy-dride (**5**). Introduction of L-HisOMe into this carboxylic acid using DCC unfortunately failed. Several unknown products were detected. In contrast, the same coupling using benzotriazol-1-yloxytris(dimethylamine)phosphon-ium hexafluorophosphate (BOP) in a dry DMF solution yielded the target free-base compound (**6**) in high yield (~85%). Iron insertion was carried out using FeBr₂ in dry THF to afford the corresponding iron(III) complexes.

O₂-Binding Properties of FeRP(B)s in Organic Solvents. The UV—vis absorption spectrum of the tolu-ene solution of **FecycP(Im)** with a 2-methyl-1-imid-azolylalkyl arm under an N₂ atmosphere showed the formation of the five-N-coordinated complex (λ_{max}: 441, 539, 558 nm) as well as **FepivP(Im)** (not shown) (Tsuchida et al., 1995). The **FepivP(His)** and **FecycP(His)** with a proximal histidine also displayed the same spectral pattern (λ_{max}: 441, 544, 564 nm), which was constant in the range from 5 μM–1 mM at 10–70 °C. Resonance Raman (RR) spectroscopy of **Fepiv(His)** demonstrated a medium band at 219 cm⁻¹, which was assigned to the Fe(II)—N(imidazole) stretching mode,
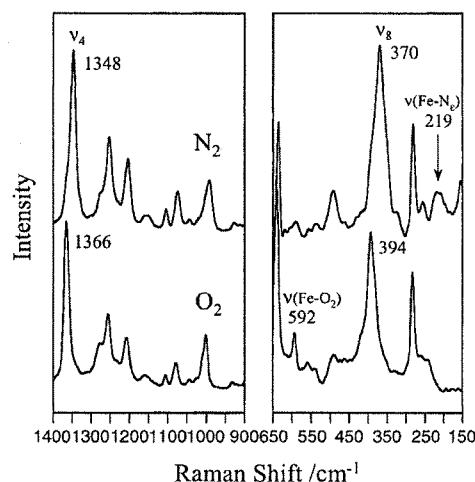
Figure 1. Resonance Raman spectra of **FepivP(His)** in benzene solution at 25 °C.

ν(Fe—N$_\epsilon$) (Figure 1) (Hori et al., 1980; Wu et al., 1998). It can be concluded that the covalently linked histidine residue at the porphine periphery binds to the central iron(II) to give the five-coordinated high-spin iron(II) complex under an N₂ atmosphere in a fashion similar to the 2-methylimidazolated analogues [**FepivP(Im)** or **FecycP(Im)**].

Upon bubbling of O₂ or CO gas into the benzene solution of **FepivP(His)**, the UV—vis absorption spec-

Table 1. O₂-Binding Parameters of FeRP(B) in Organic Solvents at 25 °C

FeRP(B)	solvent	$P_{1/2}$ (Torr)	$10^{-8} k_{on}$ ($M^{-1} s^{-1}$)	$10^{-3} k_{off}$ (s^{-1})
FepivP(Im)	toluene	38	1.6	79
FecycP(Im)	toluene	20	1.8	47
FepivP(His)	benzene	1.7	2.1	3.7
FecycP(His)	toluene	1.7	2.0	4.3

trum immediately changed to those of the O₂—adduct complex (λ_{max}: 429, 551 nm) or CO—adduct complex (λ_{max}: 428, 546 nm) (Komatsu et al., 2001). The dioxygenation was sufficiently stable and reversible at 25 °C depending on the O₂-partial pressure. In the RR spectrum, the ν(Fe—O₂) vibration of the dioxygenated **FepivP(His)** appeared at 592 cm⁻¹ after O₂ bubbling. This peak suggests a typical end-on type O₂-coordination to the porphinatoiron(II). The skeletal modes of the porphine ring (ν_8 and ν_4) were also upshifted from 370 and 1348 cm⁻¹ to 394 and 1366 cm⁻¹, respectively. These observations indicate the formation of the six-coordinated low-spin iron(II) complex of **FepivP(His)** (Burke et al., 1978; Hori et al., 1980; Wu et al., 1998). All the shifts were reversibly observed depending on the O₂ concentration. The RR spectra of **FecycP(His)** showed the same results as well.

The O₂-binding affinities ($P_{1/2}$), and O₂-association and -dissociation rate constants (k_{on}, k_{off}) of the **FeRP(B)**s in organic solvents are summarized in Table 1. The difference in the fence structure around the O₂-coordination site (pivaloyl or 1-methylhexanoyl) did not significantly influence their O₂-binding equilibria and kinetics. On the basis of the important earlier studies, the distal steric encumbrance only reduces the association rate for O₂ (Collman et al., 1983; Traylor et al., 1985). According to the hypothesis, the inner volume of the cavities, which are constructed using the four pivaloyl or 1-methylcyclohexanoyl groups on the porphine plane, should be of similar size. On the other hand, the axial histidine coordination significantly increased the O₂-binding affinity compared to those of the 2-methylimidazole bound analogues by a factor of 11—24, that is kinetically due to the low O₂-dissociation rate constants. It is generally recognized that the steric hindrance of the 2-methyl group of the axially coordinated imdazole decreases the O₂-binding affinity, giving the "Tense state" model of Hb (Collman et al., 1978). Our results on the large O₂-binding affinities of **FepivP(His)** and **FecycP(His)** correlate well with the theory of the former study.

To clarify the geometry of the bulky cyclohexanoyl fences and axial histidine coordination, the stereostructure of the dioxygenated low-spin complex of **FecycP(His)** was simulated by molecular dynamics (Figure 2). It was found that (i) the repulsions between the cyclohexanoyl fences do not induce a ruffling of the porphine plane, and (ii) the dihedral angle of the imidazole ring with respect to the porphine was 89.3°, suggesting that the imidazole N-coordination to the central iron(II) is not distorted by the rigid amide spacer between the porphine and HisOMe. It is also remarkable that (iii) the H atom of the imidazole cannot form a hydrogen bond with the neighboring carbonyl O atom, which is known to partially influence the dioxygenation of the heme.

We concluded that covalently attaching the histidine group directly to the porphine periphery provides the five-N-coordinated high-spin iron(II) complex and a large equilibrium constant for the O₂ binding in comparison to that of the 2-methylimidazolated analogue due to the
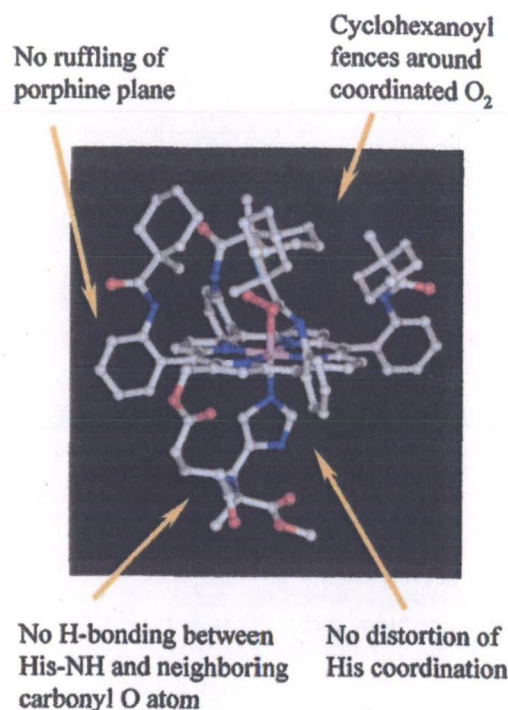

Figure 2. Simulated structure of the dioxygenated **FecycP-(His)**. Molecular dynamics and minimization (force field: esff) were performed using an Insight II system (Molecular Simulations Inc.). The structure was generated by alternative minimizations and annealing dynamic calculations from 1000 to 100 K.

small dissociation rate, even though its O₂-binding affinity was 6-fold lower than that of the *N*-alkylimidazole-coordinated one, 2-[8-(1-imidazolyl)octanoyloxymethyl]-5,10,15,20-tetrakis[(α,α,α,α-*o*-pivaloylamino)phenyl]-porphinatoiron(II) ($P_{1/2}$: 0.29 Torr) (Tsuchida et al., 1995). This is probably caused by the low σ-basicity of the histidine.

Anyway, these results are the first examples of the stable O₂—adduct complexes of the synthetic porphinatoiron(II)s with an intramolecularly coordinated proximal histidine and their O₂-binding equilibrium and kinetic parameters.

FeRP(B)s Incorporations into rHSA. A maximum of eight **FepivP(Im)** molecules were incorporated into certain domains of human serum albumin with binding constants from 10^6–10^4 M⁻¹ (Komatsu et al., 1999). Other **FeRP(B)**s were also expected to bind to rHSA in a similar fashion, and the binding sites would also be identical. From the quantitative analyses of the absorption intensity for the Soret band of aqueous rHSA—**FecycP(His)**, the maximum binding numbers of **FecycP(His)** to an rHSA were determined to be eight by using molar extinction coefficient of the carbonyl heme complex. Actually, the unbound **FecycP(His)** remaining in the flask was less than 4% of the total amount of the heme in case of **FecycP(His)**/rHSA was eight (mol/mol). The other **FeRP(B)**s [**FepivP(His)**, **FecycP(Im)**] also showed the same results. The binding numbers are always eight and independent of the substituents and axial bases.

O₂-Coordination Properties of rHSA—FeRP(B). The UV—vis absorption spectrum of the aqueous rHSA hybrid including carbonyl **FepivP(His)** showed the formation of the typical CO-coordinated low-spin tetraphenylporphinatoiron(II) derivative (λ_{max}: 433, 548 nm) (Figure 3). Light irradiation using a 500-W halogen lamp
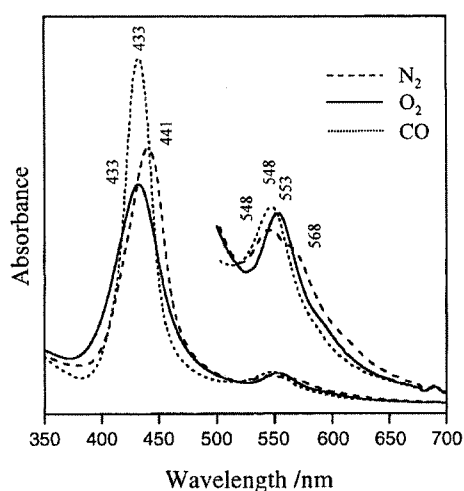
Figure 3. UV–vis absorption spectral changes of the rHSA–FepivP(His) in phosphate buffer solution (pH 7.3) at 25 °C.

Table 2. Absorption Maxima (λ_{max}) of rHSA–FeRP(B) Series in Phosphate Buffer Solution (pH 7.3) under N$_2$, O$_2$, and CO Atmosphere

rHSA–FeRP(B)	N$_2$	O$_2$	CO
rHSA–FepivP(Im)	443, 542, 567	426, 552	427, 539
rHSA–FecycP(Im)	445, 543, 567	428, 555	429, 545
rHSA–FepivP(His)	441, 548, 568	433, 553	433, 548
rHSA–FecycP(His)	442, 548, 568	429, 553	431, 548
Hb[a]	430, 555	415, 541, 576	419, 540, 569

[a] From Antonini et al. (1971).

of this solution under an O$_2$ atmosphere led to CO dissociation, affording the O$_2$–adduct complex (λ_{max}: 433, 553 nm). Upon exposure of the dioxygenated rHSA–FepivP(His) to N$_2$, the UV–vis absorption spectrum changed to that of the five-N-coordinated iron(II) complex with an intramolecularly coordinated axial histidine (λ_{max}: 441, 548, 568 nm). This O$_2$-binidng was reversibly observed and kinetically stable under physiological conditions (pH 7.3, 37 °C). Similar dioxygenations were also observed in the rHSA hybrids with **FecycP(Im)** and **FecycP(His)** (Table 2).

The laser flash photolysis experiments provided the k_{on} and k_{off} values of the O$_2$ binding to rHSA–**FeRP(B)**s, and a detailed kinetic analysis gave the following results. (i) The absorption decays accompanying the O$_2$ recombination were composed of three-phases of the first-order kinetics, therefore, the curves were fit by a triple-exponential equation, which is similar to the previously reported rHSA– **FepivP(Im)** (Komatsu et al., 2000). The minor, almost 10% component, which has the fastest rate constant, was independent of the O$_2$ concentrations. It should be correlated with a base elimination reaction (Geibel et al., 1978). (ii) From the careful inspections of the other two phases, the association rate constants for the fast and slow rebindings [k_{on}(fast) and k_{on}(slow)] of O$_2$ were calculated (Table 3). The k_{on}(fast) values are 4–6-times larger than k_{on}(slow). (iii) The concentration ratios of the fast and slow reactions were 2–3. Consequently, the O$_2$ association to the **FeRP(B)**s in the hydrophobic domains of the serum albumin is influenced by the molecular microenvironments around each O$_2$-coordination site, e.g., steric hindrance of the amino acid residue and difference in polarity. These observations coincided with our previous results on rHSA–**FepivP(Im)** (Komatsu et al., 2000).

Table 3. O$_2$-Binding Parameters of rHSA–FeRP(B) Series in Phosphate Buffer Solution (pH 7.3) at 25 °C

rHSA–FeRP(B)	$10^{-6}\,k_{on}$ (M^{-1} s^{-1})		$10^{-1}\,k_{off}$ (s^{-1})		$P_{1/2}{}^a$ (Torr)	$\tau_{1/2}{}^b$ (h)
	fast	slow	fast	slow		
rHSA–FepivP(Im)	34	9.5	75	20	13 (33)	2
rHSA–FecycP(Im)	46	7.3	98	16	13 (35)	9
rHSA–FepivP(His)	36	6.1	5.9	1.0	1 (3)	5
rHSA–FecycP(His)	54	8.8	8.9	1.4	1 (3)	25

[a] At 37 °C in parentheses. [b] At 37 °C.

The $P_{1/2}$ of the rHSA–**FeRP(B)**s were determined on the basis of the UV–vis. spectral changes during the O$_2$ titration (Table 3). According to the kinetic experiments, the $P_{1/2}$ values were divided into two components using our previously reported equation (Komatsu et al., 2000). Nevertheless, the calculated $P_{1/2}$ for the fast and slow phases were all identical in each case. The rHSA–**FepivP(Im)** and rHSA–**FecycP(Im)** showed the same O$_2$-binding affinities (13 Torr), indicating that the fence structures on the porphine plane cause only negligibly small changes in their O$_2$-equilibria and -kinetics even in albumin. In contrast, the axial histidine coordination provided a 13-fold larger O$_2$-binding affinity compared to those of the 2-methylimidazole-linked analogues, which is again ascribed to the low O$_2$-dissociation rate constants.

Accompanying the autoxidation of the central iron(II), the absorption band (λ_{max}: 552–555 nm) slowly disappeared at 37 °C, leading to the formation of the inactive iron(III) porphinate (Momenteau et al., 1994). The effect of the heme structure on the half-life ($\tau_{1/2}$) of the O$_2$–adduct complex was rather remarkable. (i) The cyclohexanoyl fences gave ca. 5-fold longer $\tau_{1/2}$ values compared to those of the pivaloyl derivatives, and (ii) the proximal histidine coordination increased $\tau_{1/2}$ by a factor of 3. As a result, (iii) the dioxygenated rHSA–**FecycP(His)** showed an unusually long lifetime ($\tau_{1/2}$: 25 h at 37 °C) which is ca. 13-fold longer than that of rHSA–**FepivP(Im)**.

In conclusion, recombinant human serum albumin incorporating **FeRP(His)**s having an intramolecularly coordinated histidine residue formed stable O$_2$–adduct complexes under physiological conditions. In particular, dioxygenated rHSA–**FecycP(His)** showed a high stability against the proton-driven oxidation, and its half-lifetime reached a value similar to that of the native Hb A ($\tau_{1/2}$: 36 h at 37 °C) (Mansouri et al., 1973). Although the O$_2$-binding affinity of rHSA–**FecycP(His)** is too high to use as a blood replacement composition, it can be utilized as an O$_2$-carrying medicine for oxygenation of the hypoxia region in cancer tissue, the preservation or circulation liquid for organs, and culture medium for the regeneration of tissues, etc. As a red blood cell substitute, rHSA–**FecycP(Im)**, which has a similar $P_{1/2}$ value to red blood cells, is full of promise. In the bloodstream, the apparent lifetime of the O$_2$-coordinated albumin–heme is prolonged by a factor of 4 (Tsuchida et al., 2000), so that the rHSA–**FecycP(Im)** is expected to transport O$_2$ in the circulatory system for more than 36 h. The preclinical test of the administration of rHSA–**FecycP(Im)** into anesthetized rats is currently underway.

ACKNOWLEDGMENT

Supporting Information Available: Experimental details of the synthesis procedures (^{1}H NMR, IR, MS, UV–vis) of the all compounds in Scheme 1. This material is available free of charge via the Internet at http://pubs.acs.org.

LITERATURE CITED

(1) Antonini, E., and Brunori, M. (1971) in Hemoglobin and Myoglobin in Their Reactions with Ligands (A. Neuberger, E. L. Tatum, C. Rivat, Ed.), North-Holland Publ., Amsterdam.

(2) Burke, J. M., Kinchrad, J. R., Peters, S., Gagne, R. R., Collman, J. P., and Spiro, T. G. (1978) Structure-Sensitive Resonance Raman Bands of Tetraphenyl and "Picket Fence" Porphyrin-Iron Complexes, Including an Oxyhemoglobin Analogue. *J. Am. Chem. Soc. 100,* 6083–6088.

(3) Collman, J. P., Brauman, J. I., Doxsee, K. M. Halbert, T. R., and Suslick, K. S. (1978) Model Compounds for the T State of Hemoglobin. *Proc. Natl. Acad. Sci. U.S.A. 75,* 564–568.

(4) Collman, J. P., Brauman, J. I., Iverson, B. L., Sessler, J. L., Morris, R. M., and Gibson, Q. H. (1983) O_2 and CO Binding to Iron(II) Porphyrins: A Comparison of the "Picket Fence" and "Pocket" Porphyrins. *J. Am. Chem. Soc. 105,* 3052–3064.

(5) Geibel, J., Cannon, J., Campbell, D., and Traylor, T. G. (1978) Model Compounds for R-State and T-State Hemoglobins. *J. Am. Chem. Soc. 100,* 3575–3585.

(6) Hori, H. and Kitagawa, T. (1980) Iron-Ligand Stretching Band in the Resonance Raman Spectra of Ferrous Iron Porphyrin Derivatives. Importance as a Probe Band for Quaternary Structure of Hemoglobin. *J. Am. Chem. Soc. 102,* 3608–3613.

(7) Komatsu, T., Hamamatsu, K., Wu, J., and Tsuchida, E. (1999) Physicochemical Properties and O_2–Coordination Structure of Human Serum Albumin Incorporating Tetrakis-(*o*-pivalamido)phenylporphyrinatoiron(II) Derivatives. *Bioconjugate Chem. 10,* 82–86.

(8) Komatsu, T., Matsukawa, Y., and Tsuchida, E. (2000) Kinetics of CO and O_2 Binding to Human Serum Albumin-Heme Hybrid. *Bioconjugate Chem. 11,* 772–776.

(9) Komatsu, T., Matsukawa, Y., Miyatake, K., and Tsuchida, E. (2001) O_2-Adduct Complex of *meso*-Tetrakis($\alpha,\alpha,\alpha,\alpha$-*o*-pivalamidophenyl)porphinatoiron(II) with an Intramolecularly Coordinated Proximal Histidine. *Chem. Lett. 2001,* 668–669.

(10) Momentau, M., and Reed, C. A. (1994) Synthetic Heme Oxygen Complexes. *Chem. Rev. 94,* 659–698.

(11) Monsouri, A., and Winterhalter, K. H. (1973) Nonequivalence of Chains in Hemoglobin Oxidation. *Biochemistry 12,* 4946–4949.

(12) Sumi, A., Ohtani, W., Kobayashi, K., Ohmura, T., Yokoyama, K., Nishida, M., and Suyama, T. (1993) Purification and Physicochemical Properties of Recombinant Human Serum Albumin, in *Biotechnology of Blood Proteins* (C. Rivat, J.-F. Stoltz, Eds.) Vol. 227, pp 293–298, John Libbey Eurotext, Montrouge.

(13) Traylor, T. G., Tsuchiya, S., Campbell, D., Mitchell, M., Stynes, D., and Koga, N. (1985) Anthracene Heme Cyclophanes. Steric Effects in CO, O_2, and RNC Binding. *J. Am. Chem. Soc. 107,* 604–614.

(14) Tsuchida, E., Komatsu, T., Kumamoto, S., Ando, K., and Nishide, H. (1995) Synthesis and O_2-Binding Properties of Tetraphenylporphyrinatoiron(II) Derivatives Bearing a Proximal Imidazole Covalently Bound at the β-Pyrrolic Position. *J. Chem. Soc., Perkin Trans. 2* 747–753.

(15) Tsuchida, E., Komatsu, T., Matsukawa, Y., Hamamatsu, K., and Wu, J. (1999) Human Serum Albumin Incorporating Tetrakis(*o*-pivalamido)phenylporphinatoiron(II) Derivative as a Totally Synthetic O_2-Carrying Hemoprotein. *Bioconjugate Chem. 10,* 797–802.

(16) Tsuchida, E., Komatsu, T., Hamamatsu, K., Matsukawa, Y., Tajima, M., Yoshizu, A., Izumi, Y., and Kobayashi, K. (2000) Exchange Transfusion with Albumin-Heme as an Artificial O_2-Infusion into Anesthetized Rats: Physiological Reponses, O_2-Delivery, and Reduction of the Oxidized Hemin Sites by Red Blood Cells. *Bioconjugate Chem. 10,* 797–802.

(17) Wu, J., Komatsu, T., and Tsuchida, E. (1998) Resonance Raman Studies of O_2-Binding to *ortho*-Substituted Tetraphenyl- and Tetranaphthyl-Porphyrinatoiron(II) Derivatives with a Covalently Linked Axial Imidazole. *J. Chem. Soc., Dalton Trans.* 2503–2506.

BC010067R

Human Serum Albumin Incorporating Synthetic Hemes as an O_2-Carrying Hemoprotein: Control of O_2-Binding Ability by Heme Structure

*Eishun Tsuchida,* Teruyuki Komatsu, Yasuko Mastukawa, Tomoyuki Okada*

Department of Polymer Chemistry, Advanced Research Institute for Science and Engineering, Waseda University, Tokyo 169-8555, Japan

Summary: Incorporation of different structured synthetic hemes, 5,10,15,20-tetraphenylporphyrinatoiron(II) derivetives with a covalently linked proximal base [FeP(1) to FeP(7)], into human serum albumin (HSA), provides seven types of albumin-heme hybrids (HSA-FeP) with different O_2-binding abilities. An HSA host absorbs a maximum of eight FeP molecules in each case. The obtained all HSA-FePs can reversibly bind and release O_2 under physiological conditions (in aqueous media, pH 7.3, 37 °C) as similar as hemoglobin and myoglobin. The difference in the fence structures did not affect the O_2-binding parameters, however the axial histidine coordination significantly increased the O_2-binding affinity, which is ascribed to the low O_2-dissociation rate constants. The most remarkable effect of the heme structure appeared in the half-lifetime ($\tau_{1/2}$) of the O_2-adduct complex. The dioxygenated rHSA-FeP(4) showed an unusually long lifetime ($\tau_{1/2}$: 25 hr at 37 °C) which is ca. 13-fold longer than that of rHSA-FeP(1).

Introduction

Human serum albumin (HSA) is the most abundant plasma protein, which binds and transports a great variety of metabolites and organic compounds in our blood stream.[1] This very common protein has suddenly become to attract much attention in many research fields, since its crystal structure was dissolved in 1989.[2] The 585 amino acids consist of a unique heart-shaped structure, that is made of three repeating domains I to III, and each one is constructed of two sub-domains. The majority of the ligand compounds are bound at one site within special hydrophobic cavities of the subdomains IIA and IIIA. We have also found that 5,10,15,20-tetrakis[$\alpha,\alpha,\alpha,\alpha$-o-(2,2-dimethylpropanamido)phenyl]-2-[8-(2-methyl-1-imidazolyl)octanoyloxymethyl]porphinatoiron(II) [FeP(1)] is incorporated into HSA, providing synthetic hemoprotein [HSA-FeP(1)] which can bind and release O_2 under physiological conditions like

hemoglobin.[3-5] The obtained HSA-FeP(1) solution has a good compatibility with human whole blood and can quantitatively transport O_2 in vivo.[6] Furthermore, recombinant HSA (rHSA) is now manufactured on a large scale by expression in the *Pichia pastoris* as a host cell, therefore rHSA-FeP becomes an entirely synthetic O_2-carrying hemoprotein.[7] These albumin-heme hybrids are recognized to be one of the most promising materials not only as a blood replacement composition, but also as an O_2-carrying medicine which will be adopted in several clinical applications, ex., myocardial infraction, anemia, and tracheal blockade, *etc.* However, to use this synthetic O_2-carrier for such diseases, its O_2-transporting abilities should be adjusted to the required conditions. We believe that the control of the O_2-binding property can be realized by the optimizing of the chemical structure of the incorporated heme. This paper describes the O_2-binding abilities of the human serum albumin incorporating seven types of synthetic hemes, 5,10,15,20-tetraphenylporphyrinatoiron(II) derivatives with a covalently linked proximal base [FeP(1) to FeP(7), Formula 1].[8,9]
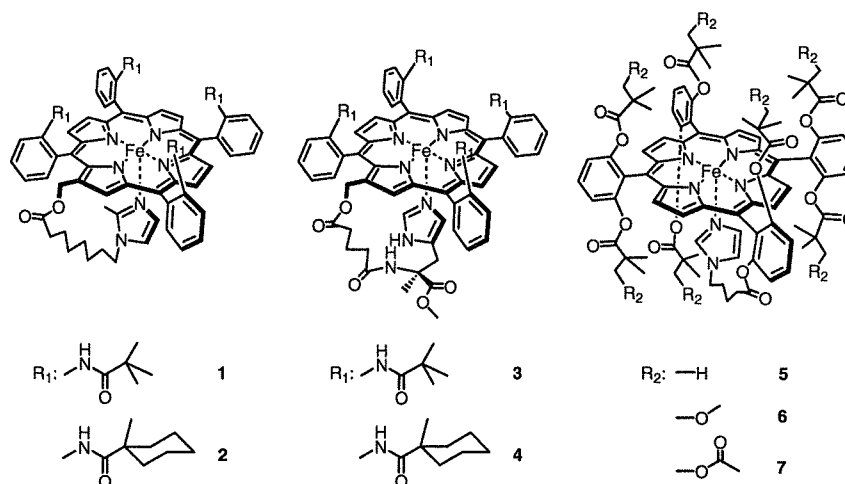
Formula 1. Synthetic hemes FeP(1) to FeP(7)

Heme incorporation into human serum albumin

A maximum of eight FeP(1) molecules were incorporated into certain domains of human serum albumin with binding constants from $10^6 - 10^4$ M^{-1}.[4] Other FePs were

also expected to bind to HSA or rHSA in a similar fashion, and the binding sites would also be identical. For instance, from the quantitative analyses of the absorption intensity for the Soret band of aqueous rHSA-FeP(4), the maximum binding numbers of FeP(4) to an rHSA were determined to be eight. The other FePs [FeP(2) – FeP(7)] also showed the same results. The binding numbers are always eight and independent of the substituents and proximal bases. The predicted 3D structure of the rHSA hybrid incorporating eight FeP(1) molecules into the hydrophobic cavities are demonstrated in Figure 1.
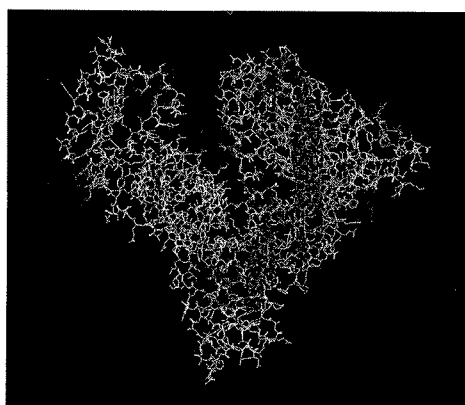
Figure 1. Predicted structure of rHSA hybrid incorporating eight FeP(1) molecules by molecular simulation using Insight II.

O_2-binding parameters of human serum albumin–hemes

The UV-vis. absorption spectrum of the aqueous rHSA hybrid including carbonyl FeP(3) showed the formation of the typical CO-coordinated low-spin tetraphenyl-porphinatoiron(II) derivative (λ_{max}: 433, 548 nm). Light irradiation of this solution under an O_2 atmosphere led to CO dissociation, affording the O_2-adduct complex (λ_{max}: 433, 553 nm). Upon exposure of the dioxygenated rHSA-FeP(3) to N_2, the UV-vis. absorption spectrum changed to that of the five-N-coordinated high-spin iron(II) complex with an intramolecularly coordinated axial histidine (λ_{max}: 441, 548, 568 nm). This O_2-binidng was reversibly observed and kinetically stable under physiological

conditions (pH 7.3, 37 °C). Similar dioxygenations were also observed in the human serum albumin hybrids with FeP(2) – FeP(7) (Table 1).

Table 1. Absorption maxima (λ_{max}) of human serum albumin-heme hybrids in phosphate buffer solution (pH 7.3) under N_2, O_2 and CO.

	N_2	O_2	CO
rHSA-FeP(1)	443,542,567	426,552	427,539
rHSA-FeP(2)	445,543,567	428,555	429,545
rHSA-FeP(3)	441,548,568	433,553	433,548
rHSA-FeP(4)	442,548,568	429,553	431,548
HSA-FeP(5)	438,539,558	425,549	427,545
HSA-FeP(6)	438,540,560	426,549	427,546
HSA-FeP(7)	438,542,563	426,549	427,546

The O_2-coordinations to FePs in human serum albumin are expressed by equation 1.

$$FeP + O_2 \underset{k_{off}}{\overset{k_{on}}{\rightleftharpoons}} FeP-O_2 \qquad \cdots (1)$$

$$[K = (P_{1/2})^{-1} = k_{on}/k_{off}]$$
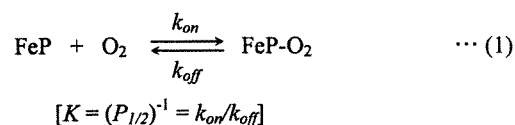
The O_2-association and dissociation rate constants (k_{on}, k_{off}) were explored by laser flash photolysis.[5] The detailed kinetic evaluation of human serum albumin-heme hybrids gave the following three results.

(i) The absorption decays accompanying the O_2 recombination were composed of three-phases of the first-order kinetics; the curves were fit by a triple-exponential equation.[5] The minor (<10%) and the fastest component was independent of the O_2 concentrations. It should be correlated with a base elimination.[10]

(ii) From the careful inspections of the two slower phases, the association rate constants for the fast and slow rebindings [$k_{on}(fast)$ and $k_{on}(slow)$] of O_2 were calculated (Table 2). The $k_{on}(fast)$ values are 4 – 7-times larger than $k_{on}(slow)$.

(iii) The concentration ratios of the fast and slow reactions were 2 – 3.

Based on these findings, we can conclude that the O_2 association to the FePs in the hydrophobic domains of the serum albumin is influenced by the molecular microenvironments around each O_2-coordination site, e.g., steric hindrance of the amino acid residue and difference in polarity.

Table 2. O_2-Binding parameters of human serum albumin-heme hybrids in phosphate buffer solution (pH 7.3) at 25°C.

| | $10^{-6} k_{on}$ ($M^{-1} s^{-1}$) | | $10^{-1} k_{off}$ (s^{-1}) | | $P_{1/2}$ | $\tau_{1/2}$ |
	fast	slow	fast	slow	(Torr)	(hr)
rHSA-FeP(1)	34	9.5	75	20	13	2
rHSA-FeP(2)	46	7.3	98	16	13	9
rHSA-FeP(3)	36	6.1	5.9	1.0	1	5
rHSA-FeP(4)	54	8.8	8.9	1.4	1	25
HSA-FeP(5)	11	1.5	50	6.9	28	5
HSA-FeP(6)	11	2.0	41	7.6	23	2
HSA-FeP(7)	8.9	2.3	34	8.8	23	2

The $P_{1/2}$ of the human serum albumin-heme hybrids were determined on the basis of the UV-vis. spectral changes during the O_2 titration (Table 2).[5] According to the kinetic experiments, the $P_{1/2}$ values were divided into two components using our previously reported equation.[5] Nevertheless, the calculated $P_{1/2}$ for the fast and slow phases were all identical in each case. The rHSA-FeP(1) and rHSA-FeP(2) showed the same O_2-binding affinities (13 Torr), indicating that the fence structure on the porphyrin plane causes only small changes in their O_2-equilibria and -kinetics. The double-sided series, FeP(5), FeP(6), and FeP(7) in albumin, showed very similar O_2-binding parameters, also supporting the above assumption. In contrast, the axial histidine coordination provided a 13-fold larger O_2-binding affinity compared to those of the 2-methylimidazole linked analogues [FeP(1) or FeP(2)], which is ascribed to the low O_2-dissociation rate constants.

Stability of O_2-adduct complex of human serum albumin–hemes

Accompanying the autooxidation of the central iron(II), the absorption band (λ_{max}: 549–555 nm) slowly disappeared at 37 °C, leading to the formation of the inactive iron(III) porphinate.[11] The effect of the heme structure on the half-lifetime ($\tau_{1/2}$) of the O_2-adduct complex was rather remarkable. (i) The cyclohexanoyl fences gave ca. 5-fold longer $\tau_{1/2}$ values compared to those of the pivaloyl derivatives, and (ii) the proximal histidine coordination increased $\tau_{1/2}$ by a factor of 3. As a result, (iii) the dioxygenated rHSA-FeP(4) showed an unusually long lifetime ($\tau_{1/2}$: 25 hr at 37 °C)

which is ca. 13-fold longer than that of rHSA-FeP(1). In double-sided series, the introduction of the polar-substituents on the fence groups led to reduce the stability of the O_2-adduct species.

Conclusions

Human serum albumin incorporating FePs having an intramolecularly coordinated histidine residue formed stable O_2-adduct complexes under physiological conditions. In particular, dioxygenated rHSA-FeP(4) showed a high stability, and its half-lifetime reached a value similar to that of the native Hb A ($\tau_{1/2}$: 36 hr at 37 °C).[12] Although the O_2-binding affinity of rHSA-FeP(4) is too high to use as a blood replacement composition, it can be utilized as an O_2-carrying medicine for dioxygenation of the hypoxia region in cancer tissue, *etc.* As a red blood cell substitute, rHSA-FeP(2), which has a similar $P_{1/2}$ value to red blood cells, is promising. In the blood stream, the apparent lifetime of the O_2-coordinated albumin-heme is prolonged by a factor of 4,[6] so that the rHSA-FeP(2) is expected to transport O_2 in the circulatory system for more than 1.5 days.

[1]   T. Peters Jr., "All about Albumin, Biochemistry, Genetics, and Medical Applications", Academis Press Inc., San Diego, 1996.
[2]   D. C. Carter, X.-M. He, S. H. Munson, P. D. Twigg, K. M. Gernert, M. B. Broom, T. R. Miller, *Science* **1989**, *244*, 1195.
[3]   T. Komatsu, K. Ando, N. Kawai, H. Nishide, E. Tsuchida, *Chem. Lett.* **1995**, 813.
[4]   T. Komatsu, K. Hamamatsu, J. Wu, E. Tsuchida, *Bioconjugate Chem.* **1999**, *10*, 82.
[5]   T. Komatsu, Y. Matsukawa, E. Tsuchida, *Bioconjugate Chem.* **2000**, *11*, 772.
[6]   E. Tsuchida, T. Komatsu, K. Hamamatsu, Y. Matsukawa, A. Tajima, A. Yoshizu, Y. Izumi, K. Kobayashi, *Bioconjugate Chem.* **2000**, *11*, 46.
[7]   E. Tsuchida, T. Komatsu, Y. Matsukawa, K. Hamamatsu, J. Wu, *Bioconjugate Chem.* **1999**, *10*, 797.
[8]   T. Komatsu, Y. Matsukawa, E. Tsuchida, *Bioconjugate Chem.* **2001**, *12*, submitted.
[9]   T. Komatsu, T. Okada, M. Moritake, E. Tsuchida, *Bull. Chem. Soc. Jpn.* **2001**, *74*, in press.
[10]   J. Geibel, J. Cannon, D. Campbell, T. G. Traylor, *J. Am. Chem. Soc.* **1978**, *100*, 3575.
[11]   M. Momentau, C. A. Reed, *Chem. Rev.* **1994**, *94*, 659.
[12]   A. Monsouri, K. H. Winterhalter, *Biochemistry* **1973**, *12*, 4946.

Self-Organized Lipid-Porphyrin Bilayer Membranes in Vesicular Form: Nanostructure, Photophysical Properties, and Dioxygen Coordination

Teruyuki Komatsu, Miho Moritake, Akito Nakagawa, and Eishun Tsuchida*[a]

Abstract: An amphiphilic tetraphenyl-porphyrin and its iron complex bearing four phospholipid substituents, in which a trimethylolethane residue connects the two acyl chains (lipid-porphyrins), have been synthesized. The free-base lipid-porphyrin **6a** self-organizes in aqueous media to form spherical unilamellar vesicles with a diameter of 100 nm and a uniform thickness of 10 nm, which corresponds to twice the length of the molecule. In the visible absorption spectrum, the porphyrin Soret band was significantly red-shifted (12 nm) relative to that of the monomer in benzene/MeOH solution due to the excitonic interaction of the porphyrin chromophores. The $\Pi-A$ isotherm of **6a** gave an area per molecule of 2.2 nm², which allowed the estimation of the number of molecules in a single vesicle (2.3×10^4). Double-layered Langmuir–Blodgett (LB) films of **6a** on a glass surface exhibited an absorption spectrum identical to that of the **6a** vesicles in bulk aqueous solution, and this suggests that they contain similar geometric arrangements of the porphyrin moieties. Exciton calculations on the basis of our structural model reproduced the bathochromic shift of the Soret band well. In the photophysical properties of the **6a** vesicles, the characteristics of J-aggregated porphyrins substantially predominate: strong fluorescence and extremely short triplet lifetime. The iron complex **6b** with a small molar excess of 1-dodecylimidazole (DIm) also formed spherical unilamellar vesicles (100 nm Φ).

Keywords: dioxygen ligands · nanostructures · porphyrinoids · self-assembly · vesicles

Scanning force microscopy after evaporation on a graphite surface revealed **6b**/DIm vesicles with a vertical height of 19.8 nm, which coincided with the thickness of the double bilayer membranes. The ferrous **6c** formed a bis(DIm)-coordinated low-spin Fe^{II} complex under an N$_2$ atmosphere. Upon addition of O$_2$ to this solution, a kinetically stable O$_2$ adduct was formed at 37°C with a half-life of 17 h. Distinct gel-phase (liquid-crystal) transitions of the lipid-porphyrin membranes were clearly observed; the free base **6a** displayed a higher transition temperature (56°C) than the iron complex. Magnetic circular dichroism and infrared spectroscopic studies proved that molecular O$_2$ coordinates to the self-organized lipid-porphyrinatoiron(II) vesicles in aqueous media.

Introduction

It is of current interest to construct self-organized porphyrin assemblies by formation of noncovalent bonds (metal–ligand coordination, hydrogen bonding, and electrostatic attraction) to mimic the diverse biological reactivity of porphyrinoids in nature.[1, 2] Such vectorial binding forces have built highly complicated porphyrin architectures that are difficult to prepare by general organic synthetic procedures. However, most of them were prepared in organic solvents. If we are to reproduce the various biochemical reactions that rely on the natural porphyrins, aqueous systems are particularly important. Hence, over the past few decades substantial efforts have directed towards embedding synthetic model porphyrins in phospholipid vesicles;[3] ground-state or photoinduced electron transfer,[4, 5] dioxygen (O$_2$) transport,[6] selective oxidation reactions,[7] and ATP production[8] have been reported. Unfortunately, the locations of the porphyrin co-factors in these ensembles are not always accurate, because of the low guest-to-host molecular ratio. To counter this problem, porphyrin amphiphiles become attractive building blocks for constructing well-defined three-dimensional porphyrin assemblies in aqueous media. Coulombic forces were first successfully employed in the preparation of beautiful porphyrin fibers, but they are relatively unstable and tend to precipitate because of their low solubility.[9] We are now convinced that hydrophobic interaction is the most useful driving force for preparing large-scale supramolecular systems in which thousands of metalloporphyrins are aligned with great regularity and longevity. Indeed, some porphyrins with amphiphilic side chains at the periphery self-organize in water to form supramolecular aggregates (fibers, tubes, vesicles, and sheets).[10, 11] A tetraphenylporphyrin (TPP) derivative with four dialkylglycerophosphocholine groups on one side of the ring plane produced spherical unilamellar

[a] Prof. E. Tsuchida, Dr. T. Komatsu, M. Moritake, A. Nakagawa
Advanced Research Institute for Science and Engineering
Waseda University, Tokyo 169-8555 (Japan)
Fax: (+81) 3-3205-4740
E-mail: eishun@waseda.jp

vesicles with reversible O_2-binding ability, similar to those of hemoglobin and myoglobin under physiological conditions (pH 7.3, 37°C).[12] The only drawback of this compound is laborious introduction of the phospholipid substituents, in which a glycerol residue connects the two acyl chains. We recently found that the role of glycerol can be adopted by a similar triol, namely, trimethylolethane. To the best of our knowledge, there has been no report on a phospholipid amphiphile involving a trimethylolethane residue as the connecting moiety of the acyl chains, and its self-assembly behavior. Here we report the first synthesis of and bilayer membrane formation by novel TPP derivatives with four phospholipid substituents on the porphyrin ring (lipid-porphyrins): free base **6a**, Fe^{III} complex **6b**, and Fe^{II} complex **6c**. The nanostructure of the lipid-porphyrin aggregate was elucidated by transmission electron microscopy (TEM) and scanning force microscopy (SFM). Exciton calculations on the basis of our bilayer model reproduces well the bathochromic shift observed in the UV/Vis absorption of the **6a** membranes. The free-base lipid-porphyrin vesicles fluoresce strongly, and the vesicles of the Fe^{II} complex formed a stable and reversible O_2 adduct under physiological conditions, with an O_2-binding affinity similar to that of human erythrocytes. Magnetic circular dichroism (MCD) and infrared (IR) spectroscopic studies on the O_2 coordination mode have also been made.

6

M: 2H	a
Fe^{III}	b
Fe^{II}	c
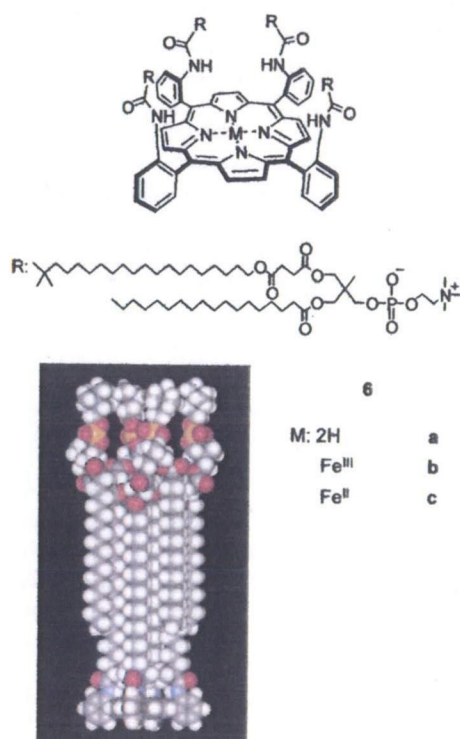
Results and Discussion

Synthesis: The synthesis of lipid-porphyrins is summarized in Scheme 1. The phospholipid precursor **3** is easily synthesized in three steps starting from trimethylolethane, whereas five
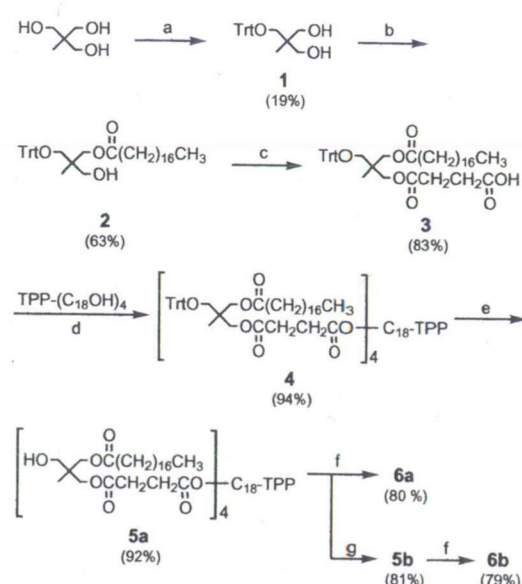
TPP-($C_{18}OH$)$_4$: 5,10,15,20-Tetrakis{α,α,α,α-o-(2,2-dimethyl-20-hydroxyicosanamido)phenyl}porphine

Scheme 1. Synthetic scheme for lipid-porphyrin **6a** and its iron(III) bromide complex **6c**. a) Trityl chloride/DMF, pyridine. b) Stearic acid anhydride, 4-DMAP/THF. c) Succinic acid anhydride/THF. d) DCC, 4-DMAP/CH_2Cl_2. e) $BF_3 \cdot Et_2O/CH_2Cl_2$. f) 2-chloro-1,3,2-dioxaphospholane 2-oxide/CH_2Cl_2, TEA. g) $FeBr_2$/THF, 2,6-lutidine. DCC = dicyclohexyl carbodiimide, 4-DMAP = 4-dimethylamino pyridine.

steps are required to obtain the corresponding material from glycerol. The coupling of **3** with the parent TPP derivative TPP-($C_{18}OH$)$_4$[13] was performed by dicyclohexyl carbodiimide (DCC) in DMF at room temperature to give **4a** in 94% yield. $BF_3 \cdot MeOH$ selectively cleaved the trityl protecting groups to yield **5a** (92%). The phosphocholine head groups were introduced in the final step by a general procedure with 2-chloro-1,3,2-dioxaphospholane 2-oxide. This is in contrast to our glycerol-based lipid-porphyrin, for which only mild, acidic phosphorylation could be used to introduce phosphocholine residues into the 3-hydroxyl group of glycerol.[12] As a result, the free-base lipid-porphyrin **6a** was synthesized in six steps by using the parent TPP-($C_{18}OH$)$_4$, whereas the glycerol analogue requires twelve steps, including zinc insertion at the porphyrin center and complicated reactions in low yields. The Fe^{III} complex **6b** was prepared from **5b** in the same manner as for **6a** from **5a**; all the compounds are available in gram quantities. The α^4 structure of the porphyrins did not atropisomerize throughout the entire process, as was confirmed by ^1H NMR spectroscopy: the chemical shift of the singlet for the 2,2-dimethyl groups ($\delta = -0.4$) remained constant. For the Fe^{III} complex **6b**, ^1H NMR spectra were recorded after removing the iron center with $FeCl_2$ in HCl/acetic acid.[14] The Satisfactory analytical data were obtained for all compounds described here (see Experimental Section).

Morphology and nanostructure of the free-base lipid-porphyrin assembly: The free-base lipid-porphyrin **6a** was dispersed in deionized water by ultrasonication ([**6a**] = 1 –

-34-

3000 μM) to give a red solution that was stable for a year without precipitation. The TEM of the negatively stained and evaporated sample revealed that **6a** forms perfectly spherical vesicles with a diameter of 100 nm (Figure 1a). The thickness
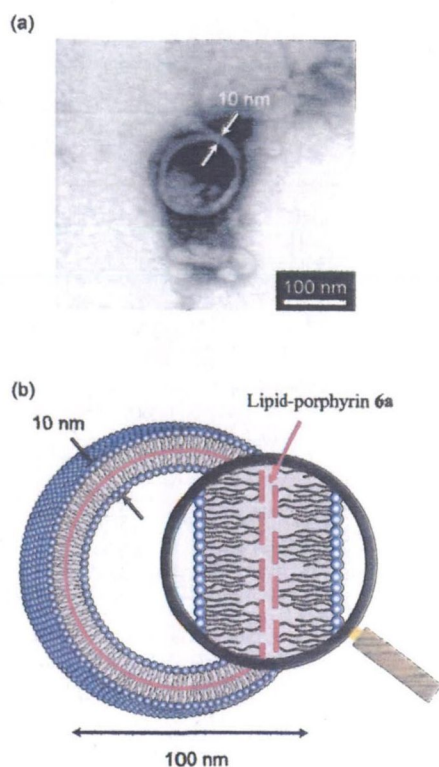
(a)

(b)

Figure 1. a) Transmission electron micrograph of a vesicle of the free-base lipid-porphyrin **6a** negatively stained with uranyl acetate. b) Schematic of the bilayer membrane.

of the unilamellar membrane was 10 nm, which corresponds to twice the length of the **6a** molecule (4.6 nm) (Figure 1b). Light-scattering measurements gave a sharp peak with a narrow distribution (100 ± 36 nm) and supported the TEM result. In general, ultrasonic irradiation of phospholipids provides small unilamellar vesicles. However, the spherical membrane consisting of the giant porphyrin amphiphile **6a** ($M = 4564$) cannot produce a large curvature; therefore, the vesicles are much larger than the usual ones. They neither coagulate nor photodegrade for a long time.

The visible absorption spectrum of the **6a** vesicles showed a porphyrin Soret band at 434 nm ($\varepsilon_{max} = 3.1 \times 10^5 \, M^{-1} cm^{-1}$), which was significantly shifted to the red region relative to that of the monomer in benzene/MeOH (4:1; $\lambda_{max} = 422$ nm; Figure 2). The bandwidth at half-height ($\Delta\lambda_{1/2} = 16$ nm) was slightly wider than that of the monomer ($\Delta\lambda_{1/2} = 14$ nm). The intensity and absorption maxima of the Q-bands demonstrated even smaller shifts of 3 nm, which may be a van der Waals shift caused by the replacement of solvent. Thus, the larger bathochromic shift of the Soret band (12 nm) should include some excitonic interactions owing to a lateral arrangement (J-aggregate) of the transition moments of the porphyrin
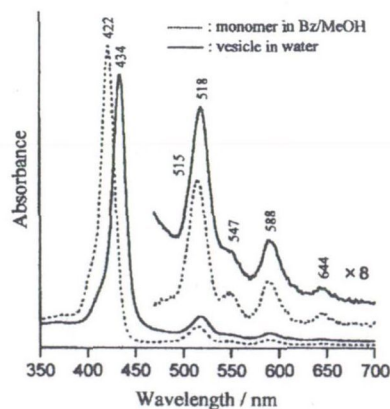

Figure 2. UV/Vis absorption spectra of lipid-porphyrin **6a** at 25 °C.

chromophores. Hence, we are certain that the hydrophobic TPP planes of **6a** form two-dimensional planar sheets in the vesicles, and stack at the middle of the bilayer membranes (Figure 1b). The quantitative evaluation of the excitonic interactions of these stacked porphyrin sheets are described below.

Surface pressure – molecular area ($\Pi - A$) isotherm and exciton calculation of the Langmuir-Blodgett (LB) film: The $\Pi - A$ isotherm of the giant porphyrin amphiphile **6a** exhibited essentially the same features as that of typical amphiphilic lipids (Figure 3).[15] At large areas
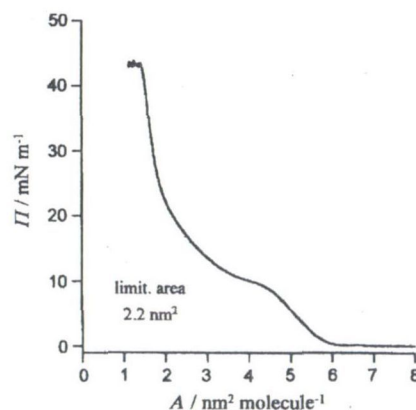
Figure 3. $\Pi - A$ isotherm of lipid-porphyrin **6a**. The subphase was pure water, and the film was compressed at a rate of 10 mN min^{-1}.

(>6.0 nm^2 molecule^{-1}) the film is in an expanded state. Upon compression, the film undergoes a transition from the expanded phase to the liquid expanded phase (4.5 nm^2 molecule^{-1}). Further compression led to the liquid-expanded/liquid-condensed transition (3.5 nm^2 molecule^{-1}), and finally to a solid condensed phase. The collapse pressure reached 43 mN m^{-1}, and this indicates formation of a relatively close packed solid membrane. Extrapolation of the second linear portion of the isotherm to zero surface pressure gave, as the intercept, the area per **6a** molecule. The value of 2.2 nm^2 coincides with the sum of the areas of four phosphocholine head groups, and we infer that the lipid-porphyrin in

——— 5471

the oriented layer is likely to have a cylindrical form with a TPP bottom of 1.5 nm² (see the space-filling model above). Based on this value, the number of constituent molecules of **6a** in one vesicle (100 nm Φ) was estimated to be 2.3×10^4 (1.4×10^4 in the outer phase and 9.0×10^3 in the inner phase).

The **6a** monolayer on the LB trough was then slowly transferred onto a glass plate to give a porphyrin monolayer in which the hydrophilic head groups likely face the glass surface, while the hydrophobic TPP plane is toward the air. Further immersion and removal of the substrate perpendicular to the trough should result in formation of trilayered LB films. Interestingly, the visible absorption spectra of these films provided good clues to the in-plane and interlayer arrangements of the TPP moieties in the **6a** vesicles. The monolayer showed distinct TPP absorption with sufficiently high intensity for spectroscopic analysis (Figure 4a). The Soret band at 430 nm is clearly red-shifted (8 nm) relative to that of the monomer in benzene/MeOH ($\lambda_{max} = 422$ nm). The absorption intensity of the **6a** trilayers is three times as high as that of the monolayer with a small bathochromic shift (2 nm) in the Soret band; the λ_{max} of the Q-bands were essentially unaltered. This observation suggested formation of triple-layer **6a** films on the glass plate. Here, it is of interest to subtract the spectrum of the monolayer from that of the trilayer, presumably to give the absorption of a bilayer in which the outer and inner TPP sheets are stacked at the center of the membrane (Figure 4b). In fact, the difference spectrum ($\lambda_{max} = 433$, $\Delta\lambda_{1/2} = 15$ nm) closely resembles that of the **6a** vesicles in bulk aqueous solution ($\lambda_{max} = 434$, $\Delta\lambda_{1/2} = 16$ nm, Figure 2), that is, the spherical **6a** vesicles and double-layered films on a solid substrate contain similar porphyrin arrangements.

Then we employed simple point-dipole exciton coupling theory to predict the porphyrin alignment in the LB mono- and bilayers.[16] First, for the **6a** monolayer film on the glass surface, we assumed that the tightest packing of the TPP moieties is realized by a rhomboidal lattice with diagonal distances of 2.6 nm for $2a$ and 1.48 nm for $2b$ (Figure 4c), as observed in the triclinic unit cell of a single crystal of unsolvated free-base TPP.[17] The head-group area of 2.2 nm² could be fitted on an individual porphyrin platform without overlap. This assumption was also made in our excitonic calculation on the monomolecular porphyrin platelets.[11h] The exciton interaction ΔE between two porphyrins is given by Equation (1):

$$\Delta E = M^2 r_{mn}^{-3}(1 - 3\cos^2\theta) \tag{1}$$

where M is the transition dipole moment of **6a**, r_{mn} is the center-to-center distance between the original porphyrin (P_o) and neighboring porphyrin (P_{mn}), and θ is the tilt angle between the line connecting the centers and the molecular axes. We took into account all the interactions with the infinite porphyrin neighbors on the 22 lines through the origin of the coordinate axes. The excitonic interaction ΔE is always considered as V_{mn} and V'_{mn} in two different Soret transitions S_x and S_y (see Experimental Section). With our **6a** monolayer model, the difference was very small. With $M^2 = 81.8 D^2$ for the dipole strength of the monomer, total V and V' were

calculated to be -519.9 and -515.4 cm⁻¹, respectively. The wavelength difference between the corresponding transitions is much smaller than the half-width of the Soret band of the monomer. Consequently, splitting of the Soret band could not
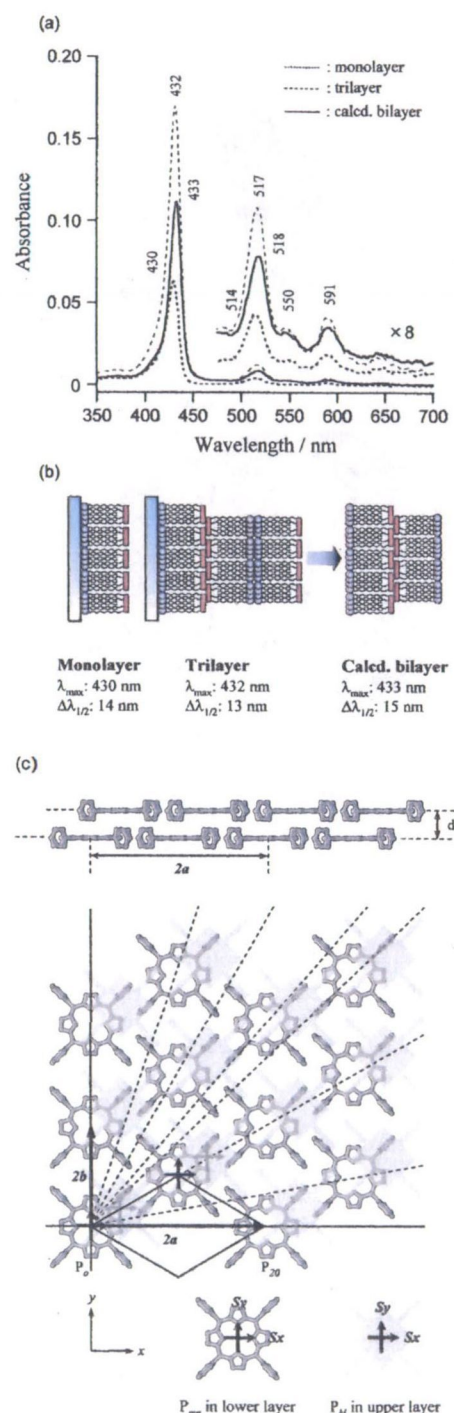

Figure 4. a) UV/Vis absorption spectra of LB films of lipid-porphyrin **6a** on a glass plate at 25 °C. b) Schematics of the mono-, tri-, and bilayers of lipid-porphyrin **6a** on the glass surface. c) Predicted arrangement of the porphyrin planes as a model for the bilayer membranes of lipid-porphyrin **6a**. The porphyrin P_o is located at the origin of the coordinate axes.

-36-

be expected, and the result was one exciton band, red-shifted by $517.7\ \text{cm}^{-1}$ with respect to the monomer. This calculated shift is almost identical to the observed value of the **6a** monolayer (only $76.8\ \text{cm}^{-1}$ larger). A van der Waals shift, which occurs on going from solution to a dense-packed LB film, was not seen. The real lattice of the LB monolayer might be slightly different from our model, because of the direct contact between the phosphocholine head groups and the solid glass surface. The use of an extended transition dipole instead of the point dipole also gave nearly the same results.[18, 19]

To predict the absorption of the bilayer, we made the additional hypothesis that the interlayer TPP arrangements are also similar to those found in crystals of free-base TPP. Based on the structural data reported by Strauce et al., two postulates are made: 1) a slipped face-to-face stacking of the porphyrin sheets with a minimum spacing d of $4.1\ \text{Å}$ (Figure 4c),[17] and 2) a porphyrin core in the upper layer is shifted by $+4.0$, $+2.7$, and $+4.1\ \text{Å}$ in the x, y, and z directions, respectively, from the center of the nearest core in the layer below. The distances and angles from the porphyrin P_o to the neighbors in the upper layer were estimated. Then we calculated all the interactions of these porphyrin pairs (total of 46 combinations), but stopped summation at a distance of some $5\ \text{nm}$. The difference was relatively wide in this calculation: -805.9 and $323.8\ \text{cm}^{-1}$ for S_x and S_y, respectively. If this is true, the Soret bands should be split or blue-shifted with significant broadening. However, the reverse was the case; only a $3\ \text{nm}$ bathocromic shift from the monolayer and still narrow bandwidth were observed. In our structural model, the most unreliable parameter is the layer spacing d. For a slightly larger value of $d = 6.0\ \text{Å}$ the difference decreased (-152.0 and $268.2\ \text{cm}^{-1}$ for the x and y directions). This means a rather small shift from λ_{max} of the monolayer, and is in good agreement with the fact that the absorptions of the monolayer and the bilayer are quite similar (Figure 4a). Since the spherical **6a** vesicles in bulk aqueous solution showed a spectrum similar to that of the double-layered LB films of **6a** on the glass plate, we can conclude that they are both describable by equivalent exciton interactions. The small wavelength difference between the predicted λ_{max} in our model ($431\ \text{nm}$) and experimentally obtained values ($\lambda_{\text{max}} = 433\ \text{nm}$ on the glass surface and $434\ \text{nm}$ in water) is likely due to the van der Waals shift. In this case, the head group–glass contact effect, which was considered in the monolayer, can be ignored, since the stacking of the second porphyrin layer probably weakens it. Of course, the porphyrin lattice in the bilayers is somewhat flexible, because of the fluidity of the membrane, despite its being below the phase transition temperature (vide infra); therefore, the observed shift in the Soret band always comes from the averaged exciton interaction.

Photophysical properties of free-base lipid-porphyrin vesicles:
The most remarkable photophysical property of the aqueous solution of **6a** vesicles is to fluoresce strongly; its fluorescence emission intensity was 76% of that of the monomer in benzene/MeOH (4:1; Figure 5). The three-dimensional excitation–emission spectrum revealed that the

fluorescence emission maxima ($\lambda_{\text{em}} = 649$, $713\ \text{nm}$) correlates with the Soret band absorption of the vesicles ($\lambda_{\text{max}} = 434\ \text{nm}$), which indicates that the strong fluorescence is due to the membrane, and not to a small amount of monomer dissociated from the aggregates. Thus, the lifetime of the excited
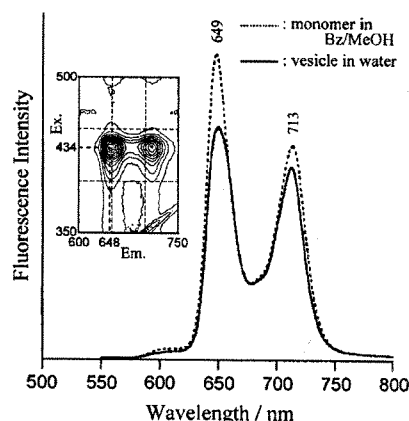

Figure 5. Fluorescence emission spectra of lipid-porphyrin **6a** (1.7 μM) at 25 °C (excitation at 428 nm). The inset shows emission–excitation correlation image.

singlet state of the vesicles ($\tau_F = 6.8\ \text{ns}$) was not dramatically different from that of the monomers ($\tau_F = 10\ \text{ns}$).

Laser flash photolysis experiments were carried out with nanosecond laser excitations. The transient absorption spectrum of the **6a** monomer in benzene/MeOH after laser flash illumination displayed the typical triplet–triplet (TT) absorption of TPP, in which the dark decay obeyed first-order kinetics (triplet lifetime $\tau_T = 2.0\ \text{ms}$) and is strongly accelerated by the presence of O_2 (Figure 6). Excitation of the **6a**
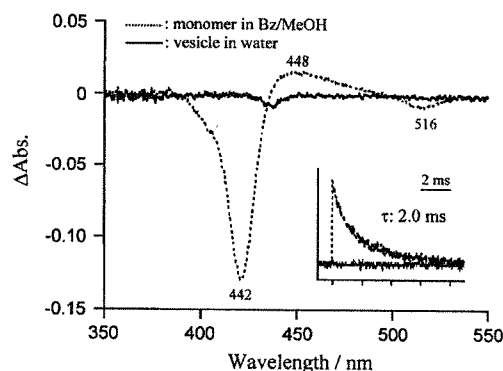
Figure 6. Transission–absorption differential spectra of lipid-porphyrin **6a** in solution 50 ns after laser-flash photolysis (excitation at 516 nm) under an Ar atmosphere ([**6a**] = 1.7 μM). The inset shows the absorption decay at 450 nm.

bilayer vesicles, on the other hand, gave small-magnitude signals with a lifetime that was too small to observe with our nanosecond instrumentation. If internal conversion is the only process influenced by self-assembly, the triplet state would be quenched to the same extent as the fluorescence, but this was not seen. These observations on the excited singlet and triplet

states of the **6a** vesicles are almost the same as those on monolayered porphyrin platelets, which consist of laterally aligned porphyrins.[11h] Whitten et al. also reported a significant decrease in τ_T for 5,10,15,20-tetrakis(α^4-hexanamidophenyl)porphyrin J-aggregates in the presence of a small amount of surfactant in water.[20] There are two possible interpretations for the reduction of the triplet yield: 1) a decrease in the rate constant of intersystem crossing k_{isc}, and 2) an increase in the rate constant of triplet deactivation k_o. Based on our previous calculation for a similar porphyrin assembly,[11h] we can predict that the triplet lifetime of the **6a** vesicles may decrease by some 2 ns. The extremely short-lived triplet state of the lipid-porphyrin vesicles could be further evaluated using a picosecond laser flash apparatus.

Nanostructure of lipid-porphyrinatoiron assembly: The iron (III) complex of lipid-porphyrin **6b** also self-organizes in water to form spherical unilamellar vesicles with a diameter of 100 nm. The presence of a small excess of 1-dodecylimidazole (DIm, DIm/**6b** = 2.2 – 3.4 mol mol^{-1}) as an axial base did not hinder vesicle formation. The TEM of the evaporated **6b**/DIm solution on the copper grid showed an identical membrane with a thickness of 10 nm, which again corresponds to twice the length of the molecule (Figure 7). Light-scattering measurements gave a main diameter peak at 97 nm with a distribution of ±73 nm. The visible absorption spectrum (λ_{max} = 421, 570 nm) suggested the formation of a six-coordinate low-spin iron(III) complex with DIm ligands on both axial sites.

The aqueous **6b**/DIm was then transferred to highly oriented pyrolytic graphite (HOPG) and subjected to SFM under ambient conditions. The collapsed vesicles became detectable; they are obviously images of flattened **6b**/DIm assemblies on the graphite surface (Figure 7b). The thickness measured from the height profile of the evaporated vesicle was 19.5 nm (vertical distance a–a in Figure 7b), which corresponds to twice the thickness of the bilayer membrane. For evaluation of the lateral size, we should normally consider the horizontal broadening effect due to the shape of the tip, but this is not necessary for the vertical distance.[21] We can therefore conclude that the iron complex with DIm produces bilayer vesicle membranes, like free-base **6a**.

O$_2$ coordination to lipid-porphyrinatoiron(II) vesicles: The UV/Vis absorption spectrum of a phosphate buffer solution of the Fe^{II} **6c**/DIm vesicles revealed the presence a typical six-coordinate low-spin Fe^{II} species (λ_{max} = 436, 538, 568 nm) (Figure 8).[22] The TEM of the solution again exhibited spherical unilamellar vesicles with a wall of bilayer thickness (10 nm, not shown). Upon exposure of these vesicles to O$_2$ gas, the absorption spectrum immediately changed to that of an O$_2$ adduct (λ_{max} = 435, 543 nm). This dioxygen complex was kinetically stable in the wide range of 5 – 50 °C, depending on the O$_2$ partial pressure. Reversion of the O$_2$ adduct to the bis(DIm)-ligated species on bubbling N$_2$ gas was observed, that is, the dissociated DIm remains in the membrane interior during the dioxygenation and rebinds rapidly to the iron center after deoxygenation. The constant morphology of the vesicle throughout the reversible O$_2$ coordination cycle was
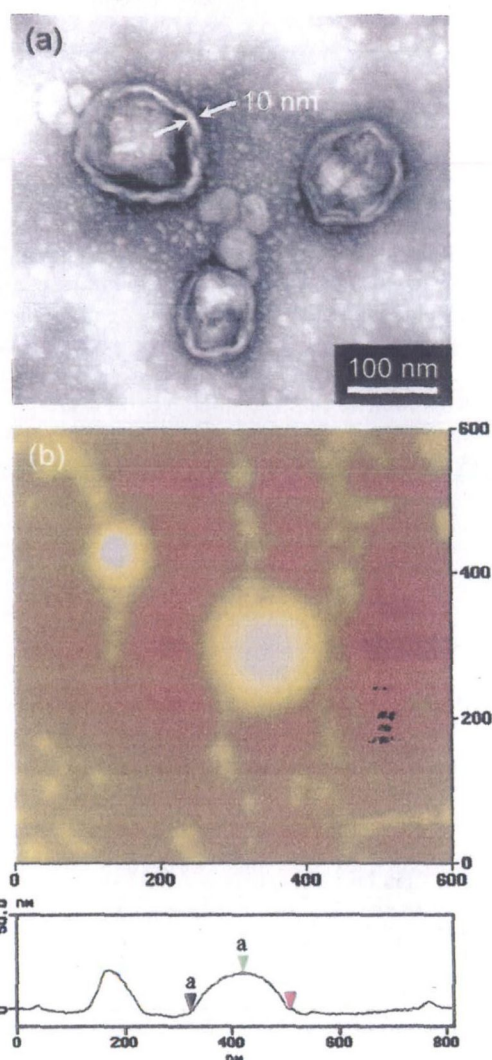
Figure 7. a) Transmission electron micrograph of vesicles of the lipid-porphyrinatoiron(III) complex **6b**/DIm negatively stained with uranyl acetate. b) SFM images (tapping mode) of the evaporated sample of **6b**/DIm vesicles on HOPG. Image size is 600×600 nm (z range: 50 nm), and its cursor profile 19.5 nm (vertical distance a–a).

Figure 8. Visible absorption spectral changes for vesicles of the lipid-porphyrinatoiron(II) complex **6c**/DIm in phosphate buffer solution (pH 7.3) at 25 °C.

-38-

confirmed by TEM. Bubbling carbon monoxide into this solution gave the more stable carbonyl complex ($\lambda_{max} = 433$, 545 nm).

Oxidation to the Fe^{III} species was very slow; the half-life of the O_2 adduct was 17 h at 37 °C. The relationship between the O_2 binding ratio and O_2 pressure, that is, the $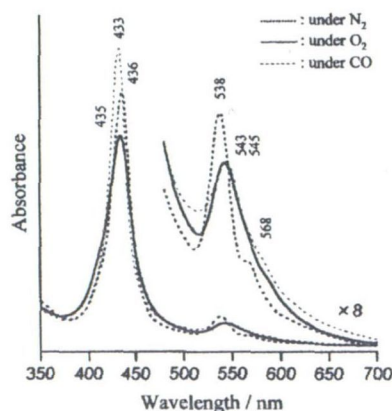O_2$ equilibrium curve, was plotted on the basis of the UV/Vis absorption spectral changes on O_2 titration (Figure 9). The apparent O_2 binding affinity [$P_{1/2}$ is the gas pressure at half O_2 coordination of porphyrinatoiron(II)] of the 6c/DIm vesicles was determined to be 30 Torr at 37 °C, a value similar to that of human erythrocytes.[23] Although the O_2-binding profile did not show any cooperativity like that seen in hemoglobin, their O_2-transporting efficiency between the lungs ($P_{O_2} = 110$ Torr) and muscle tissue ($P_{O_2} = 40$ Torr) is 20 %, which is nearly the same value (22 %) as that of human erythrocytes.
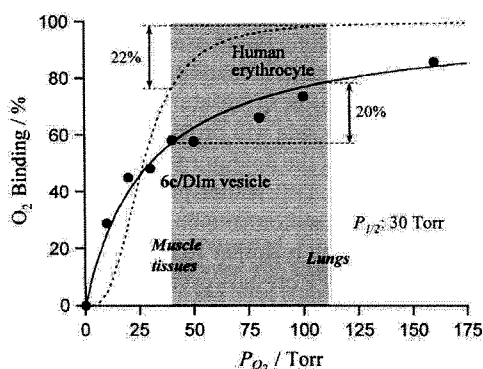

Figure 9. O_2 equibllium curve of vesicles of the lipid-porphyrinatoiron(II) complex 6c/DIm in phosphate buffer solution (pH 7.3) at 37 °C.

Differential scanning calorimetry (DSC): The thermal behavior of the lipid-porphyrin bilayer membranes was studied by DSC. Three samples, 6a, 6b, and 6b/DIm vesicles, demonstrated gel-phase (liquid-crystal) transitions (Table 1). Free

Table 1. Phase transition temperatures of the lipid-porphyrin vesicles and their thermodynamic parameters.

System	T_c [°C]	ΔH [kcal mol^{-1}]	ΔS [cal mol^{-1}deg^{-1}][a]	ΔS_{CH_2} [cal mol^{-1}deg^{-1}]
6a	56	4.1	73.2	0.54
6b	49	3.7	75.5	0.56
6b/DIm	40	1.5	29.4	–
DPPC[b]	41	8.6	27.3	0.90

[a] $\Delta S = \Delta H T_c^{-1}$. [b] DPPC = 1,2-diparmytoyl-sn-glycero-3-phosphatidyl-choline.[24]

base 6a showed a relatively sharp transition at 56 °C with an enthalpy change ΔH of 4.1 kcal mol^{-1}; this suggests that the long acyl chains on the porphyrin are responsible for formation of close-packed layers. We are certain that the trimethylolethane residue in the lipid group plays the same role as a glycerol residue. It is remarkable that the ferric complex 6b had a lower phase-transition temperature T_c of 49 °C. This decrease may result from the different geometric alignments of the TPP planes in the membrane. As described above, free-base TPP forms triclinic crystals in which each

porphyrin array shows a parallel arrangement of the nearest neighbor phenyl groups and a constant repeat distance. The stacking of all the phenyl rings is expected to provide some lattice stabilization. By contrast, the Fe^{III} – TPP complex aligns in a random conformation.[17] The porphyrin moieties in the 6a bilayer are presumably oriented in a fashion similar to that in the free-base TPP crystal, which may afford additional stabilization to the membrane packing. Indeed, the temperature dependence of the absorption spectrum of the 6a vesicles showed a small hypsochromic shift with broadening and a decrease in intensity at T_c (56 °C; Figure 10). This was observed only for the free-base 6a porphyrin vesicles, and not for the iron complex.
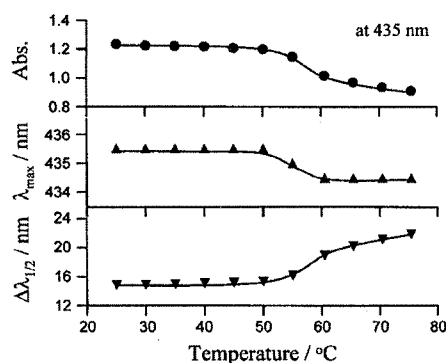

Figure 10. Temperature dependence of the Soret band absorption λ_{max} and half-width $\Delta\lambda_{1/2}$ of vesicles of the lipid-porphyrin 6a in water.

Although the lipid-porphyrin vesicles have distinct phase transitions, their low ΔH values mean the alkyl chains are less dense than those of a 1,2-diparmytoyl-sn-glycero-3-phosphatidylcholine (DPPC) membrane. The increased amount of entropy per methylene unit (ΔS_{CH_2}), which is often used to evaluate the molecular packing (0.90 for DPPC),[24] was also low (0.54 and 0.56 for the 6a and 6b vesicles, respectively). The thermotropic characteristics of the iron-complex vesicles were further altered by addition of DIm, which resulted in a significant decrease in T_c and a drop of 2.2 kcal mol^{-1} in the enthalpy change of the transition.

Magnetic circular dichroism (MCD) and IR spectroscopy: For porphyrins and hemoproteins, MCD is a sensitive probe for oxidation state, spin state, and axial ligation of the metal center. It has been therefore used as a fingerprint for the coordination structure of various model hemes.[25] We applied the MCD and IR spectroscopy to characterize the O_2 adduct of the self-organized 6c/DIm vesicles. Under an N_2 atmosphere, the MCD showed a well-characterized spectrum of bis(imidazole)-ligated six-coordinate low-spin Fe^{II} porphyrin, which differs strongly to that of a five-coordinate high-spin complex with mono-imidazole ligation (Figure 11). This observation indicates that axial coordination is not affected by the dense packing of the four phospholipid groups on the porphyrin plane. Admission of O_2 gas yields the six-coordinate 6c/DIm(O_2) complex, which shows an S-shaped A-term MCD in the Soret region, as observed in the spectra of other dioxygenated Fe^{II}TPP derivatives.[25] The CO adduct is also
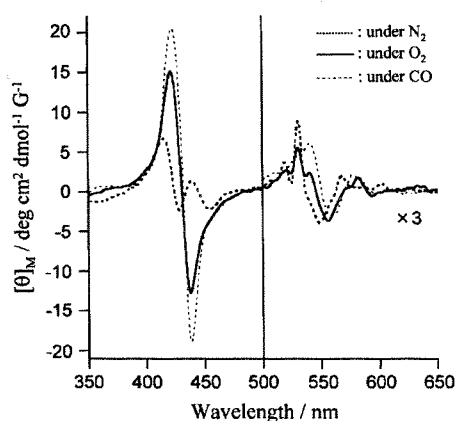
Figure 11. MCD spectra of vesicles of the lipid-porphyrinatoiron(II) complex 6c/DIm in phosphate buffer solution (pH 7.3) at 25 °C.

low-spin and is expected to show a similar A-term MCD band with strong intensity; such a band was actually observed. In all cases, the complicated pattern in the Q-band regions coincided well with those previously reported (Table 2).[25]

Table 2. Absorption maxima of MCD spectra of the 6c/DIm vesicles in phosphate buffer solution (pH 7.3) at 25 °C.

Atmosphere	MCD λ_{max} [nm]
N_2	416(+), 429(−), 439(+), 454(−), 519(+)
	531(+), 537(−), 549(−), 568(+), 574(−)
O_2	421(+), 438(−), 531(+), 541(+)
	555(−), 572(+), 581(+), 593(−)
CO	422(+), 438(−), 538(+), 543(+)
	557(−), 578(+), 545(−)

Difference IR spectra in solution of 6c/DIm vesicles for CO versus $^{16}O_2$ complexes displayed a distinct positive band at the stretching frequency of coordinated CO at 1969 cm^{-1} (Table 3). In the spectrum for the $^{16}O_2$ versus the $^{18}O_2$ adduct, we

Table 3. IR spectral data of vesicles of the lipid-porphyrinatoiron(II) complex 6c/DIm in phosphate buffer solution (pH 7.3) at 25 °C.

System	$\nu(^{16}O-^{16}O)$	$\nu(^{18}O-^{18}O)$	$\nu(^{12}C-^{16}O)$
6c/DIm vesicles	1155	1081	1969
FeT$_{piv}$PP/MIm[a]	1159	1075	1969
hemoglobin[27]	1107	1065	1951
O_2 or CO gas	1556	–	2143
O_2^-	1145	–	–

[a] FeT$_{piv}$PP/MIm = 5,10,15,20-Tetrakis($\alpha,\alpha,\alpha,\alpha$-o-pivalamidophenyl)porphyrinatoiron(II) – 1-methylimidazole complex.[26]

observed the appearance of a positive band at 1155 cm^{-1} and a negative peak at 1081 cm^{-1}, both of which correspond to the stretching frequencies of the coordinated O_2 molecules. The frequency shifts between $^{16}O_2$ and $^{18}O_2$ adducts (74 cm^{-1}) is in good agreement with the value calculated from the harmonic-oscillator prediction of the O–O stretching vibration. Their ν(O–O) bands are close to not only those of ionic superoxides, but also to those of the bent end-on O_2 bound to other synthetic Fe^{II}TPP systems in benzene or Nujol.[26] On the basis

of these findings, we conclude that the self-organized 6c bilayer vesicles coordinate molecular O_2 like hemoglobin and model hemes,[26, 27] without any hinderance by aggregation.

Conclusion

The synthesized lipid-porphyrins are giant porphyrin amphiphiles with the ability to form perfectly round bilayer vesicles in aqueous solution. The glycerol in the phospholipids can be replaced by trimethylolethane. Indeed, phospholipids in which trimethylolethane residues links diparmytoyl chains and phosphocholine head group assemble in water to give unilamellar vesicles similar to those formed by DPPC.[28] The advantages of the trimethylolethane-based approach are: 1) the synthetic procedures to connect the acyl chains are easier than with glycerol, as shown in this work; and 2) the two acyl groups are bound in a symmetric form, which is not realized in natural lecithin.[29] This could give parallel geometric arrays of alkyl chains in membrane layers. For instance, for radical polymerization of unsaturated lipids, the double bonds oriented side by side will provide high polymerization yields. In the interior of the lipid-porphyrin vesicle, two sheets made of J-aggregated TPP planes presumably stack with a lateral displacement. Exciton coupling theory confirmed our predicted models, which is similar to that seen in the triclinic unit cell of free-base TPP crystals, except for the slightly wider interlayer distance (ca. 6.0 Å), and it reproduced the Soret band bathochromic shifts in the visible absorption of the 6a vesicles. The free-base lipid-porphyrin bilayers form a strongly fluorescent aggregate, but show an extraordinarily short triplet lifetime. We consider that this unique photophysical behavior is due to the edge-to-edge alignment of the porphyrin platforms. Furthermore, the N-coordinated high-spin Fe^{II} complex 6c/DIm membranes can bind one equivalent of O_2 molecules. An aqueous solution of the 6c/DIm vesicles with high concentration (>mM) is an entirely synthetic O_2 carrier that could act as a substitute for red blood cells. These bilayer membranes possess a spherical architecture consisting of 23000 porphyrins in water, and are a new class of a supramolecular assembly that can realize important biological reactions of porphyrinoids in nature: not only O_2 transport, but also metabolic oxidation and photo-induced electron or energy transfer. In particular, there has been substantial recent interest in the construction of cyclic multiporphyrin assemblies, since a wheel-shaped bacterio-chlorophyll circuit has been found in a light-harvesting antenna complex.[30] More recently, we have prepared multicomponent vesicles made of differently metalated lipid-porphyrins, in which efficient energy transfer due to the tightest packing of the chromophores is observed. A new investigation of the photoinduced electronic communication in the lipid-porphyrin architecture is underway.

Experimental Section

Materials and apparatus: All commercially available reagents of high-purity grades were used without further purification, unless otherwise

stated. Solvents were normally purified by distillation before use. Dichloromethane was refluxed over and distilled from P_2O_5. Tetrahydrofuran was refluxed over and distilled from sodium wire. Water was deionized by using an ADVANTEC GS-200 system. Thin-layer chromatography (TLC) was carried out on 0.2 mm precoated plates of silica gel 60 F_{254} (Merck). Purification was performed by column chromatography on silica gel (Merck, Keiselgel 60, Art 7736) or Sephadex LH-60 gel (Amersham Pharmacia Biotech). Infrared spectra were recorded on a JASCO FT/IR-410 spectrometer. ^{1}H NMR spectra were measured on a JEOL Lambda 500 spectrometer (500 MHz), and chemical shifts are expressed in parts per million downfield from Me_4Si as internal standard. FAB-MS spectra were obtained on a JEOL JMS-SX102A spectrometer. Elemental analysis was performed on a Yanagimoto MT3 CHN corder. UV/Vis absorption spectra were recorded on a JASCO V-570 spectrophotometer, and steady-state fluorescence spectra on a HITACHI F-4500 spectrofluorometer. Magnetic circular dichroism spectra were obtained on a JASCO J-820 spectropolarimeter. Light-scattering measurements were performed on a COULT-ER Model N4SD. All these measurements were normally carried out at 25 °C. 5,10,15,20-Tetrakis[$\alpha,\alpha,\alpha,\alpha$-$o$-(2,2-dimethyl-20-hydroxyicosanamido)phenyl]porphine [TPP-($C_{18}OH$)$_4$] and 2-chloro-1,3,2-dioxaphospholane 2-oxide were prepared according to the previously reported procedures.[13]

2,2-Bis(hydroxymethyl)-1-trityloxypropane (1): A solution of trityl chloride (13 g, 46.6 mmol) in dry DMF (150 mL) was added dropwise over about 90 min to a solution of 2-hydroxymethyl-2-methyl-1,3-propanediol (6.0 g, 50 mmol) and pyridine (8.4 mL) in dry DMF (24 mL) at 85 °C under an N_2 atmosphere. Then the mixture was stirred for a further 3 h at 95 °C. The DMF and pyridine were removed in vacuo, and the residue was extracted with $CHCl_3$ and washed with water. The organic layer was dried over anhydrous Na_2SO_4 and the solvent was evaporated. Excess methanol was then poured into the mixture, and the resulting precipitate was filtered off. The mother liquor was again evaporated. The product was separated by column chromatography on silica gel with $CHCl_3$/MeOH (10:1) as eluent. The major band was collected and dried at room temperature for several hours in vacuo to give compound **1** as a viscous solid (3.37 g, 19 %). $R_f =$ 0.40 ($CHCl_3$/MeOH, 10:1); IR (NaCl): $\tilde{v} = 1154$ (COC, ether), 3390 cm^{-1} (OH, alcohol); ^{1}H NMR (500 MHz, CDCl$_3$, 25 °C, TMS): $\delta = 0.9$ (s, 3H; CH$_3$), 3.0 (s, 2H; CH_2OTri), 3.5 (s, 4H; CH_2OH), 7.2–7.4 ppm (m, 15H; Tri). MS: m/z calcd for $C_{24}H_{26}O_3$: 362.19; found: 362.26 [M^+].

2-Hydroxymethyl-2-octadecanoyloxymethyl-1-trityloxypropane (2): Compound **1** (3.37g, 9.30 mmol), stearic acid anhydride (5.12 g, 9.30 mmol), and 4-DMAP (568 mg, 4.65 mmol) were dissolved in dry THF (100 mL), and the solution was refluxed for 12 h under an N_2 atmosphere. After evaporation of the solvent, excess methanol was added, and a white precipitate was removed. The mother liquor was evaporated and the resulting mixture was separated by column chromatography on silica gel with $CHCl_3$/Et$_2$O (30:1) as eluent. The major band was collected and dried at room temperature for several hours in vacuo to give compound **2** as a viscous liquid (3.67 g, 63 %). $R_f = 0.50$ ($CHCl_3$/Et$_2$O, 30:1); IR (NaCl): $\tilde{v} =$ 1176 (COC, ether), 1737 (C=O, ester), 3490 cm^{-1} (OH, alcohol); ^{1}H NMR (500 MHz, CDCl$_3$, 25 °C, TMS): $\delta = 0.8$ (t, 3H; (CH$_2$)$_{16}$CH_3), 0.9 (s, 3H; CH$_3$), 1.3 (s, 28H; (CH_2)$_{14}$CH$_3$), 1.6 (m, 2H; C(=O)CH$_2$CH_2), 2.3 (t, 2H; C(=O)CH_2), 3.1(q, 2H; CH_2OTri), 3.5 (q, 2H; CH_2OH), 4.2 (q, 2H; CH_2OC(=O)), 7.2–7.5 ppm (m, 15H; Tri). MS: m/z calcd for $C_{42}H_{60}O_4$: 628.45; found: 627.5 [M^+ − H].

2-(3-Carboxypropanoyloxy)methyl-2-octadecanoyloxymethyl-1-trityloxypropane (3): A solution of **2** (3.67 g, 5.85 mmol), succinic acid anhydride (4.09 g, 40.9 mmol), and 4-DMAP (1.43 g, 11.7 mmol) in dry THF (170 mL) was refluxed for 12 h under an N_2 atmosphere. The resulting mixture was brought to dryness on a rotary evaporator and extracted with $CHCl_3$. The organic layer was washed with water and dried over anhydrous Na_2SO_4. The solvent was then evaporated, and the residue was separated by column chromatography on silica gel with $CHCl_3$/MeOH (20:1) as eluent. The major band was collected and dried at room temperature for several hours in vacuo to give compound **3** as a white solid (3.42 g, 83 %). $R_f = 0.45$ ($CHCl_3$/MeOH, 20:1); IR (NaCl): $\tilde{v} = 1160$ (COC, ether), 1714 (C=O, carboxyl), 1741 cm^{-1} (C=O, ester); ^{1}H NMR (500 MHz, CDCl$_3$, 25 °C, TMS): $\delta = 0.9$ (t, 3H; (CH$_2$)$_{16}$CH_3), 1.0 (s, 3H; CH$_3$), 1.3 (s, 28H; (CH_2)$_{14}$CH$_3$), 1.6 (m, 2H; C(=O)CH$_2$CH_2(CH$_2$)$_{14}$), 2.2 (t, 2H; OC(=O)CH_2(CH$_2$)$_{15}$), 2.6 (m, 4H; (CH_2)$_2$COOH), 3.1 (s, 2H; CH_2OTri), 4.2 (d, 4H; CH_2OC(=O)), 7.3–7.5 ppm (m, 15H; Tri). MS: m/z calcd for $C_{46}H_{64}O_7$: 728.47; found: 751.53 [M^++Na].

5,10,15,20-Tetrakis{$\alpha,\alpha,\alpha,\alpha$-$o$-{20-[3-(2-octadecanoyloxymethyl-2-trityloxymethylpropanoxycarbonyl)propanoyloxy]-2,2-dimethylicosanamido}phenyl}porphine (4): TPP-($C_{18}OH$)$_4$[13] (607 mg, 0.299 mmol) was added to a solution of **3** (2.4 g, 1.19 mol), DCC (676 mg, 3.27 mmol), and 4-DMAP (182 mg, 0.3 mmol) in dry CH_2Cl_2 (25 mL). The mixture was stirred for 20 h at room temperature in darkness. After evaporation of CH_2Cl_2, the residue was redissolved in benzene, and the undissolved white DC urea was removed by filtration. The mother liquor was brought to dryness on a rotary evaporator. Then a $CHCl_3$ solution of the obtained porphyrin was added dropwise to excess MeOH to give a purple precipitate. The filtered crude porphyrin was finally purified by column chromatography on silica gel with $CHCl_3$/Et$_2$O (30:1) as eluent. The main band was collected and dried at room temperature for several hours in vacuo to give compound **4** as a purple solid (1.36 g, 94 %). $R_f = 0.50$ ($CHCl_3$/Et$_2$O, 30:1); IR (NaCl): $\tilde{v} =$ 1156 (COC, ether), 1692 (C=O, amide), 1739 (C=O, ester), 3437 cm^{-1} (NH, amide); UV/Vis (CHCl$_3$): $\lambda_{max} = 419$, 513, 545, 587, 642 nm; ^{1}H NMR (500 MHz, CDCl$_3$, 25 °C, TMS): $\delta = -2.6$ (s, 2H; inner H), −0.2 (s, 24H; 2,2-dimethyl), 0.8 (t, 12H; (CH$_2$)$_{16}$CH_3), 1.0 (s, 12H; CH$_3$), 1.0–1.3 (m, 112H; (CH_2)$_{14}$CH$_3$, 128H; (CH_2)$_{16}$), 1.5 (m, 8H; OC(=O)CH$_2$CH_2(CH$_2$)$_{14}$, 8H; CH_2CH$_2$OC(=O)), 2.2 (t, 8H; OC(=O)CH_2(CH$_2$)$_{14}$), 2.5 (s, 16H; OC(=O)(CH_2)$_2$C(=O)O), 3.0 (m, 8H; CH_2OTri), 4.0 (m, 16H; C(CH_2OC(=O))$_2$, 8H; CH_2OC(=O)(CH$_2$)$_2$), 7.1 (s, 4H; amide), 7.2–7.3 (m, 60H; Tri), 7.4 (t, 4H; Ph H4), 7.7 (t, 8H; Ph H5), 7.8 (d, 4H; phenyl H3), 8.7 (d, 4H; Ph H6), 8.8 ppm (s, 8H; pyrrole).

5,10,15,20-Tetrakis{$\alpha,\alpha,\alpha,\alpha$-$o$-{20-[3-(2-octadecanoyloxymethyl-2-hydroxymethylpropanoxycarbonyl)propanoyloxy]-2,2-dimethylicosanamido}phenyl}porphine (5a): Boron trifluoride methanol complex (0.85 mL, 1.64 mmol) was added to a solution of **4** (1.33 g, 0.273 mmol) in dry CH_2Cl_2 (60 mL). After stirring for 4 h at room temperature, the green solution was carefully poured into ice/water to stop the reaction, and the mixture extracted with $CHCl_3$. The organic layer was dried over anhydrous Na_2SO_4 and evaporated. Then a $CHCl_3$ solution of the residue was added dropwise to the excess MeOH to precipitate the porphyrin. The filtered crude product was purified by column chromatography on silica gel with $CHCl_3$/MeOH (20:1) as eluent. The major fraction was collected and dried at room temperature for several hours in vacuo to give compound **5a** as a purple solid (1.07 g, 92 %). $R_f = 0.3–0.4$ ($CHCl_3$/MeOH, 20:1); IR (NaCl): $\tilde{v} =$ 1691 (C=O, amide), 1738 (C=O, ester), 3436 (NH, amide), 3502 cm^{-1} (OH, alcohol); UV/Vis (CHCl$_3$): $\lambda_{max} = 419$, 513, 545, 587, 642 nm; ^{1}H NMR (500 MHz, CDCl$_3$, 25 °C, TMS): $\delta = -2.6$ (s, 2H; inner H), −0.2 (s, 24H; 2,2-dimethyl), 0.8 (t, 12H; (CH$_2$)$_{16}$CH_3), 1.0 (s, 12H; CH$_3$), 1.0–1.3 (m, 112H; (CH_2)$_{14}$CH$_3$, 128H; (CH_2)$_{16}$), 1.7 (m, 8H; OC(=O)CH$_2$CH_2(CH$_2$)$_{14}$, 8H; CH_2CH$_2$OC(=O)), 2.3 (t, 8H; OC(=O)CH_2(CH$_2$)$_{14}$), 2.6 (s, 16H; OC(=O)(CH_2)$_2$C(=O)O), 3.4 (d, 8H; CH_2OH), 4.1 (m, 16H; C(CH_2OC(=O))$_2$, 8H; CH_2OC(=O)(CH$_2$)$_2$), 7.1 (s, 4H; amide), 7.5 (t, 4H; Ph H4), 7.8 (t, 8H; Ph H5), 7.9 (d, 4H; Ph H3), 8.7 (d, 4H; Ph H6), 8.8 ppm (s, 8H; pyrrole); elemental analysis calcd (%) for $C_{240}H_{394}N_8O_{32} \cdot C_6H_6$ (3981.9): C 74.20, H 10.12, N 2.81; found: C 74.34, H 9.72, N 2.71.

Iron complex of 5a (5b): A solution of **5a** (296 mg, 75.9 μmol) and 2,6-lutidine (62.5 μL) in dry THF (40 mL) was added dropwise to anhydrous FeBr$_2$ (0.7 g) under dry N_2. The mixture was refluxed for 2 h under an N_2 atmosphere. The resulting solution was brought to dryness, and the residue was extracted with $CHCl_3$ and washed with water. After drying over anhydrous Na_2SO_4, the organic layer was evaporated, and the crude compound was separated by column chromatography on silica gel with $CHCl_3$/MeOH (20:1) as eluent. The major band was collected and dried at room temperature for several hours in vacuo to give compound **5b** as dark purple solid (249 mg, 81 %). $R_f = 0.2–0.3$ ($CHCl_3$/MeOH, 20:1); IR (NaCl): $\tilde{v} = 1692$ (C=O, amide), 1737 (C=O, ester), 3433 (NH, amide), 3460 cm^{-1} (OH, alcohol); UV/Vis (CHCl$_3$): $\lambda_{max} = 357$, 417, 506, 577, 644, 683 nm.

5,10,15,20-Tetrakis{$\alpha,\alpha,\alpha,\alpha$-$o$-{20-[3-(2-octadecanoyloxymethyl-2-trimethylammonioethoxyphosphonatoxymethylpropanoxycarbonyl)propanoyloxy]-2,2-dimethylicosanamido}phenyl}porphinatoiron(II) bromide (6b): 2-Chloro-1,3,2-dioxaphospholane 2-oxide (372 μL) was added to a solution of **5b** (249 mg, 61.6 μmol) and triethylamine (0.637 mL, 4.58 mmol) in dry CH_2Cl_2 (20 mL) at 0 °C under an argon atmosphere. After stirring the mixture for 1 h and an additional 1 h at room temperature, the solvent was removed under reduced pressure. Then, the resultant phosphate triester was redisolved in dry DMF (30 mL), and anhydrous trimethylamine

(4.0 mL) was immediately added. The mixture was sealed in a pressure bottle and allowed to react for 1 h at room temperature. After an additional 16 h at 60 °C, the solvent was removed, and the residue was washed with MeOH. The remaining brown crude porphyrin was purified by gel column chromatography on Sephadex LH-60 with benzene/MeOH (2:1) as eluent to give a compound **6b** as dark purple solid (202 mg, 79%). IR (NaCl): $\tilde{v} =$ 1087 (POC, phosphate), 1216 (P=O, phosphate), 1692 (C=O, amide), 1735 (C=O, ester), 3431 cm^{-1} (NH, amide); UV/Vis (CHCl$_3$): $\lambda_{max} = 353$, 417, 501, 574, 635, 680 nm; elemental analysis calcd (%) for $C_{260}H_{440}N_{12}O_{44}P_4$. FeBr 2H$_2$O (4734.07): C 65.97, H 9.45, N 3.55; found: C 66.23, H 9.46, N 3.18.

Free-base porphyrin (6a): Phosphocholine groups were introduced into compound **5a** by using the same procedure as for **6b** (Yield: 80%). IR (NaCl): $\tilde{v} = 1089$ (POC, phosphate), 1236 (P=O, phosphate), 1692 (C=O, amide), 1734 (C=O, ester), 3430 cm^{-1} (NH, amide); UV/Vis (CHCl$_3$): $\lambda_{max} = 422$, 516, 549, 590, 646 nm; ^{1}H NMR (500 MHz, CDCl$_3$/CD$_3$OD, 25 °C, TMS): $\delta = -2.6$ (s, 2 H; inner H), -0.4 (s, 24 H; 2,2-dimethyl), 0.7 (t, 12 H; (CH$_2$)$_{16}$CH$_3$), 0.8 (s, 12 H; CH$_3$), 0.8–1.2 (m, 112 H; (CH$_2$)$_{14}$CH$_3$, 128 H; (CH$_2$)$_{16}$), 1.4 (m, 8 H; OC(=O)CH$_2$CH$_2$(CH$_2$)$_{14}$, 8 H; CH$_2$CH$_2$OC(=O)), 2.1 (t, 8 H; OC(=O)CH$_2$(CH$_2$)$_{14}$), 2.4 (s, 16 H; OC(=O)(CH$_2$)$_2$C(=O)O), 3.0 (s, 36 H; N$^+$(CH$_3$)$_3$), 3.4 (t, 8 H; CH$_2$N$^+$(CH$_3$)$_3$), 3.6 (s, 8 H; P(=O)OCH$_2$), 3.8 (m, 16 H; C(CH$_2$OC(=O))$_2$, 8 H; CH$_2$OC(=O)(CH$_2$)$_2$), 4.0 (t, 8 H; CH$_2$CH$_2$N$^+$(CH$_3$)$_3$), 7.1 (s, 4 H; amide), 7.3 (t, 4 H; Ph H4), 7.6 (t, 8 H; Ph H5), 7.7 (d, 4 H; Ph H3), 8.4 (d, 4 H; Ph H6), 8.6 ppm (s, 8 H; pyrrole).

Preparation of aqueous lipid-porphyrin solutions

Free-base lipid-porphyrin solution: A benzene/methanol stock solution of **6a** (50 µL, 2.0 mM) was placed in a 5 mL round bottom flask and slowly evaporated on a rotary evaporator under reduced pressure to give a thin film of the porphyrin at the bottom. The film was then dried in vacuo for 3 h; deionized water (5 mL) heated to 60 °C was then injected. The mixture was homogenized by vortex mixing with several small glass beads (ca. 10) and briefly ultrasonicated by a bath-type sonicator. The resulting red solution (20 µM) was incubated for at least 12 h at room temperature before use.

Lipid-porphyrinatoiron(II) *solution*. A benzene/methanol stock solution of **6b** (50 µL, 2.0 mM) and a solution of 1-dodecylimidazole in CHCl$_3$ (110–165 µL, 2.0 mM) was slowly evaporated by using a rotary evaporator, as described above, to give a thin film at the bottom of the flask. The film was dried in vacuo for 3 h, and phosphate buffer (pH 7.3, 1 mM, 5 mL) heated at 60 °C was added. Homogenization by a tip-type ultrasonicator (60 mW, 3 min) in a water bath gave a yellow-brown solution, which was incubated for at least 12 h at room temperature. Then the **6b** solution (20 µM) was deaerated by N$_2$ bubbling; addition of aqueous sodium dithionate (15 mM, 20 µL) gave a solution of the bis-imidazole iron(II) complex **6c**. Excess sodium dithionate was removed by quick passage through a Sephadex G-25 (coarse) column.

Transmission electron microscopy (TEM): The negatively stained specimens for TEM were prepared as in previously reported procedures.[11d] The grids were observed in a JEOL JEM-100CX electron microscope at an accelerating voltage of 100 kV.

Scanning force microscopy (SFM): A droplet of porphyrin solution (1–5 µM) was pipetted onto freshly cleaved, highly oriented pyrolytic graphite (HOPG STM-1, Advanced Ceramics Co.). After 1 min, excess fluid was carefully blotted off by filter paper, and air-drying was carried out for a further 1 h. SFM measurements were carried out on a Nanoscope III system (Digital Instruments Inc.) in the tapping mode under ambient laboratory conditions. Silicon cantilevers (length 125 µm) with a spring constant between 21 and 78 N m^{-1} and a resonance frequency in the range 260–410 kHz were used. The scanning rate was usually 1.0 Hz. Imaging was simultaneously performed by displaying the amplitude signal and the height signal.

Langmuir–Blodgett layer and Π–A isotherm: A monolayer of lipid-porhyrin was prepared at the air/water interface in a Nippon Laser & Electronics LB Film Deposition System. Compound **6a** was spread from a 1.17 mM solution in CHCl$_3$/MeOH (10:1) onto the pure water subphase. The area per **6a** molecule was estimated from its surface pressure versus molecular area (Π–A) isotherm. Furthermore, the monolayer was pulled onto a clean glass plate to give a lipid-porphyrin monolayer, which was

applied perpendicular to the monolayer surface and slowly pulled up to give porphyrin trilayers.

Exciton calculation

Monolayer: The center-to-center distance r_{mn} of the dipole moments between the origin porphyrin P$_o$ and the neighbor P$_{mn}$ (Figure 4c) is given by Equation (2)

$$r_{mn} = [(ma)^2 + (nb)^2]^{1/2} \tag{2}$$

the angle θ_{mn} by Equation (3)

$$\tan\theta_{mn} = nb/ma \tag{3}$$

and the exciton interaction energies V_{mn} for the S_x transitions and V'_{mn} for the S_y transitions by Equations (4) and (5).

$$V_{mn} = M^2 r_{mn}^{-3}(1 - 3\cos^2\theta_{mn}) \tag{4}$$

$$V'_{mn} = M^2 r_{mn}^{-3}(1 - 3\sin^2\theta_{mn}) \tag{5}$$

The total energy is the sum of the interactions of the infinite porphyrin alignments on the 22 lines crossing the origin of the coordinate axes: V for the S_x transitions and the V' for the S_y transitions.

Bilayer: The core of the porphyrin P$_{kl}$ in the upper layer is assumed to be shifted by $+4.02$, $+2.68$, and $+d$ Å in the x, y, and z directions, respectively, from the center of the nearest porphyrin P$_{mn}$ in the layer below. The center-to-center distance r_{kl} of the dipole moments between porphyrin P$_o$ and each porphyrin P$_{kl}$ is given by Equation (6).

$$r_{kl} = [(ma + 4.02)^2 + (nb + 2.68)^2 + d^2]^{1/2} \tag{6}$$

The angles θ_{kl} for the S_x transitions and θ'_{kl} for the S_y transitions are are given by Equations (7) and (8).

$$\cos\theta_{kl} = (ma + 4.02)r_{kl}^{-3} \tag{7}$$

$$\cos\theta'_{kl} = (nb + 2.68)r_{kl}^{-3} \tag{8}$$

The exciton interaction energy V_{kl} for the S_x transitions and V'_{kl} for the S_y transitions is given by Equations (9) and (10).

$$V_{kl} = M^2 r_{kl}^{-3}(1 - 3\cos^2\theta_{kl}) \tag{9}$$

$$V'_{kl} = M^2 r_{kl}^{-3}(1 - 3\cos^2\theta'_{kl}) \tag{10}$$

The total energy is the sum of the interactions between P$_o$ and 46 porphyrins on the upper layer within a circle of about 5 nm: V_l for the S_x transitions and V'_l for the S_y transitions. Then the overall excitonic interaction in our bilayer model is finally defined as the sum of V and V_l for the S_x transitions and V' and V'_l for the S_y transitions.

Excited-state lifetimes: Singlet lifetimes of **6a** were measured by using a Horiba NAES-500 nanosecond fluorometer with an N$_2$ lamp (excitation-side band-path filter: MC560, emission-side color filter: R62). The samples were held in a cuvette (optical path length 1 cm). Triplet lifetime measurements on the nanosecond timescale were performed by using a Unisoku TSP-1000 time-resolved spectrophotometer system with a Continuum Surelite I-10 Q-switched Nd:YAG laser, which generated a second-harmonic (532 nm) pulse of 6 ns duration with an energy of 200 mJ per pulse (10 Hz). A 150 W Xenon arc lamp was used as the monitor light source. The triplet decay of **6a** was monitored by transient absorption at 450 nm. The concentration of the lipid-porphyrin was 1.7 µM, and experiments were carried out at 25 °C. Time-resolved transient absorption spectra after nanosecond laser flash photolysis were measured by an ANDOR DH520-18F-WR ICCD detector with an ORIEL MS-257 imaging monochromator. The excitation laser pulse with a wavelength of 516 nm was generated from the THG (355 nm; pulse width, 5 ns) of a Spectron SL803G-10 Nd:YAG laser by using a GWU BBO-OPO photoparametric oscilator. A pulsed xenon flash lamp (10 W, 10 Hz, 100 ns pulse width) was used as the monitor light source. The path length of the cuvette was 10 mm, and all measurements were carried out by a Tokyo Instruments two-channel simultaneous detection system at 25 °C.

-42-

O₂ Binding: O_2-binding to the lipid-porphyrinatoiron(II) complex is expressed by Equation (11):

$$FeLP + O_2 \rightleftharpoons FeLP-O_2 \qquad (11)$$

where FeLP is lipid-porphyrinatoiron(II) complex **6c**. The apparent O_2-binding affinity (gaseous pressure at half O_2 binding for **6c**, $P_{1/2}$) was determined by spectral changes at various partial pressure of O_2, as described in the literature.[12] The half-life of the dioxygenated species was determined by the time dependence of the absorption intensity at 540 nm, which is due to the O_2 adduct.

Magnetic circular dichroism (MCD): MCD was measured on a phosphate buffer solution of **6c**/DIm vesicles (8.0 μM) under N_2, CO, and O_2 atmospheres on a JASCO J-820 circular dichrometer fitted with a 1.5 T electromagnet. The accumulations were normally two performed twice, and from each datum the value without an electromagnetic field was subtracted as baseline.

Infrared spectroscopy: The phosphate buffer (pH 7.3, 1 mM) solution of **6c** vesicles (3 mM) containing three equivalents of DIm was prepared by a procedure similar to that described above in a bath-type ultrasonic generator, followed by reduction with sodium dithionate. Separate samples of this solution were exposed to atmospheres of CO, $^{16}O_2$, and $^{18}O_2$ (ISOTEC Inc., 99% enriched). Infrared spectra of each solution were measured between 2000 and 1000 cm^{-1} on a JASCO FT/IR-410 spectrometer at 4 cm^{-1} resolution. A CaF$_2$ cell (path length: 0.025 mm) was used for all measurements.

Differential scanning calorimetry (DSC): Aqueous solutions of **6a**, **6b**, and **6b**/DIm vesicles (1 wt%) were prepared by the same procedure as for IR measurements. DSC for all samples was measured on a SEIKO Instruments DSC120 differential scanning calorimeter at a scan rate of 2 °C min^{-1} in the temperature range 5–80 °C.

Acknowledgements

[1] J. K. M. Sanders in *Comprehensive Supramolecular Chemistry, Templating, Self-assembly, and Self-organization, Vol. 9* (Eds.: J.-M. Lehn, J. L. Atwood, J. E. D. Davies, D. D. MacNicol, F. Vögtle), Pergamon, Oxford, **1996**, pp. 131–164, and reference therein.

[2] Examples of multiporphyrinic assemblies of more than three porphyrin units in organic solvents: a) A. M. Brun, S. J. Atherton, A. Harriman, V. Heitz, J.-P. Sauvage, *J. Am. Chem. Soc.* **1992**, *114*, 4632–4639; b) H. L. Anderson, *Inorg. Chem.* **1994**, *33*, 972–981; c) S. Anderson, H. L. Anderson, A. Bashall, M. McPartlin, J. K. M. Sanders, *Angew. Chem.* **1995**, *107*, 1196-1200; *Angew. Chem. Int. Ed. Engl.* **1995**, *34*, 1096–1099; d) P. N. Taylor, H. L. Anderson, *J. Am. Chem. Soc.* **1999**, *121*, 11538–11545; e) C. C. Mak, N. Bampos, J. K. M. Sanders, *Angew. Chem.* **1998**, *110*, 3169–3172; *Angew. Chem. Int. Ed.* **1998**, *37*, 3020–3023; f) C. A. Hunter, R. K. Hyde, *Angew. Chem.* **1996**, *108*, 2064–2067; *Angew. Chem. Int. Ed. Engl.* **1996**, *35*, 1936–1939; g) S. Rucareanu, O. Mongin, A. Schuwey, N. Hoyler, A. Gossauer, *J. Org. Chem.* **2001**, *66*, 4973–4988; h) C. M. Drain, F. Nifiatis, A. Vasenko, J. D. Batteas, *Angew. Chem.* **1998**, *110*, 2478–2481; *Angew. Chem. Int. Ed.* **1998**, *37*, 2344–2347; i) K. Ogawa, Y. Kobuke, *Angew. Chem.* **2000**, *112*, 4236–4239; *Angew. Chem. Int. Ed.* **2000**, *39*, 4070–4073; j) H. A. M. Biemans, A. E. Rowan, A. Verhoeven, P. Vanoppen, L. Latterini, J. Foekema, A. P. H. J. Schenning, E. W. Meijer, F. C. de Schryver, R. J. M. Nolte, *J. Am. Chem. Soc.* **1998**, *120*, 11054–11060; k) J. L. Sessler, B. Wang, A. Harriman, *J. Am. Chem. Soc.* **1995**, *117*, 704–714; l) C. M. Drain, K. C. Russel, J.-

M. Lehn, *Chem. Commun.* **1996**, 337–338; m) C. Ikeda, N. Nagahara, E. Motegi, N. Yoshioka, H. Inoue, *Chem. Commun.* **1997**, 1759–1760; n) Y. Kuroda, K. Sugou, K. Sasaki, *J. Am. Chem. Soc.* **2000**, *122*, 7833–7834; o) K. Sugou, K. Kitajima, T. Iwaki, Y. Kuroda, *J. Am. Chem. Soc.* **2002**, *124*, 1182–1183.

[3] a) J. H. Fendler, *Membrane Mimetic Chemistry*, Wiley, New York, **1982**; b) S. Baral, J. H. Fendler in *Photoinduced Electron Transfer, Part B, Experimental Techniques and Medium Effects* (Eds.: M. A. Fox, M. Chanon), Elsevier, Amsterdam, **1988**, pp. 541–598; b) J.-H. Fuhrhop, J. Köning, *Membranes and Molecular Assemblies: The Synkinetic Approach*, The Royal Society of Chemistry, Cambridge, **1994**.

[4] a) T. J. Dannhauser, M. Nango, N. Oku, K. Anzai, P. A. Loach, *J. Am. Chem. Soc.* **1986**, *108*, 5865–5871; b) M. Nango, K. Iida, M. Yamaguchi, Y. Yamashita, K. Tsuda, A. Mizusawa, T. Miyake, A. Masuda, J. Yoshinaga, *Langmuir* **1996**, *12*, 1981–1988; c) J. Lahiri, G. D. Fate, S. B. Ungashe, J. T. Groves, *J. Am. Chem. Soc.* **1996**, *118*, 2347–2358.

[5] a) M. Calvin, *Acc. Chem. Res.* **1978**, *11*, 369–374; b) T. Matsuo, K. Itoh, K. Takaku, K. Hashimoto, T. Nagamura, *Chem. Lett.* **1980**, 1009–1012; c) J. K. Hurst, L. Y. C. Lee, M. Grätzel, *J. Am. Chem. Soc.* **1983**, *105*, 7048–7056; d) E. Tsuchida, M. Kaneko, H. Nishide, H. Hoshino, *J. Phys. Chem.* **1986**, *90*, 2283–2284; e) G. Steinberg-Yfrach, P. A. Liddell, S.-C. Hung, A. L. Moore, D. Gust, T. A. Moore, *Nature* **1997**, *385*, 239–241.

[6] a) K. Eshima, M. Yuasa, H. Nishide, E. Tsuchida, *J. Chem. Soc. Chem. Commun.* **1985**, 130–132; b) E. Tsuchida, H. Nishide, *Top. Curr. Chem.* **1986**, *132*, 64–99; c) E. Tsuchida, H. Nishide, M. Yuasa, E. Hasegawa, K. Eshima, Y. Matsushita, *Macromolecules* **1989**, *22*, 2103–2107.

[7] a) J. T. Groves, R. Neumann, *J. Am. Chem. Soc.* **1989**, *111*, 2900–2909; b) A. P. H. J. Schenning, J. H. L. Spelberg, M. C. P. F. Driessen, M. J. B. Hauser, M. C. Feiters, R. J. M. Nolte, *J. Am. Chem. Soc.* **1995**, *117*, 12655–12656; c) Y. Naruta, M. Goto, T. Tawara, F. Tani, *Chem. Lett.* **2002**, 162–163.

[8] G. Steinberg-Yfrach, J.-L. Rigaud, E. N. Durantini, A. L. Moore, D. Gust, T. A. Moore, *Nature* **1998**, *392*, 479–482.

[9] a) J.-H. Fuhrhop, U. Bindig, U. Siggel, *J. Am. Chem. Soc.* **1993**, *115*, 11036–11037; b) C. Endisch, C. Böttcher, J.-H. Fuhrhop, *J. Am. Chem. Soc.* **1995**, *117*, 8273–8274.

[10] J.-H. Fuhrhop in *Comprehensive Supramolecular Chemistry, Templating, Self-assembly, and Self-organization, Vol. 9* (Eds.: J.-M. Lehn, J. L. Atwood, J. E. D. Davies, D. D. MacNicol, F. Vögtle), Pergamon, Oxford, **1996**, pp. 407–450.

[11] a) R. Guilard, N. Senglet, Y. H. Liu, D. Sazou, E. Findsen, D. Fanre, T. D. Courieres, K. M. Kadish, *Inorg. Chem.* **1991**, *30*, 1898–1905; b) J.-H. Fuhrhop, C. Demoulin, C. Böttcher, J. Köning, U. Siggel, *J. Am. Chem. Soc.* **1992**, *114*, 4159–4165; c) T. Komatsu, K. Nakao, H. Nishide, E. Tsuchida, *J. Chem. Soc. Chem. Commun.* **1993**, 728–730; d) E. Tsuchida, T. Komatsu, N. Toyano, S. Kumamoto, H. Nishide, *J. Chem. Soc. Chem. Commun.* **1993**, 1731–1733; e) E. Tsuchida, T. Komatsu, K. Arai, K. Yamada, H. Nishide, C. Böttcher, J.-H. Fuhrhop, *J. Chem. Soc. Chem. Commun.* **1995**, 1063–1064; f) T. Komatsu, K. Yamada, E. Tsuchida, U. Siggel, C. Böttcher, J.-H. Fuhrhop, *Langmuir* **1996**, *12*, 6242–6249; g) T. Komatsu, E. Tsuchida, C. Böttcher, D. Donner, C. Messerschmidt, U. Siggel, W. Stocker, J. P. Rabe, J.-H. Fuhrhop, *J. Am. Chem. Soc.* **1997**, *119*, 11660–11665; h) T. Komatsu, T. Yanagimoto, E. Tsuchida, U. Siggel, J.-H. Fuhrhop, *J. Phys. Chem. B* **1998**, *102*, 6759–6765; i) T. Komatsu, T. Yanagimoto, Y. Furubayashi, J. Wu, E. Tsuchida, *Langmuir* **1999**, *15*, 4427–4433; j) S. Schell, H. K. Hombrecher, *Chem. Eur. J.* **1999**, *5*, 587–598; k) K. Kano, K. Fukuda, H. Wakami, R. Nishiyabu, R. F. Pasternack, *J. Am. Chem. Soc.* **2000**, *122*, 7494–7502; l) T. Komatsu, S. Hayakawa, T. Yanagimoto, M. Kobayakawa, A. Nakagawa E. Tsuchida, *Bull. Chem. Soc. Jpn.* **2001**, *74*, 1703–1707; m) N. Nagata, S. Kugimiya, Y. Kobuke, *Chem. Commun.* **2001**, 689–690.

[12] a) E. Tsuchida, T. Komatsu, K. Arai, H. Nishide, *J. Chem. Soc. Chem. Commun.* **1993**, 730–732; b) E. Tsuchida, T. Komatsu, K. Arai, K. Yamada, H. Nishide, C. Böttcher, J.-H. Fuhrhop, *Langmuir* **1995**, *11*, 1877–1884.

[13] Y. Matsushita, E. Hasegawa, K. Eshima, E. Tsuchida, *Chem. Lett.* **1983**, 1387–1390.

-43-

[14] J. H. Espenson, R. J. Cristiensen, *Inorg. Chem.* **1977**, *16*, 2561–2564.

[15] G. Roberts, *Langmuir–Blodgett*, Plenum Press, New York, **1990**; b) K. Larsson in *The Lipid Handbook* (Eds.: F. D. Gunstone, J. L. Harwood, F. B. Padley), Chapman and Hall, London, **1986**, pp. 321–382.

[16] a) E. G. McRae, M. Kasha, *J. Chem. Phys.* **1958**, *28*, 721–722; b) M. Kasha, *Radiation Res.* **1963**, *20*, 51–71.

[17] a) M. P. Byrn, C. J. Curtis, I. Goldberg, Y. Hsiou, S. I. Khan, P. A. Sawin, S. K. Tendick, C. E. Strouse, *J. Am. Chem. Soc.* **1991**, *113*, 6549–6557; b) M. P. Byrn, C. J. Curtis, Y. Hsiou, S. I. Khan, P. A. Sawin, S. K. Tendick, A. Terzis, C. E. Strouse, *J. Am. Chem. Soc.* **1993**, *115*, 9480–9497.

[18] C. A. Hunter, J. K. M. Sanders, A. J. Stone, *Chem. Phys.* **1989**, *133*, 395–404.

[19] U. Siggel, C. Endisch, T. Komatsu, E. Tsuchida, J. Voigt, J.-H. Furhop, *Ber. Bunsen-Ges.* **1996**, *100*, 2070–2075.

[20] D. C. Barber, R. A. Freitag-Beeston, D. G. Whitten, *J. Phys. Chem.* **1991**, *95*, 4074–4086.

[21] C. Odin, J. P. Aimé, Z. El Kaakour, T. Bouhacina, *Surf. Sci.* **1994**, *317*, 321–340.

[22] a) J. P. Collman, R. R. Gagne, C. A. Reed, T. R. Halbert, G. Lang, W. T. Robinson, *J. Am. Chem. Soc.* **1975**, *97*, 1427–1439; b) J. R. Budge, P. E. Ellis, Jr., R. D. Jones, J. E. Linard, F. Basolo, J. E. Baldwin, R. L. Dyer, *J. Am. Chem. Soc.* **1979**, *101*, 4760–4762; c) M. Momenteau, B. Loock, E. Bisagni, M. Rougee, *Can. J. Chem.* **1979**, *57*, 1804–1813.

[23] H. F. Bunn, B. G. Forget, *Hemoglobin: Molecular, Genetic and Clinical Aspects*, W. B. Sunders Company, Philadelphia, **1986**.

[24] a) D. W. Deamer, A. D. Bangham, *Biochim. Biophys. Acta.* **1976**, *443*, 629–634; b) M. Pozansky, S. Tong, P. C. White, J. M. Milgram, A. K. Solomon, *J. Gen. Physiol.* **1976**, *67*, 46–66.

[25] a) J. P. Collman, J. I. Brauman, K. M. Doxsee, T. R. Halbert, E. Bunnenberg, R. E. Linder, G. N. LaMar, J. D. Guadio, G. Lang, K. Spartalian, *J. Am. Chem. Soc.* **1980**, *102*, 4182–4192; b) J. P. Collman, F. Basolo, E. Bunnenberg, T. C. Collins, J. H. Dawson, P. E. Ellis, M. L. Marrocco, A. Moscowitz, J. L. Sessler, T. Szymanski, *J. Am. Chem. Soc.* **1981**, *103*, 5636–5648; c) J. P. Collman, J. I. Brauman, T. J. Collins, B. L. Iverson, G. Lang, R. B. Pettman, J. L. Sessler, M. A. Walters, *J. Am. Chem. Soc.* **1983**, *105*, 3038–3052.

[26] a) J. P. Collman, J. I. Brauman, T. R. Halbert, K. S. Suslick, *Proc. Natl. Acad. Sci. USA* **1976**, *73*, 3333–3337; b) E. Tsuchida, T. Komatsu, T. Nakata, E. Hasegawa, H. Nishide, H. Inoue, *J. Chem. Soc. Dalton Trans.* **1991**, 3285–3289.

[27] a) C. H. Barlow, J. C. Maxwell, W. J. Wallace, W. S. Caughey, *Biochem. Biophys. Res. Commun.* **1973**, *55*, 91–95; b) W. S. Caughey, *Ann. N. Y. Acad. Sci.* **1970**, *174*, 148–153.

[28] T. Komatsu, S. Ishihara, H. Nishide, E. Tsuchida, unpublished results.

[29] R. H. Pearson, I. Pascher, *Nature* **1979**, *281*, 499–501.

[30] G. McDermott, S. M. Prince, A. A. Freer, A. M. Hawthornthwaite-Lawless, M. Z. Papiz, R. J. Cogdell, N. W. Isaacs, *Nature* **1995**, *374*, 517–521.

自己組織化リピドヘム小胞体のナノ構造と酸素結合能

Nano-structure and Oxygen-binding Ability of Self-assembled Lipid-heme Vesicles

小松晃之, 森武美保, 土田英俊

Teruyuki Komatsu, Miho Moritake, Eishun Tuchida

和文抄録

　生理条件下（生理塩水中，pH7.3，37℃）で酸素を可逆的に吸脱着できる鉄ポルフィリン（ヘム）の組織体を構築し，それを臨床応用可能な完全合成型の人工酸素運搬体として利用する試みを進めている．リン脂質類似構造の置換基を有する両親媒性ヘム（リピドヘム）は，水相系で自発的に会合して様々な形態の組織を形成するが，特に4つのジアルキルホスホコリン基をポルフィリン面上に共有結合したテトラフェニルポルフィリン鉄錯体は二分子膜小胞体を構成し，安定な酸素配位錯体を与える．今回，ジアルキル鎖の結合部位として新たにトリメチロールエタンを導入した新しいリピドヘムを設計・合成し，それが自己集合して形成する小胞体のナノ構造と酸素結合能を明らかにした．電子顕微鏡観察，原子間力顕微鏡観察から，リピドヘムと1-ドデシルイミダゾールが水中で均一分散して，粒径約100nmの一枚膜小胞体を形成することを解明．その膜厚（10nm）がリピドヘム分子長（4.6nm）の二倍に相当したことから，小胞体はリピドヘムの分子二層膜からなると考えられる．酸素親和性（$P_{1/2}$）は30Torr（37℃）でヒト赤血球の値に近く，酸素錯体半減期は17hr（37℃）と長い．レーザーフラッシュホトリシス法から決定した酸素結合・解離速度定数は，ヘモグロビンの値と同等で，これは酸素吸脱着の速度が赤血球に比べ1,500倍速いことを意味する．また，酸素分子の配位構造を磁気円二色性，赤外吸収スペクトル測定から解析し，ヘモグロビンと同じbent end-on型であることを実証した．

Abstract

Molecular assemblies made of iron-porphyrins (hemes), which can reversibly bind and release oxygen molecule under physiological conditions (in saline solution, pH 7.3, 37°C), have been synthesized and tried to use as totally synthetic oxygen-carriers in clinical situations. It is known that amphiphilic hemes having phospholipid-like substituents are self-organized in aqueous media to form various shaped assemblies, in particular, tetraphenylporphinatoiron complexes with four dialkylphosphocholine groups on the porphyrin ring plane produce bilayer vesicles and form stable oxygen-adduct complexes. Recently, we have synthesized new lipid-heme, in which trimethyrolethane is introduced as an attaching moiety for two long acylchains, and evaluated the nano-structure and oxygen-binding ability of its self-assembled vesicles. Electron microscopy and atomic force microscopy revealed that lipid-heme and 1-dodecylimidazole were homogeneously organized in water to give spherical unilamellar vesicles with a diameter of approximately 100 nm. Since the thickness of the membrane (10 nm) coincided to the twice of the length of lipid-heme molecule (4.6 nm), it can be supposed that the vesicles were composed of double layer membrane structure. The oxygen-binding affinity ($P_{1/2}$) was 30 Torr (37°C), which is close to that of human red blood cells, and its half-life time ($\tau_{1/2}$) was enough long (17 hr at 37°C). The oxygen association- and dissociation-rate constants determined by laser flash photolysis showed similar values of hemoglobin's, which indicates that oxygen absorption rate of the lipid-heme vesicles is 1,500-fold faster than that of red blood cells. Furthermore, the coordination structure of oxygen molecule was evaluated by magnetic circular dichroism and infrared spectroscopies, and found to be bent/end-on structure as same as hemoglobin.

1．緒　言

　ヘモグロビン（Hb）の酸素結合席である鉄プロトポルフィリンIX（ヘム）の酸素吸脱着能を合成のポルフィリン鉄錯体で再現しようとする試みは1970年代から始まり[1-3]，これまでに有機化学の英知を結集した数多くの修飾ヘム誘導体が精密合成されてきた[4,5]．合成化学，生物無機・有機化学からのアプローチが主流であったため，そのほとんどは非プロトン性有機溶媒中の修飾ヘムを対象としたモデル研究であったが，(i)ポルフィリン骨格の立体的・電子的構造因子と酸素配位平衡の相関，(ii)酸素結合ダイナミクス，(iii)配位酸素の電荷分極構造など，重要な知見が集積されてきた．Hbからヘムを単離し室温で酸素と接触させても，水中はもちろん有機溶媒中でもヘム鉄は瞬時に不可逆酸化され，酸素分子の配位を見ることはない．一般にヘム錯体への可逆的な酸素結合を可能とするためには，(i)酸素錯体にもう一つのヘムが結合してμ-oxo二量体を形成する二分子酸化過程を禁止し，さらに(ii)配位酸素にプロトン（水）が付加する一分子酸化過程を抑制する必要がある．Hbにおけるグロビン鎖の役割の一つは，ヘムを疎水的な分子環境（ヘムポケット）内へ固定し，上記条件を満足させることにあるといってよい．加えて，ヒスチジン残基（E7 His）のイミダゾールπ-軌道から鉄d_{xz}へのπ-donationが，軌道の電子密度を増大させ，中心鉄から酸素へのback donationを促進，ヘムの酸素親和性を増大させている．

　実際に合成ヘムを利用して，生理条件下で酸素輸送のできる人工酸素運搬体を具体化した最初の例は，著者らの両親媒性ヘムをリン脂質二分子膜中に包埋した系であった[6]．つまり我々は，両親媒性のポルフィリン鉄（II）錯体（リピドヘム）をリン脂質が構成する二分子膜層間に配置固定すると，水中でも安定な酸素錯体が得られることを初めて見出したのである．この発見を契機にリピドヘム誘導体の設計・合成を幅広く展開[7-11]，興味あることに，ジアルキルホスホコリン基をポルフィリン面上に導入した化合物の一群が，水中で自発的に集合してヘム鉄のみからなる二分子膜小胞体を形成することを明らかにした[12,13]．アルキレン側鎖が規則配列して構築する疎水場の中央にヘムが二次元配列するため，結果として上記二つの酸化過程が同時に抑制され，安定な酸素錯体が得られる．リピドヘム小胞体の酸素親和性はヒト赤血球と同程度で，酸素結合解離速度もヘモグロビンと同等，所望の濃度（[ヘム]＝5-10mM）に調整したリピドヘム小胞体水分散液は，赤血球の酸素輸送能を十分に代替できる完全合成型の人工酸素運搬体となり得る．また，この自己組織化リピドヘムの完成により，従来共成分として混合していたリン脂質の添加は不要となり，同ヘム濃度水分散液中の固形成分量は，大幅に低減できるようになった．唯一この系に残された課題は，リピドヘムの合成工程が多段階からなるため，総収率が低く，量産が難しいことにあった．

　ごく最近我々は，ジアルキルホスホコリン基の骨格部位であるグリセロールを同じ三価アルコールであるトリメチロールエタンに変換すると合成工程が大幅に簡略化され，収率高くジアシル鎖構造が構築できることを見出した[14]．得られた新しいリピドヘム（I, Fig. 1）は，二分子膜小胞体を形成し，酸素を可逆的に結合解離できる．本報では，この自己組織化リピドヘム小胞体のナノ構造と酸素結合能，酸素配位構造について報告する．
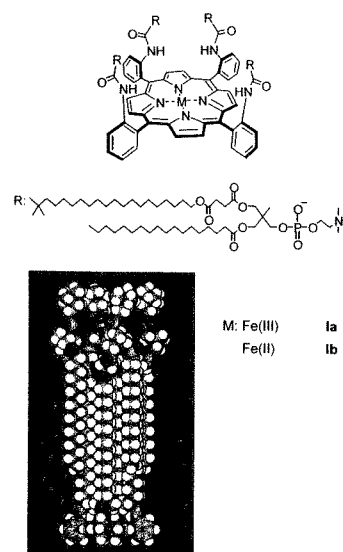
Fig. 1 Structure of lipid-heme molecule and its space-filling model.

2．実験方法

2.1 試薬，装置

　リピドヘム（Ia），1-ドデシルイミダゾール（DIm）は，既報に従い合成した[14]．イオン交換水はADVANTEC GS-200を用いて調製．紫外可視吸収（UV-vis.）スペクトルはJASCO V-570を用い，300-700nmの範囲で測定した．

2.2 リピドヘム水分散液の調製と集合構造観察

　Ia/DImの混合薄膜（1/2.2-3.4（モル比））をナス型フラスコ底部に作成し，そこへ60℃に加温したリン酸緩衝液（1mM，pH7.3）を加え，十分に水和させた後，水浴中，N_2雰囲気下で超音波照射（日本精機 TS-600，60mW，3min）すると，茶褐色透明のリピドヘム水分散液（[ヘム]＝20μM）が得られた．室温で少なくとも12時間静置してから，各測定に供した．

　得られたIa/DIm水溶液と酢酸ウラニル水溶液を混合し，親水化処理装置（JEOL HDT-400）で前処理した電子顕微鏡用支持膜付きグリッドの上にのせ，室温で乾燥させた後，透過型電子顕微鏡（TEM）観察を行った（JEOL，JEM-100CX）（ネガティブ染色法）．また別途グラファイト（HOPG）基板上に乾燥させたIa/DIm水分散液について，原子間力顕微鏡（AFM）観察（Digital Instruments，Nanoscope III）を実施した．小胞体の粒径とその分布は動的光散乱粒径分布測定装置（COULTER MODEL N4SD）を用いて測定した．

2.3 酸素結合パラメーター

　Ia/DIm水分散液（[Ia]＝20μM，pH7.3）に窒素雰囲気気下で小過剰の$Na_2S_2O_4$水溶液を添加すると，中心鉄（III）が還元され，酸素配位活性な鉄（II）錯体が得られる．余剰の$Na_2S_2O_4$を

ゲル濾過（Sephadex G-25）により除去した後，分光分析用石英製セル（1cm×1cm）に移し，セプタムラバーで密栓した．そこへ酸素，一酸化炭素を通気し，UV-vis.スペクトルを測定，スペクトルパターンから酸素錯体，一酸化炭素錯体の形成を観測した．また，異なる酸素分圧に対するUV-vis.スペクトルの連続変化から，酸素結合解離曲線を作成，酸素親和性（$P_{1/2}$）を決定した．酸素錯体吸収帯（λ_{max}：542nm）吸光度の経時変化から酸素錯体半減期（$\tau_{1/2}$）を算出．さらに，レーザーフラッシュホトリシス分光装置(UNISOKU TSP-600，Nd:YAGレーザー第二高調波（532nm））を用いて，酸素，一酸化炭素結合解離速度定数（k_{on}, k_{off}）を決定した[15]．

2.4 磁気円偏光二色性（MCD）スペクトル，赤外吸収（IR）スペクトル

Ib/DIm水分散液（[**Ib**] = 8μM，pH7.3）を，窒素，酸素，一酸化炭素雰囲気下で，各々2.5mLずつ分光分析用石英製セル（1cm×1cm）に分注し，1.5T（15kG）の磁場下，300-700nmの範囲でMCDスペクトルを測定した(JASCO J-820，積算回数：2回，25℃)．また，0TにおけるCDスペクトルをベースラインとして使用した．

Ib/DIm水分散液（[ヘム] = 3mM，pH7.3）を，窒素，一酸化炭素，酸素（$^{16}O_2$），$^{18}O_2$（Isotec Inc.（USA）99%）雰囲気下で，各々150μL採取し，CaF_2セル（JASCO，1103-7157E，セル長：0.025mm）に注入，400-4000cm^{-1}の範囲でIRスペクトルを測定した(JASCO FT-IR-410，分解能：4cm^{-1}，積算回数：64回，25℃)．

3．結果および考察
3.1 集合組織の形態とナノ構造

得られたリピドヘム水分散液（**Ia**/DIm，[ヘム] = 10μM-10mM）はきわめて安定で，調製6ヶ月後でも沈殿凝集は認めない．この水溶液の透過型電子顕微鏡（TEM）観察から**Ia**とDImが水中で均一に分散して，粒径約100nmの一枚膜小胞体を形成することを明らかにした（Fig.2(A)）．膜厚（10nm）がリピドヘム分子長（4.6nm）の二倍に相当したことから，小胞体はリピドヘムの分子二層膜からなると考えられる．著者らは以前，ジアシル鎖の結合部位として天然のリン脂質（例えば，ジパルミトイルホスファチジルコリン（DPPC））と同じグリセロールを用いたリピドヘムを合成し，それが水中で自己集合して二分子膜小胞体を形成することを報告しているが[12]，このリピドヘム（**Ia**）も単独，または軸塩基配位子としてのDImが共存する条件下でも同様な小胞体を形成できる．グリセロール部分をトリメチロールエタンに変換しても，小胞体形成能に変化はなかった．動的光散乱法により測定した小胞体の粒径は97±73nmで，TEM観察の結果と一致した．

また，**Ia**/DIm水分散液をグラファイト基板上で乾燥させ原子間力顕微鏡（AFM）観察を行うと，小胞体が潰れて変形した円盤状組織像が認められた(Fig.2(B))．これはDPPCなどのリン脂質からなる小胞体に見られる現象と類似しており，内水相を有する小胞組織のAFM観察では一般的である[10]．円盤の高さは均一で19.5nm．この高さがリピドヘム二分子膜の厚みの二倍と一致したことからも，分子二層膜構造が裏付けられた．
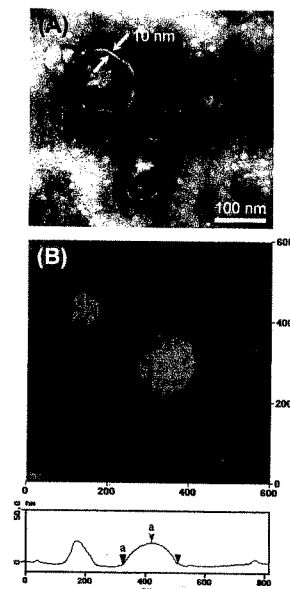

Fig.2 (A) TEM of **Ia**/DIm vesicle stained by uranyl acetate. (B) AFM image of the evaporated sample of **Ia**/DIm vesicles on HOPG.

3.2 酸素結合能

Ib/DIm小胞体のUV-vis.スペクトルは，窒素雰囲気下でλ_{max}：436，538，568nmを示し，**Ib**の両軸配位座にDImが結合した6配位鉄（II）低スピン錯体の形成を示した．そこへ酸素を通気するとスペクトルパターンは速やかに酸素錯体型（λ_{max}：435，543nm）へ移行し，この酸素結合解離は酸素／窒素の吹き込みに伴い可逆的に変化した（Fig.3）．また，一酸化炭素を吹き込むときわめて安定なカルボニル錯体（λ_{max}：433，545nm）が得られた．異なる酸素分圧に対するUV-vis.スペクトル変化から算出した酸素親和性（$P_{1/2}$）は30Torr（37℃）でヒト赤血球の値（27Torr）に近く[16]，酸素錯体の半減期も17hr（37℃）と長い．酸素結合サイトであるヘム部が小胞体表面から約4.0nm内側の疎水場に規則正しく二次元配列して固定されているため[14]，μ-oxo二量体形成とプロトン酸化が同時に抑制されるのである．また，この二分子膜小胞体は約23,000分子のリピドヘムから構成されており，その全てに酸素分子が結合できる(Fig.4)．Hbの酸素結合過程に見られる協同現象（いわゆるアロステリック効果）は観測されないが，例えば肺（P_{O_2}：110Torr）〜末梢組織（P_{O_2}：40Torr）間におけるリピドヘム小胞体の酸素運搬効率（20%）は，赤血球の値（22%）に匹敵することから，人工酸素運搬体として十分な酸素輸送能力を有しているといってよい（Fig.5）．
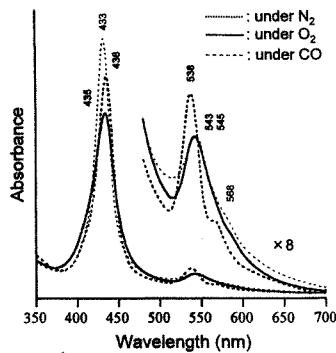
Fig. 3 UV-vis. absorption spectral changes of **Ib/DIm** vesicles in phosphate buffer solution (pH 7.3) at 25°C.
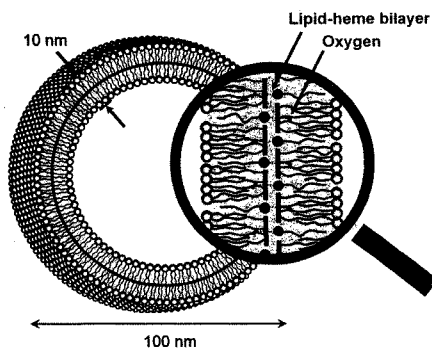

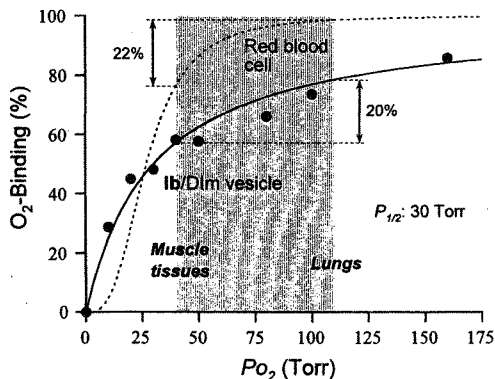**Fig. 4** Schematic illustration of **Ib/DIm** bilayer vesicles.

Fig. 5 O₂-equilibrium curve of **Ib/DIm** vesicles in phosphate buffer solution (pH 7.3) at 37°C.

Ib/DIm (CO) 小胞体水分散液にレーザーフラッシュを照射すると，配位COの解離と再結合が観測される．この瞬時に起こる非平衡状態から平衡状態へのUV-vis.スペクトル変化から，配位気体分子の結合解離速度定数（k_{on}, k_{off}）が算出できる．レーザー照射10μs後における過渡吸収スペクトルは，窒素，一酸化炭素雰囲気下における吸収帯の差スペクトルとは異なるパターンを示した．つまりこの実験条件下では，レーザー照射により一酸化炭素が解離した後，近傍に存在するDImが第6配位座に配位することなく，一酸化炭素の再結合が先行して生起する．レ

ーザフラッシュホトリシス法により決定したリピドヘム小胞体のk_{on}, k_{off}はHbの値と同等値を示し[17,18]，これは生体膜に内包されている構造の赤血球と比較した場合，酸素吸脱着の速度が1,500倍速いことを意味する[19]．

Table 1 O₂- and CO-binding rate constants of **Ib/DIm** vesicle in phosphate buffer solution (pH 7.3) at 25 °C.

	O₂		CO
	k_{on} [M⁻¹s⁻¹]	k_{off} [s⁻¹]	k_{on} [M⁻¹s⁻¹]
Ib/DIm vesicle	1.6×10^7	2.5×10^2	1.2×10^7
Hb(T-state)α[a]	2.9×10^6	1.8×10^2	2.2×10^5
Red blood cell[b]	1.1×10^4	1.6×10^{-1}	1.4×10^4

[a] pH 7.0-7.4, 20 °C, ref.17, 18.　[b] pH 7.4, ref. 19.

3.3 リピドヘムの軸配位構造と酸素配位構造

ヘムやヘム蛋白質の磁気円偏向二色性（MCD）スペクトル測定からは，その酸化状態，スピン状態，配位構造に関する重要な知見が得られる[20,21]．Ib/DIm小胞体の窒素，酸素，一酸化炭素雰囲気下におけるMCDスペクトルは，それぞれ異なるパターンを示した（Fig. 6）．これらはCollmanらが報告しているテトラフェニルポルフィリン鉄（II）-ビス（N-メチルイミダゾール）[FeTPP (N-MeIm)₂] 錯体，FeTPP (N-MeIm) (CO) 錯体，および近位結合型置換FeTPP (O₂) 錯体のパターンとよく一致した[21]．つまり，窒素雰囲気下では，2つのDImが両軸配位座に結合した鉄(II) 6配位低スピン錯体構造をとるが，そこへ酸素，一酸化炭素を通気すると，DImの1つがO₂，COに置き換わりSoret帯領域に対称性の高い大きなMCDが出現する．この結果は，従来UV-vis.スペクトルから考察していたIb/DIm小胞体の軸配位構造変化が正しいことを示している．
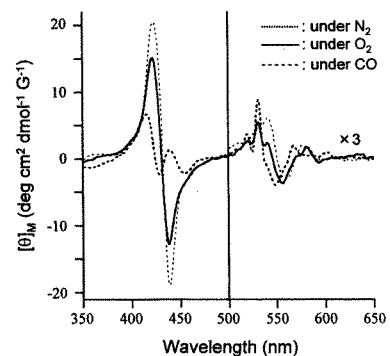

Fig. 6 MCD spectral changes of **Ib/DIm** vesicles in phosphate buffer solution (pH 7.3) at 25°C.

ヘム錯体における配位酸素の伸縮振動（ν_{O_2}）は，IRスペクトルにより直接観測することができるが，一般に水溶液の場合，水の吸収が大きいため，差スペクトル法を用いて定量する．Ib/DIm (^{16}O₂) 錯体からIb/DIm (CO) 錯体のIRスペクトルを差し引くと，1155cm⁻¹に配位酸素の伸縮振動（ν^{16}O₂）が観測された（Table 2）．この値がスーパーオキサイド（1145cm⁻¹）に近いこ

とから，類似のFeTPP誘導体と同様，リピドヘムの酸素配位構造はbent end-on型と考えられる[22]．さらに，Ib/DIm（$^{18}O_2$）錯体−Ib/DIm（CO）錯体の差スペクトルには$\nu^{18}O_2$（1081cm^{-1}）が出現し，$\nu^{16}O_2$−$\nu^{18}O_2$間 同位体シフト値（74cm^{-1}）は，計算値（74cm^{-1}）とよく一致した．これらの事実は，間違いなく分子状酸素がリピドヘム小胞体のヘム鉄に配位していることを示す結果である．また，配位一酸化炭素の伸縮振動（$\nu_{CO}=1969$cm^{-1}）も類似のFeTPP誘導体の値と一致した．自己組織化したリピドヘム小胞体の中でも，軸塩基であるDImの中心鉄への配位に歪みはないと考えられる．

Table 2 IR spectral data of Ib/DIm vesicle in phosphate buffer solution (pH 7.3) at 25 ℃.

	O$_2$		CO
	$\nu^{16}O\text{-}^{16}O$ [cm^{-1}]	$\nu^{18}O\text{-}^{18}O$ [cm^{-1}]	$\nu^{12}C\text{-}^{16}O$ [cm^{-1}]
Ib/DIm vesicle	1155	1081	1969
FeTpivPP(MIm)[a]	1159	1075	1969
O$_2$ or CO (gas)	1556	-	2143
O$_2$$^-$	1145	-	-

[a]FeTpivPP(MIm): Picket-fence Fe(II)porphyrin(1-methyl-imidazole) complex (Nujol) (ref. 22).

4．結 論

リン脂質置換基のジアシル鎖結合部位としてトリメチロールエタンを導入した新しいリピドヘムを合成し，それが水相系で自己集合して形成する二分子膜小胞体のナノ構造と酸素結合能を明らかにした．グリセロールをトリメチロールエタンに置換しても，小胞体形成能に変化はない．実際に，二つのパルミトイル鎖をトリメチロールエタンで連結したリン脂質も，DPPCと同様に水相系で自発的に会合して二分子膜小胞体を与えた．グリセロールより対称性の高いトリメチロールエタンを含む分子構造のほうが，二分子膜を形成した際の分子充填率は高い可能性もある．このリピドヘムに軸塩基配位子として1-ドデシルイミダゾールを添加して調製した粒径約100nmの一枚膜小胞体は，酸素の吹き込みに伴い，安定な酸素錯体を形成した．酸素親和性は30Torr（37℃）でヒト赤血球の値に近く，酸素錯体半減期は17hr（37℃）と実用に耐える安定度を持つ．この二分子膜小胞体は約23,000分子のリピドヘムから構成されているので，その全てに酸素分子が結合できることになる．酸素結合・解離速度定数は，ヘモグロビンの値と同等で，これは酸素の吸脱着速度が赤血球に比べ1,500倍速いことを意味している．さらに，酸素の配位構造がヘモグロビンと同じbent end-on型であることを証明した．現在，高濃度リピドヘム小胞体水分散液の溶液物性，血液適合性，生体内酸素輸送能について検討を進めている．

参考文献

1. Collman JP, Gagne RR, Halbert TR, Marchon JC, Reed CA. Reversible oxygen adduct formation in ferrous complexes derived from a "picket fence" porphyrin. A model for oxymyoglobin. J Am Chem Soc 1973;95:7868-7870.

2. Chang CK, Traylor TG. Solution behavior of a synthetic myoglobin active site. J Am Chem Soc 1973;95:5810-5811.

3. Almog J, Baldwin JE, Huff J. Reversible Oxygenation and autooxidation of a "capped" porphyrin iron(II) complex. J Am Chem Soc 1975;97:227-228.

4. Momenteau M, Reed CA. Synthetic heme dioxygen complexes. Chem Rev 1994;94:659-698.

5. Collman JP, Fu L. Synthetic models for hemoglobin and myoglobin. Acc Chem Res 1999;32:455-463.

6. Matsushita Y, Hasegawa E, Eshima K, Tsuchida E. Synthesis of amphilic porphinato iron complexes having phosphoryl-choline groups. Chem Lett 1983;1983:1387-1390.

7. Komatsu T, Nakao K, Nishide H, Tsuchida E. Octopus-porphyrins. Their assembly and oxygen-binding in aqueous medium. J Chem Soc Chem Commun 1993;1993;728-730.

8. Tsuchida E, Komatsu T, Toyano N, Kumamoto S, Nishide H. Lipid-porphyrin fibers: morphology and incorporation into phospholipid vesicle. J Chem Soc Chem Commun 1993;1993:1731-1733.

9. Komatsu T, Yamada K, Tsuchida E, Siggel U, Böttcher C, Fuhrhop JH. Micellar fibers of octopus porphyrin. Photoinduced electron transfer reactions in aqueous media. Langmuir 1996;112:6242-6249.

10. Komatsu T, Tsuchida E, Böttcher C, Donner D, Messersch-midt C, Siggel U, Stocker W, Rabe JP, Fuhrhop JH. Solid vesicle membrane made of meso-tetrakis[(bixinylamino)-o-phenyl]porphyrins. J Am Chem Soc 1997;119:11660-11665.

11. Komatsu T, Yanagimoto T, Tsuchida E, Siggel U, Fuhrhop JH. Monolayer assemblies made of octopusporphyrins with pyridinium headgroups: Electron transfer reactions in non-covalent porphyrin-quinone platelets in aqueous media. J Phys Chem B 1998;102: 6759-6765.

12. Tsuchida E, Komatsu T, Arai K, Yamada K, Nishide H, Fuhrhop JH. Self-assembled lipidporphyrin bilayer vesicles. Microstructure and dioxygen binding in aqueous medium. Langmuir 1995;11:1877-1884.

13. Tsuchida E, Komatsu T, Arai K, Yamada K, Nishide H, Böttcher C, Fuhrhop JH. Monolayered octopus-porphyrin vesicle: Microstructure and oxygen-binding in aqueous medium. J Chem Soc Chem Commun 1995;1995:1063-1064.

14. Komatsu T, Moritake M, Nakagawa A, Tsuchida E. Self-organized lipid-porphyrin bilayer membranes in vesicular form: Nanostructure, photophysical properties and dioxygen coordination. Chem Eur J 2002;8:5469-5480.

15. Tsuchida E, Komatsu T, Arai K, Nishide H. Synthesis and

dioxygen-binding properties of double-sided porphyrinatoiron(II) complexes bearing covalently bound axial imidazole. J Chem Soc Dalton Trans 1993;1993:2465-2469.

16. Severinghaus JW. Blood gas calculator. J Appl Physiol 1966; 21:1108-1116.

17. Sawicki CA, Gibson QH. Properties of the T state of human oxyhemoglobin studied by laser photolysis. J Biol Chem 1977;252:7538-7547.

18. Steinmeier RC. Parkhurst LJ. Kinetic studies on the five principal components of normal adult human hemoglobin. Biochemistry 1975;14:1564-1571.

19. Tsuchida E, Yuasa M, Nishide H. Rate parameters for oxygen and carbon monoxide binding to liposome-embedded heme unde physiological conditions. J Chem Soc Dalton Trans 1985;1985:65-68.

20. Collman JP, Basolo F, Bunnenberg E, Collins TJ, Dawson JH, Ellis Jr PE, MMarrocco ML, Moscowitz A, Sessler JL, Szymanski T. Use of magnetic circular dichroism to determine axial ligatiion for some sterically encumbered iron(II) porphyrin complexes. J Am Chem Soc 1981;103:5636-5648.

21. Collman JP, Bruman JI, Doxsee KM, Halbert TR, Bunnenberg E, Linder RE, LaMar GN, Gaudio JD, Lang G, Spartalian K. Synthesis and characterization of "tailed picket fence" porphyrins. J Am Chem Soc 1980;102:4182-4192.

22. Collman JP, Bruman JI, Halbert TR, Suslick KS. Nature of O_2 and CO binding to metalloporphyrins and heme proteins. Proc Natl Acad Sci USA 1976;73:3333-3337.

-50-

www.rsc.org/chemcomm ChemComm

meso-Tetrakis[o-(N-methyl)pyridinium]porphyrin ensembles with axially coordinated cyclodextrin-penetrating phenethylimidazole: reversible dioxygen-binding in aqueous DMF solution

Teruyuki Komatsu,[a] Shoichi Hayakawa,[b] Eishun Tsuchida[a] and Hiroyuki Nishide[*b]

[a] Advanced Research Institute for Science & Engineering, Waseda University, Tokyo 169-8555, Japan
[b] Department of Applied Chemistry, Waseda University, Tokyo 169-8555, Japan.
     E-mail: nishide@waseda.jp; Fax: +81 3-3209-5522; Tel: +81 3-3200-2669

α-Cyclodextrin (αCD)-penetrating 2-methyl-1-phenethyl-imidazole coordinates to the zinc(II) and iron(II) complexes of meso-tetrakis[o-(N-methyl)pyridinium] porphyrinate, giving non-covalently linked αCD-porphyrin ensembles; the iron(II) complex can reversibly bind and release dioxygen in aqueous DMF solution.

Modified porphyrinatoiron(II) complexes with a highly-complicated structure, which are prepared by general organic synthetic procedures, namely covalent bonding, have been extensibly studied to mimic the diverse reactivities of hemoproteins.[1,2] In particular, the designs of single-face or double-face encumbered models have been a topic of great interest for the preparation of dioxygen (O₂)-carrying hemes as hemoglobin and myoglobin analogues.[3,4] Based on these significant efforts, we now recognize that two crucial factors are necessary for the dioxygenation of the synthetic heme; (i) bulky-substituents on the porphyrin ring plane to prevent μ-oxo dimer formation, and (ii) a hydrophobic environment to exclude the protons, especially in aqueous media.[5] However, a great deal of labor is generally required to introduce the encumbrance on the porphyrin macrocycle and the total synthetic yields are rather low. If a suitable molecular structure, which provides the O₂-binding capability to the porphyrin platform, is constructed by non-covalent bond formations in water, a totally new class of porphyrin architectures will appear in this chemistry. We report herein for the first time the formation of meso-tetrakis[o-(N-methyl)pyridinium]porphyrinato-zinc(II) and -iron(II) ensembles with axially coordinated α-cyclodextrin-penetrating 2-methyl-1-phenethylimidazole (αCD-MPIm), and the reversible O₂ binding to the iron(II) complex in aqueous DMF solution (Fig. 1). We have employed an αCD to prepare the water-soluble bulky proximal base, and its binding to the flat tetracationic porphyrinato-iron(II) leads to a stable O₂-adduct formation. This is the first example of dioxygenation of a non-covalently linked supramolecular architecture of a cyclodextrin-heme complex.

meso-Tetrakis(o-pyridyl)porphine (TPyP), prepared by Adler's method,[6] was reacted with CH₃I in CHCl₃-EtOH solution to yield the quaternarized 5,10,15,20-tetrakis[o-(N-methyl)pyr-

idinium]porphine tetraiodide (47%). The Zn(II) insertion was carried out using Zn(OAc)₂ in MeOH, affording the Zn(II) complex (1a). In the case of the iron complex (1b), the central metal was formerly introduced to TPyP by FeBr₂ in DMF, and then quaternarized using CH₃I. Both materials were finally passed through an ion exchange column (Dowex 1-2X) to convert their counter anions to Cl⁻. Analytical data for all the compounds were satisfactorily obtained.

As Miskelly et al. reported, four rotational atropisomers of 1a could be separated on silica gel using an eluent of 2-butanone–conc. aq. NH₃–NH₄PF₆–N-methylimidazole (MIm).[7] However, attempts to separate these isomers without PF₆⁻ counter anions and axially coordinated MIm were unsuccessful. Anyhow, it is true that the αααβ isomer is the most dominant species of 1a (ca. 50%) at thermal equilibrium.[8]

From the aqueous suspension of αCD and MPIm (20-fold molar excess), the equivalent inclusion compound, αCD-MPIm, was isolated as a white solid. The ¹H NMR spectrum, where all signals were carefully assigned by ¹H–¹H COSY, showed that (i) it exactly consists of a 1:1 complex of the host and guest molecules, and (ii) MPIm is incorporated into the apolar cavity of the αCD on the basis of the upfield shifts of the proton signals for the 3- and 5-positions inside the αCD ring; Δppm = +0.075 and +0.049 for 3H and 5H, respectively. However, the magnitudes of these shifts were relatively small compared to the previously reported examples.[9] The molecular length of MPIm (9.5 Å) is longer than the depth of the αCD (6.7 Å), therefore, the ethylene moiety of MPIm may be located in the middle of the cyclic hexaglucopyranose. Hence, the ring current shift observed in the inner-H of αCD by the phenyl and imidazolyl groups is somewhat small. The FAB-MS also demonstrated a molecular-mass ion peak of αCD-MPIm at 1159.9 [M⁺]. The hydrophobic and dipole–dipole interactions are probably responsible for the driving force of this inclusion.[10] The MOPAC calculations suggested that the conformer, in which the phenyl ring of MPIm (4.2 Debye) is oriented to the secondary hydroxyl side (the narrower rim) of αCD (9.4 Debye), is energetically more favorable than the reverse one.

The addition of this αCD-MPIm ligand to the aqueous solution of 1a gave a five-N-coordinate Zn(II) complex (λmax: 430, 559, 594 nm). Although anionic tetraarylporphyrins are known to form 1:2 complexes with β-cyclodextrin, the cationic porphyrins have no interaction with any cyclodextrin family.[11] The binding constant of αCD-MPIm (K_B = 1.0 × 10² M⁻¹ in water) to 1a was nearly the same as that of the 1,2-dimethylimidazole (DMIm) (K_B = 0.9 × 10² M⁻¹), indicating that the αCD-complexation produced no effect on the axial imidazole association constant. The most remarkable observation in the αCD-MPIm binding to the Zn(II) center is inducing the rotation of the C–C bond between the meso-C and the pyridinium 1-C. In the ¹H NMR spectrum of 1a itself in D₂O, the signals of pyrrole β-H and the pyridinium 6-H appeared as a singlet at 8.85 and 9.25 ppm, respectively. On the contrary, after the αCD-MPIm coordination, they both became doublets and the pyridium 3-H signals significantly shifted upfield (Δppm: −0.12 ppm). Since the DMIm binding to 1a did not induce such
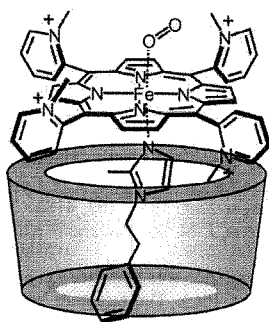

Fig. 1 The possible dominant αααβ structure of the dioxygenated 1c(αCD-MPIm) ensemble.

dramatic changes, we concluded that the bulky αCD-MPIm coordination influences the atropisomer equilibrium of **1a** in statistical distribution.[12] The chemical shifts for 2-CH₃ hydrogens of the pyridinium groups in **1a**(αCD-MPIm) might be more informative on which isomers exist,[7] but they were interfered with by the αCD signals.

The ferric **1b** was reduced to the corresponding ferrous complex (**1c**) in water by adding a two-fold molar excess of aqueous Na₂S₂O₄ under an N₂ atmosphere with αCD-MPIm. The UV-vis absorption spectrum showed the typical five-*N*-coordinate high-spin Fe(II) complex (λ_{max}: 431, 533, 562 nm).[3,4] However, upon exposure to O₂ gas, **1c**(αCD-MPIm) was oxidized to the ferric state even at low temperature (5 °C).

In a DMF–water (3/2, v/v) solution, the identical five-*N*-coordinate complex (λ_{max}: 435, 538, 564, 621 nm) of **1c**(αCD-MPIm) was formed under an N₂ atmosphere as well, and the obtained complex was stable in the range of 10 μM–1 mM at 5–40 °C (Fig. 2). After bubbling O₂ gas through this solution, the UV-vis absorption immediately changed to that of the O₂-adduct complex [λ_{max}: 422, 542, 570 (sh.) nm] at 5 °C.[3-5] This dioxygenation was sufficiently kinetically stable, and reversibly observed depending on the O₂ partial pressure. After the addition of CO, **1c**(αCD-MPIm) produced a very stable carbonyl complex [λ_{max}: 420, 535, 564 (sh.) nm]. The resulting O₂ and CO adduct species are both diamagnetic and the ¹H NMR spectra showed characteristics of $S = 0$.[13] Oxidation to the Fe(III)porphyrin slowly took place; the final product was the Fe(III)OH complex with a λ_{max} at 415 and 589 nm.[14] It is quite remarkable that the oxidation process obeyed first-order kinetics (half-life was *ca.* 40 min at 5 °C) even under a relatively low O₂-partial pressure (*ca.* 20 Torr) (Fig. 2 inset). The positively charged pyridinium groups at the porphyrin periphery could prevent μ-oxo dimer formation by an electrostatic repulsion. Neutral 5,10,15,20-tetraphenylporphyrinato-iron-(II)(αCD-MPIm) [FeTPP(αCD-MPIm)] rapidly oxidized after the O₂ bubbling under the same conditions. We considered that the αCD-MPIm coordination to the ααβ and αααα isomers of **1c** took place from the β-side of the porphyrin plane by steric hindrance to the 2-CH₃ groups of the pyridinium rings. As a result, there were at least two pyridinium cations surrounding the O₂-coordination site of **1c**(αCD-MPIm), and then the proton driven oxidation was retarded.

The three-dimensional structure of the dioxygenated **1c**(αCD-MPIm) ensemble was simulated by molecular dynamics calculations.[15] The significant properties of the architecture are: (i) MPIm penetrates the cavity of αCD and half of the imidazole- and phenyl-rings are forced out from the cyclic

hexaglucopyranose, which supports the ¹H NMR spectral data, (ii) the *meso*-pyridinium groups and the rim of the αCD bucket contact within the van der Waals distance, and (iii) the imidazole coordination angle does not distort and is identical to that observed in the same calculation for other dioxygenated FeTPP derivatives.

In conclusion, the non-covalently linked αCD-porphyrin ensemble consisting of the simple flat tetracationic-porphyrinato-iron(II) and αCD-penetrating proximal imidazole showed the following unique characteristics. (i) The synthetic yield of the architecture based on the porphyrin is in principle ≈ 100%. (ii) The O₂-adduct complex of **1c**(αCD-MPIm) is the first example of a new class of synthetic O₂-carrying hemoprotein models which is constructed by non-covalent bond formations. The molecular O₂ can bind from the aqueous side to the flat porphyrinato-iron(II) and no oxidation occurs in polar environment, because protons cannot reach the dioxygen active site. (iii) The obtained ensemble was easily dissociated by the addition of methanol, and each building block was withdrawn by gel column chromatography. Further investigations to evaluate the O₂-binding behavior of these porphyrin architectures are now underway.

Fig. 2 Visible absorption spectra of the **1c**(αCD-MPIm) ensemble and its O₂-, CO-adduct complexes in DMF–H₂O (3/2 v/v) solution at 5 °C. The inset demonstrates the first-order plots of the absorption decay at 542 nm (O₂-adduct species).

Notes and references

1 For a review, see: for example, *The Porphyrin Handbook*, ed. K. M. Kadish, K. M. Smith and R. Guilard, Academic Press, Oxford, 1999, vol. 4.

2 (*a*) Y. Kuroda, T. Hiroshige, T. Sera, Y. Shiroiwa, H. Tanaka and H. Ogoshi, *J. Am. Chem. Soc.*, 1989, **111**, 1912; (*b*) Y. Naruta, F. Tani and K. Maruyama, *Chem. Commun.*, 1990, 1378; (*c*) H.-Y. Zhang, A. Blasko, J.-Q. Yu and T. C. Bruice, *J. Am. Chem. Soc.*, 1992, **114**, 6621; (*d*) T. Sasaki and Y. Naruta, *Chem. Lett.*, 1995, 663; (*e*) J. P. Collman, M. Rapta, M. Bröring, L. Raptova, R. Schwenninger, B. Boitrel, L. Fu and M. L'Her, *J. Am. Chem. Soc.*, 1999, **121**, 1387.

3 M. Momenteau and C. A. Reed, *Chem. Rev.*, 1994, **94**, 659 and references therein.

4 (*a*) J. P. Collman and L. Fu, *Acc. Chem. Res.*, 1999, **32**, 455; (*b*) E. Tsuchida, T. Komatsu, S. Kumamoto, K. Ando and H. Nishide, *J. Chem. Soc., Perkin Trans. 2*, 1995, 747; (*c*) T. Komatsu, K. Sano and E. Tsuchida, *Chem. Commun.*, 1998, 977; (*d*) D. L. Jiang and T. Aida, *Chem. Commun.*, 1996, 1523; (*e*) A. Kossanyi, F. Tani, N. Nakamura and Y. Naruta, *Chem. Eur. J.*, 2001, **7**, 2862.

5 (*a*) E. Tsuchida, T. Komatsu, K. Arai and H. Nishide, *Chem. Commun.*, 1993, 730; (*b*) E. Tsuchida, T. Komatsu, K. Arai, K. Yamada, H. Nishide, C. Böttcher and J.-H. Fuhrhop, *Langmuir*, 1995, **11**, 1877; (*c*) T. Komatsu, M. Moritake, A. Nakagawa and E. Tsuchida, *Chem. Eur. J.*, 2002, **8**, in press.

6 J. B. Kim, A. D. Adler and F. R. Longo, in *The Porphyrins*, ed. D. Dolphin, Academic Press, New York, 1978, vol. 1, p. 85.

7 T. Kaufmann, B. Shamsai, R. S. Lu, R. Bau and G. M. Miskelly, *Inorg. Chem.*, 1995, **34**, 5073.

8 R. A. Freitag and D. G. Whitten, *J. Phys. Chem.*, 1983, **87**, 3918.

9 (*a*) L. Bender and M. Komiyama, in *Bioinorganic Chemistry*, ed. E. E. van Tameleon, Academic Press, New York, 1977, vol. I, ch. 2; (*b*)) Saenger, *Angew. Chem., Int. Ed. Engl.*, 1980, **19**, 344.

10 M. Kitagawa, H. Hoshino, M. Sakurai, Y. Inoue and R. Chujo, *Bull. Chem. Soc. Jpn.*, 1988, **61**, 4225.

11 K. Kono, N. Tanaka, H. Minamizono and Y. Kawakita, *Chem. Lett.*, 1996, 925.

12 R. Fiammengo, P. Timmerman, F. de Jong and D. N. Reinhoudt, *Chem. Commun.*, 2000, 2313.

13 J. P. Collman, J. I. Brauman, K. M. Doxsee, T. R. Halbert, E. Bunnenberg, R. E. Linder, G. N. LaMar, J. D. Gaudio, G. Lang and K. Spartalian, *J. Am. Chem. Soc.*, 1980, **102**, 4182.

14 D. Lexa, M. Momenteau, J.-M. Saveant and F. Xu, *Inorg. Chem.*, 1985, **24**, 122.

15 The esff forcefield simulation was performed using an Insight II system (Molecular Simulations Inc.). The structure was generated by alternative minimizations and annealing dynamic calculations from 298 to 100 K. Dielectric constant was fixed at 54.5 D, corresponding to DMF–H₂O (3/2 v/v) solution.
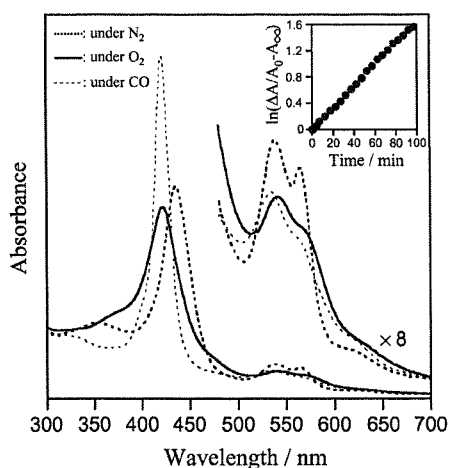
Synthetic Dioxygen-carrying Hemoprotein. Human Serum Albumin Including Iron(II) Complex of Protoporphyrin IX with an Axially Coordinated Histidylglycyl-propionate

Akito Nakagawa, Teruyuki Komatsu, Naomi Ohmichi, and Eishun Tsuchida*

Advanced Research Institute for Science and Engineering, Waseda University, 3-4-1 Okubo Shinjuku-ku, Tokyo 169-8555

Human serum albumin incorporating the iron(II) complex of protoporphyrin IX having an axially coordinated histidylglycyl-propionate formed a dioxygen-adduct complex in aqueous media (pH 7.3). The O_2-binding affinity ($P_{1/2}$) was 0.1 Torr at 25 °C.

Apomyoglobin spontaneously incorporates an iron(III) complex of protoporphyrin IX (hemin) and enable the prosthetic group to bind a dioxygen molecule (O_2).[1,2] Human serum albumin (HSA), the most abundant plasma protein in our blood stream, also captures a hemin dissociated from methemoglobin and accommodates it in the subdomain IB.[3,4] However, this HSA-hemin hybrid cannot form the O_2-adduct complex, even if one reduces the central ferric ion of the hemin to the ferrous state. We have shown that HSA including highly encumbered tetraphenylporphinato-iron(II) ($Fe^{2+}TPP$) derivatives can only bind and release O_2 under physiological conditions similar to hemoglobin (Hb) and myoglobin (Mb).[5] The prerequisites of these stable dioxygenations were believed to provide the $Fe^{2+}TPP$ structure with (i) steric hindrance around the O_2-binding site to prevent proton access, and (ii) a covalently bound proximal imidazole. More recently, we have found that the iron(II) complex of protoporphyrin IX having an axially coordinated histidylglycyl-propionate is also included into the HSA interior and forms an O_2-adduct in aqueous media at 25 °C. This communication reports for the first time the HSA hybrids incorporating natural protoheme IX derivatives as novel synthetic O_2-carrying hemoproteins.
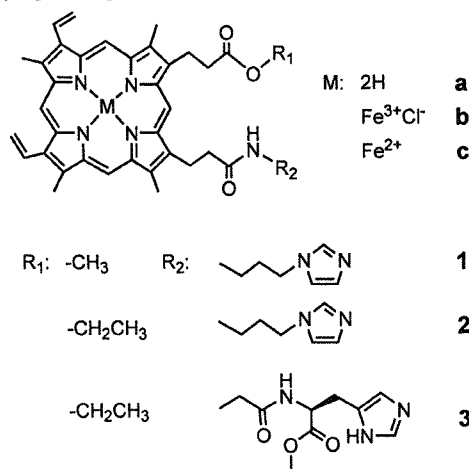
The free-base porphyrin of the pioneering Mb model, chelated heme 1a,[6] was synthesized by our one-pot reaction procedure using benzotriazol-1-yloxytris(dimethylamino)phosphonium hexafluorophosphate (BOP) at room temperature in pyridine. After the reaction, the mixture, when poured into excess water, led to precipitation of the crude product; the pyridine, water soluble BOP, and formed hexamethylphosphoramide were easily filtered off. Compound 2a with an ethyl propionate, and compound 3a having a histidylglycyl-propionate were also prepared in the same manner (Yield: 30%).[7] The iron insertion was performed using $FeCl_2$ in DMF to give the corresponding hemin derivatives. The analytical data of all compounds were satisfactorily obtained.[8]

The UV–vis absorption spectrum of the ferrous complex 3c (λ_{max}: 423, 533, 555 nm) in DMF showed the formation of the typical five-N-coordinated high-spin iron(II) complex as well as 1c and 2c. Upon the bubbling of O_2 gas through this solution, the UV–vis absorption immediately changed to that of the O_2-adduct complex (λ_{max}: 408, 540, 575 nm). The dioxygenated 3c transferred to the stable carbonyl species (λ_{max}: 419, 537, 568 nm) after the exposure of carbon monoxide (CO). The O_2-binding affinity ($P_{1/2}$) of 3c was determined to be 0.2 Torr in DMF solution, which is slightly lower (high affinity) than those of 1c and 2c ($P_{1/2}$: 0.3 Torr) (Table 1).[6d] The O_2-binding affinity normally elevates in proportion to an increase in the basicity of the trans-coordinated imidazole,[9] but histidine in 3c showed a smaller pK_a (6.0) in comparison to the value of 1-(acetoamidopropyl)imidazole (pK_a = 6.6) for 2c. The high O_2-binding affinity of 3c is presumably due to a favorable geometry of the imidazole bonding to the central iron, which was supported by the preliminary results on our molecular simulations of the dioxygenated 3c complex.[10]

The hybridization of HSA and the protoheme IX derivatives (molar ratio: 1/1) were carried out as follows. The ethanol solution of the carbonylated heme (1.6 mM, 50 µL) was slowly injected into the phosphate buffered solution (pH 7.3, 1 mM) of the recombinant HSA (rHSA)[11] (20 µM, 4 mL) under an argon atmosphere. The obtained aqueous solutions were stable for a few months without precipitation. The UV–vis absorption spectra of the rHSA-heme hybrids showed formation of the CO-ad-

Table 1. O_2-binding parameters of rHSA-protoheme IX derivatives at 25 °C

	pK_a	$P_{1/2}$ (Torr)		$\tau_{1/2}$ (min)
		in DMF	rHSA hybrid in water	rHSA hybrid in water
1c	6.6[a]	0.3	0.1	20
		0.3[b]	1.0[c]	—
2c	6.6[a]	0.3	0.1	50
3c	6.0[d]	0.2	0.1	90

[a]pKa value of 1-(acetoamidoprpoyl)imidazole in water (Ref. 6b), [b]Ref. 6d, [c]2% Aqueous myristyltrimethylammonium-bromide suspension (Ref. 6c). [d]pKa value of histidine in water.
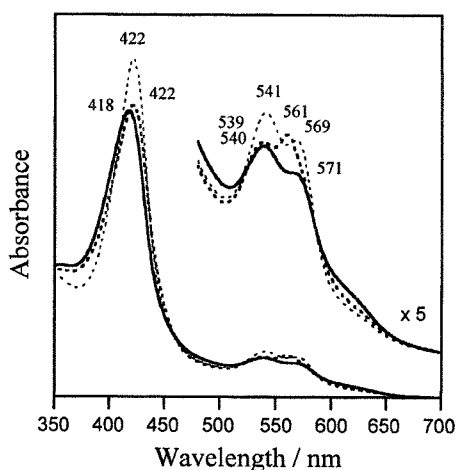
Figure 1. UV–vis absorption spectral changes of rHSA-**3c** in phosphate buffered solution (pH 7.3, 25 °C); under Ar: ----, under O₂: —, under CO: ······.

duct complexes (Figure 1). The binding number of protoheme IX derivative in one albumin molecule was confirmed to be one by assay of the each concentration and the relatively high binding constants of the hemes for rHSA (K_1: ca. $4 \times 10^6 \, \text{M}^{-1}$). The isoelectric points ($pI = 4.8$) and circular dichloism spectra of rHSA-hemes were identical to those observed for rHSA itself, which indicated that the surface net charges and second-order structure of rHSA host did not change after incorporation of the heme guest. Light irradiation of the carbonyl complex of rHSA–**3c** led to CO dissociation and a changing of spectrum, in which two peaks appeared in the Q band region; the resulting spectral shape resembles that of the six-coordinated low-spin mesoheme derivatives.[6b] This result implies that the sixth coordination site of **3c** is occupied by some amino acid residue of albumin. The spectral feature of rHSA–**1c** and rHSA–**2c** also showed the same trend.

Upon exposure of the rHSA–**3c** solution to O₂, the UV–vis absorption spectrum rapidly changed to that of the O₂-adduct complex (Figure 1). From the recent result on our crystal structural analysis of rHSA-hemin hybrid,[4] we infer that the protoheme derivatives **1c**, **2c**, and **3c** are also accommodated into the hydrophobic site of the subdomain IB, and it may contribute to their O₂-adduct complex formation. The O₂-binding affinity ($P_{1/2}$) of rHSA–**2c** and rHSA–**3c** were determined to be both 0.1 Torr. Accompanying the autooxidation of the central iron(II), the absorption band (λ_{max}: 540, 571 nm) slowly decreased, leading to the formation of the inactive protohemin. The half life-times ($\tau_{1/2}$) of the O₂-adduct species for rHSA–**2c** and rHSA–**3c** were 50 min and 90 min, respectively (Table 1). We concluded that the axially bound histydylglycyl-propionate to protoheme IX provided a more stable O₂-adduct compared to the imidazolyl one, and the ethyl propionate on the other side also contributed the increased stability for the dioxygenated complex relative to the methyl-propionate ($\tau_{1/2}$ of rHSA–**1c**: 20 min).

In conclusion, rHSA successfully incorporated protoheme IX derivatives with an intramolecularly coordinated proximal base, giving rHSA-heme hybrids, which form O₂ adducts at 25 °C. These are the first examples of the synthetic O₂-carrying

hemoproteins containing the natural protoheme IX derivative as a prosthetic group, which may also act as a very new class of artificial hemoprotein enzymes as well.

References and Notes
1   T. Hayashi, H. Dejima, T. Matsuo, H. Sano, D. Murata, and Y. Hisaeda, *J. Am. Chem. Soc.*, **124**, 11226 (2002).
2   S. Neya, K. Imai, H. Hori, H. Ishikawa, K. Ishimori, D. Okuno, S. Nakatomo, T. Hoshino, M. Hata, and N. Funasaki, *Inorg. Chem.*, **42**, 1456 (2003).
3   M. Wardell, Z. Wang, J. X. Ho, J. Robert, F. Ruker, J. Ruble, and D. C. Carter, *Biochem. Biophys. Res. Commun.*, **291**, 813 (2002).
4   P. A. Zunszain, J. Ghuman, T. Komatsu, E. Tsuchida, and S. Curry, "Protein Data Bank," code: 1O9X, paper in preparation.
5   a) T. Komatsu, K. Ando, N. Kawai, H. Nishide, and E. Tsuchida, *Chem. Lett.*, **1995**, 813. b) T. Komatsu, K. Hamamatsu, J. Wu, and E. Tsuchida, *Bioconjugate Chem.*, **10**, 82 (1999). c) E. Tsuchida, T. Komatsu, Y. Matsukawa, K. Hamamatsu, and J. Wu, *Bioconjugate Chem.*, **10**, 797 (1999). d) T. Komatsu. T. Okada, M. Moritake, and E. Tsuchida, *Bull. Chem. Soc. Jpn.*, **74**, 1695 (2001). e) T. Komatsu, Y. Matsukawa, and E. Tsuchida, *Bioconjugate Chem.*, **13**, 397 (2002).
6   a) W. S. Brinigar, C. K. Chang, J. Geibel, and T. G. Traylor, *J. Am. Chem. Soc.*, **96**, 5597 (1974). b) J. Geibel, J. Cannon, D. Chambell, and T. G. Traylor, *J. Am. Chem. Soc.*, **100**, 3575 (1978). c) T. G. Traylor, C. K. Chang, J. Geibel, A. Berzinis, T. Mincey, and J. Cannon, *J. Am. Chem. Soc.*, **101**, 6716 (1979). d) T. G. Traylor and P. S. Traulor, *Annu. Rev. Biophys. Bioeng.*, **11**, 105 (1982).
7   Glycyl-L-histidine methyl ester dihydrochloride was prepared according to the previously reported procedures [E. Monzani, L. Linati, L. Casella, L. D. Gioia, M. Favretto, M. Gullotti, and F. Chillemi, *Inorg. Chim. Acta*, **273**, 339 (1998)].
8   Spectoscopic data: **2a**; ¹H-NMR (500 MHz, CDCl₃) δ −3.6 (s, 2H, inner-H), 0.9 (t, -COO-CH₂CH₃, 3H), 1.1–1.5 (m, 2H, -CH₂CH₂-imidazole (Im)), 2.9–3.1 (m, -C(=O)NH-CH₂CH₂-, 2H), 3.1–3.3 (m, -CH₂CH₂COO-, 4H), 3.4–3.7 (m, porphyrin (por.)-CH₃, -CH₂CH₂-Im, 14H), 3.7–3.9 (m, -COO-CH₂CH₃, 2H), 4.1–4.4 (m, por.-CH₂-, 4H), 5.9–6.4 (m, vinyl =CH₂, 1m, 5H), 6.6 (d, 1m , 1H), 6.9 (s, 1m , 1H), 8.1–8.3 (m, vinyl-CH=, 2H), 9.8–10.1 (m, meso, 4H), FAB-MS (m/z): 698.4 [M-H⁺]. IR (cm⁻¹): 1650 (ν_C=O (amido)), 1732 (ν_C=O (ester)). UV–vis (CHCl₃) λ_max: 409, 509, 544, 580, 633 nm. **2b**; FAB-MS (m/z): 752.4 [M-Cl⁻]. IR (cm⁻¹): 1651 (ν_C=O (amido)), 1725 (ν_C=O (ester)). UV–vis (CHCl₃) λ_max: 406, 520, 578 nm. **3a**; ¹H-NMR (500 MHz, CDCl₃) δ −4.6 (s, 2H, inner-H), 2.7–2.9 (m, Im-CH₂-, 2H), 3.0–3.5 (m, por.-CH₃, -CH₂CH₂CONH-, -CH₂ CH₂-COO-CH₂CH₃, 18H), 3.6 (s, -CONH-CH₂CONH-, 2H), 4.0–4.3 (d, por.-CH₂, 4H), 4.3–4.5 (m, α-CH, 1H), 6.0–6.4 (m, vinyl =CH₂, 4H), 7.4 (s, 1m , 1H), 8.0–8.3 (m, vinyl-CH=, 1m, 5H), 9.8–10.0 (m, meso, 4H), FAB-MS (m/z): 785.4 [M-H⁺]. IR (cm⁻¹): 1635 (ν_C=O (amido)), 1725 (ν_C=O (ester)). UV–vis (CHCl₃) λ_max: 405, 505, 541, 577, 627 nm. **3b**; FAB-MS (m/z): 838.4 [M-Cl⁻]. IR(cm⁻¹): 1660 (ν_C=O (amido)), 1734 (ν_C=O (ester)). UV–vis (CHCl₃) λ_max: 388, 508, 637 nm.
9   D. V. Stynes, H. C. Stynes, B. R. James, and J. A. Ibers, *J. Am. Chem. Soc.*, **95**, 1796 (1973).
10 The esff forcefield simulation was performed using an Insight II system (Molecular Simulation Inc.). The structure was generated by alternative minimization and annealing dynamic calculation.
11 A. Sumi, W. Ohtani, K. Kobayashi, T. Ohmura, K. Tokoyama, M. Nishida, and T. Suyama, "Biotechnology of Blood Proteins," John Libbey Eurotext, Montrouge (1993), Vol. 227, p 293.

Molecular Energy and Electron Transfer Assemblies Made of Self-Organized Lipid-Porphyrin Bilayer Vesicles

Teruyuki Komatsu, Miho Moritake, and Eishun Tsuchida*[a]

Abstract: Novel molecular energy and electron transfer assemblies in vesicular form, which are made of self-organized amphiphilic porphyrins bearing phospholipid-like substituents (lipid-porphyrins), have been photochemically characterized. Tetraphenylporphyrin (TPP) derivatives with four dialkylphosphocholine groups [free-base (**1a**), Zn^{2+} complex (**1b**), and Fe^{3+} complex (**1c**)] are spontaneously associated in water to form spherical unilamellar vesicles with a diameter of 100–150 nm. Exciton calculations based on the bilayered sheet model of **1b**, which has a porphyrin packing similar to that seen in the triclinic unit cell of the Zn^{2+}TPP crystals, reproduced the Soret band bathochromic shift appearing in the aqueous solution of **1b** well. The UV/Vis absorption spectrum of the **1a/1b** hybrid vesicles (molar ratio: 1/1) showed no electronic interaction between the two porphyrin chromophores in the ground state, but efficient intermolecular singlet–singlet energy transfer took place from the excited **1b** donors to the **1a** acceptor within the vesicle. Near-field scanning optical microspectroscopy of the **1a/1b** vesicles on a graphite surface also showed only free-base porphyrin fluorescence. The efficiency of the energy transfer was 0.81 and the rate constant was $3.1 \times 10^9 \, s^{-1}$. On the other hand, protoporphyrin IX bearing two alkylphosphocholine propionates (**2**) was incorporated into the **1a** or **1c** bilayer vesicles (ca. 100 nm ϕ, molar ratio: **1a/2** or **1c/2** = 10). The UV/Vis absorption spectrum showed that **2** was successfully anchored into the fluid alkylene region of the membrane without stacking. Photoirradiation (λ_{ex}: 390 nm) of the **1c/2** vesicles in the presence of triethanolamine led a vectorial electron transfer from the outer aqueous phase to the membrane center, which allowed reduction of the ferric ion of the Fe^{3+}TPP platform.

Keywords: electron transfer · energy transfer · porphyrinoids · self-assembly · vesicles

Introduction

In nature, solar energy conversion is triggered by the capturing of sunlight by hundreds of chlorophyll arrays. That excited energy is funneled to a reaction center by an extremely efficient transfer of energy and is converted to chemical potential in the form of a long-lived charge-separated state.[1] To obtain insight into these natural light-harvesting events, numerous porphyrinoid arrays linked by covalent bonds have been synthesized.[2, 3] Nonetheless, general organic synthetic procedures did not allow the construction of a large-scale supramolecular architecture in which more than hundreds of metalloporphyrins are ordered with great regularity. Thus, noncovalent approaches could present considerable advantages.[4, 5] Furthermore, if we are to reproduce any biochemical reaction, the aqueous medium is particularly important. From these points of view, self-organized porphyrin assemblies have attracted attention as a potential light-harvesting antennae model in water. Whereas

porphyrin H-aggregates are generally quenched due to the large exciton couplings,[6] J-aggregated porphyrins show strong fluorescence.[7] One of the most significant examples of the emitting assemblies is our spherical bilayered vesicles made of amphiphilic tetraphenylporphyrin (TPP) with four phospholipid-like substituents (lipid-porphyrin, **1a**); its fluo-

M: 2H	1a
Zn^{2+}	1b
$Fe^{3+}Br^-$	1c
Fe^{2+}	1d
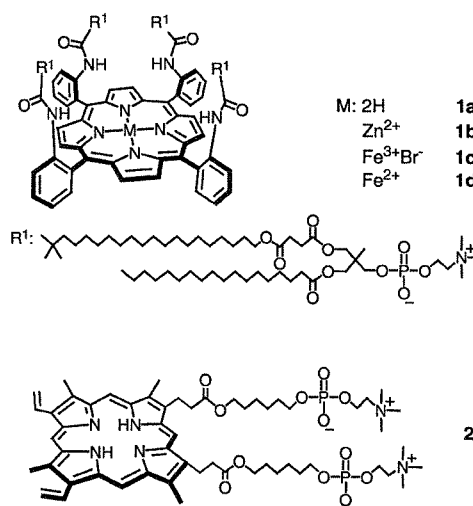
[a] Prof. E. Tsuchida, Dr. T. Komatsu, M. Moritake
Advanced Research Institute for Science and Engineering Waseda University, Tokyo 169-8555 (Japan)
Fax: (+81)3-3205-4740
E-mail: eishun@waseda.jp

rescence intensity remained 76 % of that of the monomer in organic solvent.[8] Herein, we report on novel bilayer vesicles consisting of two lipid-porphyrin ensembles [free-base (**1a**) and Zn^{2+} complex (**1b**)], in which an efficient singlet–singlet energy transfer took place based on the in-plane tightest packing of the porphyrin platforms. In addition, we present vectorial electron migration from the bulk aqueous phase to the membrane center of the Fe^{3+} complex lipid–porphyrin (**1c**) vesicles. The amphiphilic protoporphyrin IX (**2**) anchored into the highly oriented alkylchain region acts as an electron transfer mediator. Photoirradiation (λ_{ex}: 390 nm) under the coexistence of triethanolamine allowed reduction of the central ferric ions of the Fe^{3+} porphyrins and gave an O_2-coordinating ability to the vesicles.

Figure 2. UV/Vis absorption spectra of **1b** at 25 °C: a) in benzene/MeOH (4:1 v/v) (dotted line) and b) in water (solid line).

Results and Discussion

Nanostructure and fluorescence of the lipid-porphyrin vesicles: The newly synthesized Zn^{2+} complex of lipid-porphyrin **1b** was dispersed in deionized water by ultrasonication to give a pink-colored colloidal solution. Transmission electron microscopy (TEM) of the negatively stained and evaporated sample on a copper grid showed that **1b** forms spherical unilamellar vesicles with a diameter of 100–150 nm as well as the corresponding free-base porphyrin **1a** and the Fe^{3+} complex **1c** (Figure 1a).[8c] The thickness of the membrane
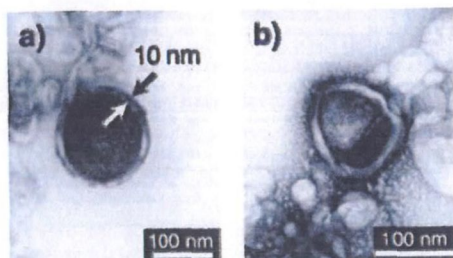

Figure 1. Transmission electron micrographs of evaporated aqueous solutions of a) **1b** and b) **1a/1b** ensemble (molar ratio: 1/1). The samples were negatively stained by uranylacetate.

was 10 nm, which is twice the molecular length of **1b** (4.6 nm). Most probably, the hydrophobic Zn^{2+}TPP platforms were arranged in two-dimensional planar sheets, which were stacked with a lateral displacement at the center of the membrane. It could be an identical conformation to that seen in the **1a** vesicles.[8c] The huge lipid-porphyrins (molecular weight over 4500) cannot produce a large curvature, so that they form giant unilamellar vesicles. This is in contrast to the fact that the usual phospholipids form small unilamellar vesicles (30–40 nm ϕ) by the same preparation.

The UV/Vis absorption spectrum of the aqueous solution of **1b** showed a porphyrin Soret band at 443 nm (ε_{max}: 2.7 × $10^5 M^{-1} cm^{-1}$), and its maximum was red shifted (+16 nm) compared to that of the monomer in benzene/MeOH (4:1 v/v) solution (λ_{max}: 427 nm) (Figure 2). On the contrary, the porphyrin Q bands remained essentially unaltered (only a 1 nm red shift). This larger bathochromic shift of the Soret
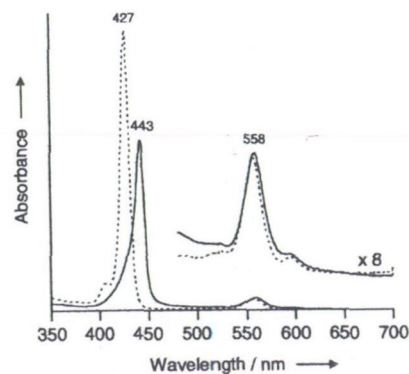
band should include excitonic interactions due to a lateral arrangement (J-aggregate) of the transition moments of the porphyrin chromophores.

We then did a quantitative analysis of the excitonic interactions of the bilayered Zn^{2+} porphyrin sheets according to our previously reported procedure.[8c] The simple point-dipole exciton coupling theory was employed,[9] and two hypotheses were postulated: 1) the tightest packing of the Zn^{2+}TPP moieties is realized within a rhomboidal lattice, which is observed in the triclinic unit cell of the single crystal of the unsolvated Zn^{2+}TPP (Figure 3, 2a: 2.6 nm, 2b: 1.48 nm),[10] and 2) the interlayer (d) of the face-to-face
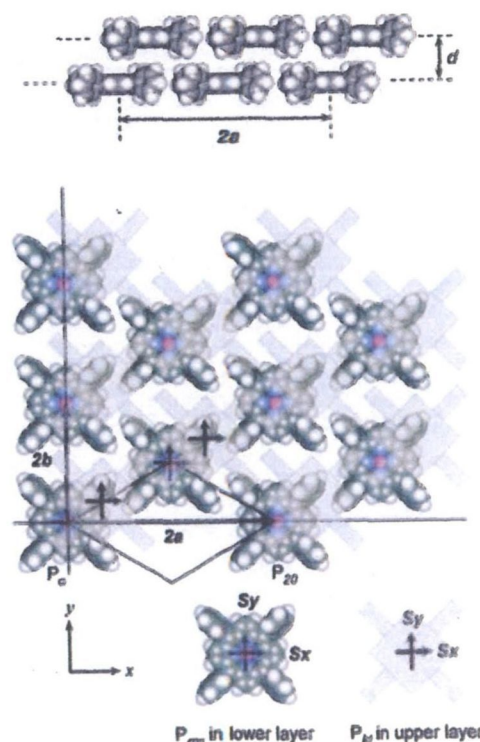

Figure 3. Predicted arrangements of the Zn^{2+}TPP platforms as a model for the bilayer membrane of **1b**. The porphyrin P_o is located at the origin of the coordinate axes.

stacking of the porphyrin sheets is 6.0 Å (Figure 3). The exciton interaction (ΔE) between the two porphyrins in the monolayer is given by Kasha's Equation (1).

$$\Delta E = M^2 r_{mn}^{-3} (1 - 3\cos^2\theta) \qquad (1)$$

M is the transition dipole moment of the Zn^{2+}TPP moiety in **1b** ($M^2 = 68.2\,D^2$),[11] r_{mn} is the center-to-center distance between the original porphyrin o (P_o) and the porphyrin mn (P_{mn}), and θ is the tilt angle between the line of centers and the molecular axes. Using the same strategy, we can estimate the exciton interactions between P_o and the porphyrin kl in the upper layer (P_{kl}).[12] These calculations eventually gave the total differences V and V' in two different Soret transitions S_x and S_y as -612.3 and $-239.0\ cm^{-1}$, respectively, that indicate split Soret peaks of 430.8 and 437.5 nm. The observed Soret band was definitely asymmetric, and it could be divided into two absorptions (438.5 and 441.4 nm). The small difference between the calculated λ_{max} and experimentally measured values is likely to be due to the van der Waals shift caused by the replacement of solvents. Thus, we can conclude that the absorption shift in the Soret band is describable by exciton interaction. Of course, the observed shift in the Soret band comes from the averaged interaction and involves some deviations, because of the fluidity of the membranes.

The most remarkable photophysical property of the lipid-porphyrin vesicles is their strong fluorescence in comparison to the other porphyrin aggregates.[6, 8c] The 3D excitation-emission spectrum of the aqueous **1b** solution showed that the fluorescence emission maxima (λ_{em}: 601, 653 nm) correlated with the absorption of the vesicles (λ_{max}: 443 nm) (not shown), which suggests that the fluorescence comes from the membrane and not the monomer dissociated from the aggregate. Single photon-counting fluorescence measurements were also done in air-equilibrated solution of **1b** vesicle. The fluorescence decay profile could be analyzed in terms of a single exponential process with a lifetime (τ_F) of 1.35 ns ($\kappa^2 = 1.14$), which was slightly shorter than the value of the **1b** monomer in benzene/MeOH (4:1 v/v) solution ($\tau_F = 2.0$ ns). The excited triplet states of the **1b** vesicles are too short to be observed by our nanosecond laser flash photolysis apparatus.

Energy transfer process within the lipid-porphyrin vesicles: Based on the exciton calculations, the alignment of the TPP planes in the free-base and the Zn^{2+} porphyrin vesicles would be identical. This result implies that they are able to produce homogeneous vesicular membranes. Indeed, the equivalent moles of **1a** and **1b** are spontaneously associated in water to yield spherical unilamellar vesicles with a diameter of 100–150 nm with a thickness of 10 nm (Figure 1b), in which the Zn^{2+} porphyrin should become the donor and the free-base porphyrin acts as the acceptor. The UV/Vis absorption spectrum of this **1a/1b** ensemble indicates that the spectral features are the sum of those from the individual lipid-porphyrin vesicles; it suggests no electronic interaction between **1a** and **1b** in the ground state (Figure 4). By contrast, its fluorescence spectrum is dramatically different from the superposition of those of the individual components. The **1a/1b** vesicles showed a decrease in fluorescence
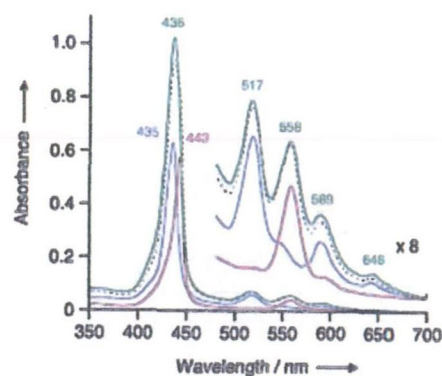

Figure 4. UV/Vis absorption spectra of **1a** vesicles (blue line), **1b** vesicles (red line), and **1a/1b** ensemble vesicles (molar ratio: 1/1, green line) in water at 25 °C. Black dotted lines represent the superposition of the spectra for **1a** and **1b**.

associated with the Zn^{2+} porphyrin and a corresponding increase in fluorescence associated with the free-base porphyrin (λ_{em}: 650, 712 nm) (Figure 5). Even on excitation at 558 nm, where the Zn^{2+} complex mainly absorbs (72 %), the emission spectral shape obviously demonstrated that of the
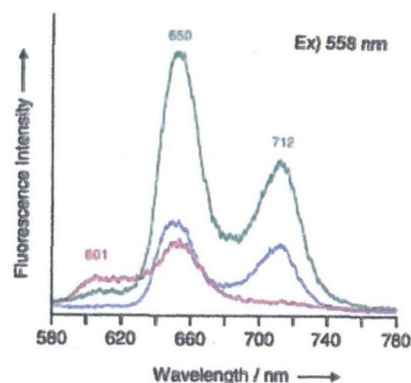

Figure 5. Steady-state fluorescence emission spectra of **1a** vesicles (blue line), **1b** vesicles (red line), and **1a/1b** ensemble vesicles (molar ratio: 1/1, green line) in water at 25 °C (Ex. 558 nm).

free-base porphyrin with stronger intensity by a factor of three. Because the fluorescence of the equivalent mixture of each vesicle solution displayed a simple sum of their spectra, efficient intermolecular singlet–singlet energy transfer could take place from the excited Zn^{2+} porphyrin donors to the statistically distributed free-base acceptor within the vesicles. Since the $\pi-\pi$ interactions between Zn porphyrins are usually somewhat stronger than those of the free-base porphyrins, there may not be a statistical dispersion of these two porphyrin chromospheres in the bilayer. However, for instance, the temperature dependence of the Soret band absorption maximum of the **1a/1b** vesicles showed a small hypsochromic shift at 56 °C, which suggests the gel-phase (liquid-crystal) transitions of the membrane. Very similar behavior was observed in the **1a** vesicles.[8a] This probably implied that the $\pi-\pi$ interactions between the Zn complexes are not so different from the free-bases in the lipid-porphyrin

-57-

vesicles. The fluorescence band of the donor considerably overlaps the acceptor absorption, therefore Förster-type excitation energy transfer would be preferable.[13]

The aqueous **1a/1b** vesicle solution was then transferred onto a graphite surface and subjected to near-field scanning optical microspectroscopy (NSOM). The bilayered membranes slowly flattened on the substrate during the water evaporation process. Unfortunately, the topology-mode measurements could not distinguish each 100 nm particle because of the low resolution. However, the dried vesicles still fluoresce on the solid surface and their emission was clearly detected by NSOM (Figure 6a). The fluorescence pattern of
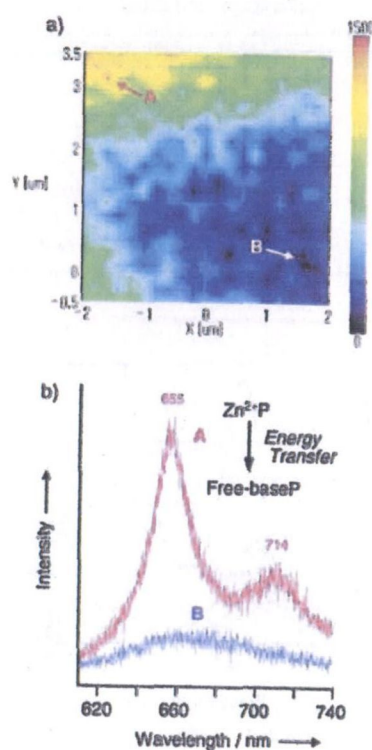

Figure 6. NSOM images of the evaporated aqueous solution of **1a/1b** ensemble vesicles (molar ratio: 1/1) on HOPG. a) fluorescence image of the flattened vesicles (4×4 μm, Ex. 442 nm, detection was effected at 650 nm), and b) fluorescence emission spectra of the flattened vesicles at the indicated parts [(A) and (B)] in the image a).

the collapsed **1a/1b** particles (λ_{em}: 655, 714 nm) was in good agreement with that of the free-base porphyrin [λ_{em}: 650, 712 nm, Figure 6b)]. Recently, Adams et al. reported interesting NSOM measurements of porphyrin thin films.[14] Our result is the first observation of an energy transfer molecular assembly made of amphiphilic porphyrin aggregates by the NSOM technique.

The fluorescence decay profile of this hybrid vesicle solution monitored at 610 nm became progressively triple-exponential with a faster decaying component being seen in addition to the original two slower kinetics ($\kappa^2 = 1.26$) (Figure 7). The longer lifetimes (6.73, 1.90 ns) are respectively assigned as those of **1a** and **1b**. The shorter-lived component (263 ps) is reflective of the singlet–singlet energy transfer
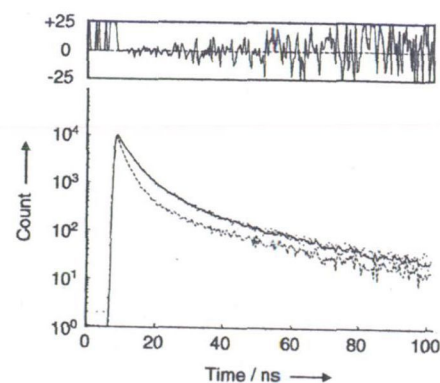

Figure 7. Time-correlated single-photon counting decay profile of **1a/1b** ensemble vesicles (molar ratio: 1/1, Ex. 558 nm, detection was effected at 610 nm). The curve is fitted to triple exponentials with lifetimes of 6.73 ns, 1.90 ns, and 263 ps ($\kappa^2 = 1.26$).

from the excited Zn^{2+} porphyrin to the free-base porphyrin within the vesicles. The rate constants for intermolecular energy transfer (k_{ET}) have been calculated from Equation (2).

$$k_{ET} = 1/\tau_{FB/Zn} - 1/\tau_{Zn} \qquad (2)$$

$\tau_{FB/Zn}$ is the measured fastest component of the excited **1a/1b** vesicles and τ_{Zn} is the lifetime of the **1b** vesicles. The k_{ET} value was 3.1×10^9 s^{-1}. The efficiency of this energy transfer (Φ_{ET}) could be determined to be 0.81 from Equation (3).[15]

$$\Phi_{ET} = k_{ET}/[k_{ET} + (1/\tau_{Zn})] \qquad (3)$$

This non-covalently constructed **1a/1b** architecture showed relatively larger k_{ET} and Φ_{ET} than the values of the free-base/Zn^{2+} porphyrin dimers linked by covalent or hydrogen bonding.[2–5, 13] From the molecular area for lipid-porphyrin (2.2 nm^2), one vesicle (100 nm ϕ) is considered to consist of 23000 porphyrin molecules.[8c] To the best of our knowledge, this is the largest molecular energy transfer assembly made of self-organized porphyrin in water. For the triplet-state process, the transient difference absorption recorded in outgassed aqueous solution of the **1a/1b** vesicles did not show any significant peaks after the laser flash photolysis.

Electron transfer process of the lipid-porphyrin vesicles: In the lipid-porphyrin vesicles, the J-aggregated TPP platforms settled under the hydrophobic barrier of 4 nm thickness, and were not sensitive to the addition of a water-soluble electron acceptor or electron donor from the bulk aqueous phase. In fact, the fluorescence intensity of the **1a** or **1b** vesicles was not quenched at all by addition of electron acceptors; N,N'-methyl-4,4'-bipyridinium dichrolides and N,N'-benzyl-4,4'-bipyridinium dichrolides in the concentration range 0 to 2 mM. Since none of the quencher molecules caused a spectroscopic shift of the porphyrin absorption bands, there is no π-overlap between the electron accepting molecules and donating porphyrins. Attempting to reduce the Fe^{3+}TPP planes in the **1c** vesicles by addition of ascorbic acid also failed. These results imply that water-soluble molecules cannot enter the membrane interior. It is, therefore, certain

-58-

that the membrane properties should be modified to realize electron communications through the lipid-porphyrin membranes. Over the past few decades, substantial efforts have also been directed towards embedding two different porphyrins geometrically in phospholipid liposomes,[6f, 16] but the location of each co-factor is not always very accurate because of the low guest-to-host ratio in the membranes.

The free-base porphyrin **1a** was coassembled with protoporphyrin IX (PPIX) bearing two alkylphosphocholine propionates (**2**) (molar ratio: **1a/2** = 10), to give similar round vesicles. Although porphyrin **2** itself produced very thin monomolecular fibers in water (Figure 8a),[6d] the TEM observation showed only spherical unilamellars (ca. 100 nm
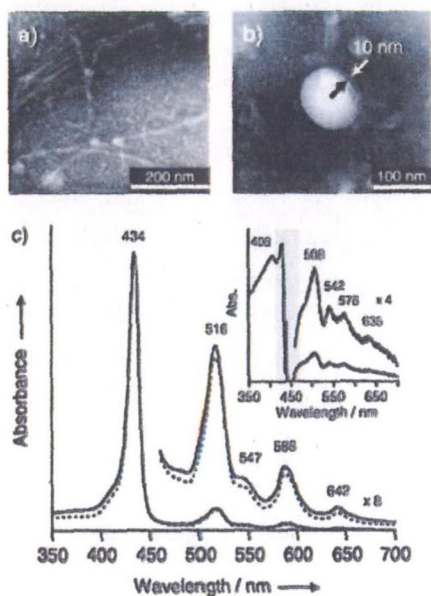
Figure 8. Transmission electron micrographs of the evaporated aqueous solutions of a) **2** and b) the **1a/2** ensemble (molar ratio: **1a/2** = 10); c) UV/Vis absorption spectra of **1a** vesicles (dotted line) and **1a/2** ensemble vesicles (solid line) in water at 25 °C. The inset shows a different spectrum for both solutions, in which the absorption maxima coincided with those of the DPPC vesicles incorporating **2** (molar ratio: DPPC/2 = 40/1) in water.

ϕ) (Figure 8b). No fibrous aggregate was detectable and the membrane did not become thicker. Increasing the amount of **2** (molar ratio: **1a/2** < 5) led to deformation of the morphology into small micelles and fibers. The subtracted difference absorption spectrum of the **1a/2** hybrids minus the homogeneous **1a** vesicles showed λ_{max} at 408, 508, 542, 578, and 635 nm (Figure 8c inset). Unfortunately, the disturbance interfered with the Soret band region. It coincided with the absorption maxima of an aqueous solution of phospholipid liposomes (ex. 1,2-dipalmytoyl-3-*sn*-glycerophosphocholine (DPPC)) incorporating **2** (molar ratio: DPPC/2 = 40, λ_{max}: 408, 509, 542, 579, and 634 nm). We concluded that **2** was homogeneously trapped into the highly oriented alkylene region of the **1a** vesicles without stacking. It may be presumed with certainty that the protoporphyrin macrocycle was anchored at the middle of the monolayer perpendicular to the membrane surface [see space-filling model in Figure 9b].
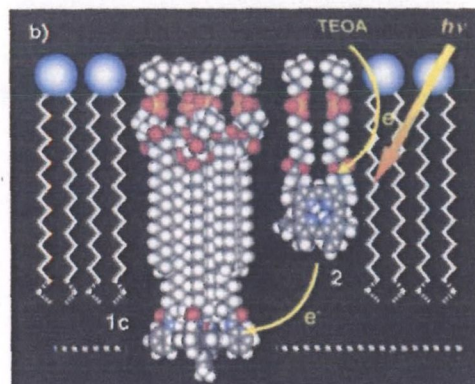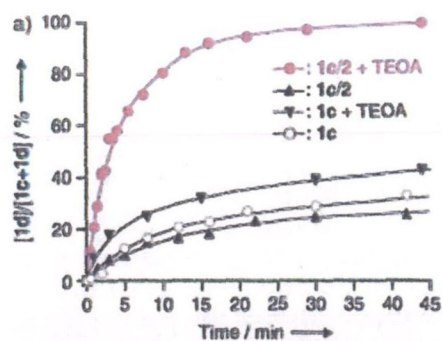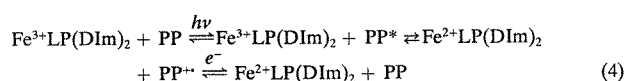
Figure 9. a) Photoreduction of $Fe^{3+}TPP$ moieties of **1c/2/DIm** vesicles in aqueous phosphate buffer (pH 7.3) at 25 °C. b) The schematic representation of the **1c/2/DIm** monolayer membrane interior using the space-filling model for the each compound (DIm is replaced by 1-methylimidazole for clarification).

In the vesicles of the Fe^{3+} complex **1c** including free-base **2** (molar ratio: **1c/2** = 10), the fluorescence of the protoporphyrin chromophore was completely quenched. This decrease in the emission would be ascribed to the intermolecular electron transfer from the excited singlet state of **2** to **1c** within the vesicles. The Fe^{3+} porphyrins are *d*-typed hyperporphyrins with an extremely short lifetime of the excited state and no fluorescence. This quenching cannot be interpreted in terms of a static mechanism and is assumed to be due to oxidative quenching. An attempt to observe the time-resolved difference spectrum of the **2** cation radical was unsuccessful, because the absorption intensity of the protoporphyrin **2** was rather low, and the reaction rate was beyond the resolution of our apparatus. The excited triplet state of **2** may also be populated by means of intersystem crossing from the singlet state, which occurs in competition with the electron transfer, but the triplet–triplet absorption of **2** was not seen in the 500–900 nm region.

The coexistence of a small excess of 1-dodecylimidazole (DIm) as an axial base for the Fe^{3+} complex **1c** did not cause morphological changes in the vesicular configuration. The UV/Vis spectrum of the **1c/2/DIm** (molar ratio: 1/0.1/3) showed maxima at 544 and 575 nm, indicating that the dominant species of **1c** is a six-coordinate ferric complex with the axially bound bis-imidazole of DIm.[17] Under an argon atmosphere, the 390 nm (Soret band of **2**) photoirradiation of the **1c/2/DIm** vesicles with triethanolamine (TEOA) in the outer aqueous phase led to efficient and

-59-

irreversible reduction of the ferric ion of **1c**; the visible absorption spectrum changed to the typical six-*N*-coordinated low-spin Fe^{2+} complex (λ_{max}: 436, 538, and 568 nm).[8c, 18] The isosbestic points (534 and 562 nm) throughout the measurement revealed that no side reaction occurred. The following results indicate that the photoreduction of **1c** takes place through the intermolecular electron transfer initiated by excitation of **2**; 1) in the absence of TEOA or **2**, the reduction proceeded by less than 40% (Figure 9a), 2) irradiation of the Soret band of **1c** also reduced the ferric center, but by less than 30%. Photoirradiation of the Soret band of **2** causes only the efficient reduction of **1c**, and TEOA acts as a sacrificial reagent to reduce the cation radical of **2**. The protoporphyrin anchors successfully serve as an electron transfer mediator, and the space-filling model of the **1c/2/DIm** hybrid demonstrated well our supposed structure (Figure 9b). The overall process of this reaction is expressed by Equation (4), where LP is lipid-porphyrin and PP is the protoporphyrin moiety of **2**.

$$Fe^{3+}LP(DIm)_2 + PP \overset{h\nu}{\rightleftharpoons} Fe^{3+}LP(DIm)_2 + PP^* \rightleftharpoons Fe^{2+}LP(DIm)_2$$
$$+ PP^{+\cdot} \overset{e^-}{\rightleftharpoons} Fe^{2+}LP(DIm)_2 + PP \qquad (4)$$

After reduction of **1c**, the membrane-trapped protoporphyrin becomes more hydrophilic and may be close enough to the bulk aqueous phase to accept an electron.

Upon exposure of the aqueous solution of the photoreduced **1d/2/DIm** vesicles to O_2, the UV/Vis absorption spectrum immediately changed to that of the corresponding O_2-adduct complex (λ_{max}: 435, 543 nm). This dioxygenation was observed to be reversibly dependent on the O_2-partial pressure the same as in our previous reported **1d/DIm** vesicles.[8c]

Conclusions

The perfectly round bilayer vesicles made of self-organized lipid-porphyrin **1a/1b** ensembles are the first molecular energy transfer assemblies with a diameter of over 100 nm in water. Singlet energy transfer occurs with a rate constant of 3.1×10^9 s^{-1} and with 81% efficiency. The non-covalently aligned J-aggregate porphyrins described herein have been shown to represent an effective approach to constructing a new class of light-harvesting antennae models in aqueous media. Indeed, effective optical cross-section per **1b** molecule in the vesicles at 558 nm is 0.73 Å^2, which is identical to that observed in benzene/MeOH homogeneous solution.[19] The 23 000 porphyrin active sites are densely packed in the vesicles and isolated from the bulk aqueous solution; therefore electron communications to the outside of the membrane have some difficulties. However, anchoring of the protoporphyrin electron-mediator to the monolayer immediately permits funneling an electron by light irradiation, and it gave a hemoglobin-like property—reversible O_2-binding activity—to the vesicles. New investigations of a photoinduced charge separation process with an external electron acceptor and light-controllable heme catalytic reactions in these supramolecular lipid-porphyrin architectures are now being undertaken.

Experimental Section

Materials and apparatus: The synthetic methods for lipid-porphyrins (**1a**, **1c**, **2**) are described elsewhere.[8c, 6d] The Zn^{2+} complex **1b** was synthesized by the insertion of zinc into the free-base lipid-porphyrin **1a** using $Zn(OAc)_2$ in MeOH solution (yield: 85%). Triethanolamine, *N,N'*-methyl-4,4'-bipyridinium dichlorides, and *N,N'*-benzyl-4,4'-bipyridinium dichlorides of high-purity grade were used without further purification. UV/Vis absorption spectra were recorded on a JASCO V-570 spectrophotometer, and steady state fluorescence spectra were obtained from a HITACHI F-4500 spectrofluorometer. All these measurements were normally carried out at 25°C.

Preparation of aqueous lipid-porphyrin solutions:

a) Lipid-porphyrin (1a, 1b, 1a/1b) solutions: A benzene/methanol stock solution of **1a** or **1b** (50—100 μL, 1.0 mM) was placed in a 5 mL round-bottom flask and slowly condensed using a rotary evaporator under reduced pressure, affording a thin film of the porphyrin at the bottom. The film was then dried in vacuo for 3 h; deionized water (5 mL) heated at 60°C was slowly injected. The mixture was homogenized by vortex mixing with several small glass beads (ca. 10 pieces) and shortly sonicated by a bath-type ultrasonicator. The obtained solution (10–20 μM) was incubated for 6 h at room temperature before use. The hybridized **1a/1b** solution was also prepared in the same manner.

b) Lipid-porphyrins 1a/2 and 1c/2/1-dodecylimidazole (DIm) hybrid solutions: A benzene/methanol stock solution of **1a** (100 μL, 1.0 mM) and methanol solution of **2** (10 μL, 1.0 mM) were slowly condensed by using a rotary evaporator under reduced pressure as described above, giving a hybrid thin-film at the bottom of the flask. The film was dried *in vacuo* for 3 h and phosphate buffer (pH 7.3, 1 mM, 5 mL) heated at 60°C was added. Homogenization by a tip-type ultrasonicator (60 mW, 3 min) in a water bath provided a pale orange solution ([**1a**] = 20 μM), which was incubated for 12 h at room temperature. The hybrid lipid-porphyrin **1c/2/DIm** (molar ratio: 1/0.1/3, [**1c**] = 20 μM) was also prepared by the same procedures.

Transmission electron microscopy (TEM): The negatively stained specimens for TEM were prepared as in previously reported procedures.[7c, 8b] The Cu grid surfaces were treated for a short period (5 s) by glow discharge using a JEOL HDF-400 to form a hydrophilic plane just before use. The obtained grids with the evaporated sample were observed in a JEOL JEM-100CX electron microscope at an acceleration voltage of 100 kV.

Exciton calculation: The overall excitonic interaction in the $Zn^{2+}TPP$ bilayer model of **1b** was calculated based on our previously reported methods.[8c]

Near-field scanning optical microspectroscopy (NSOM): A droplet of **1a/1b** vesicle solution (20 μM) was pipetted onto freshly-cleaved highly-oriented pyrolytic graphite (HOPG STM-1, Advanced Ceramics Co.). After 1 min, excess fluid was carefully blotted off with filtration paper and the surface air-dried for another 30 min. NSOM measurements were carried out using a JASCO NFS-230 Scanning Near-Field Optical Microspectrometer in the illumination collection mode under ambient laboratory conditions. The samples were excited by a He-Cd laser (442 nm) with 0.1 mW intensity for 0.5 s, and the diameter of the light probe was 400 nm. Imaging was performed by displaying the fluorescence signal and the height signal simultaneously for 4 × 4 μm (21 × 21 points).

Excited-state lifetimes: Singlet lifetimes of the lipid-porphyrin vesicles were measured by using a HORIBA NAES-500 nanosecond fluorometer with an N_2 lamp (excitation side multicavity filter: ASAHI SPECTRA MZ0560, $\lambda = 560 \pm 2$ nm; emission side multicavity filter: MZ0610, $\lambda = 610 \pm 2$ nm). The samples were held in a cuvette (optical path length, 10 mm). The concentration of the lipid-porphyrin was 9.5 μM, and experiments were carried out at 25°C. Triplet lifetime measurements on a nanosecond time scale were performed by using a Unisoku TSP-600 time-resolved spectrophotometer system with a Continuum Surelite I-10 Q-switched Nd-YAG laser, which generated a second-harmonic (532 nm) pulse of 6 ns duration with an energy of 200 mJ per pulse (10 Hz).

Steady-state electron-transfer from excited 2 to 1c: Continuous light irradiations were performed with an ORIEL 450 W xenon arc-lamp model 66021 under an argon atmosphere (25°C). The **1c** solution was deaerated by argon bubbling before photoirradiation. The light was filtered with cutoff filter (HOYA UV-32) and a multicavity filter (ASAHI SPECTRA

MY0390, $\lambda = 390 \pm 2$ nm) to isolate the desired wavelength region. The filtered light was irradiated into a solution of the **1c**/DIm (molar ratio: 1/3) vesicles or **1c**/**2**/DIm vesicles (molar ratio: **1c**/**2**/DIm = 1/0.1/3) with (or without) triethanolamine (64 mM) contained in a 10 mm cuvette at a distance of 140 mm from the center of the light source. The UV/Vis absorption spectra of the solution were measured at regular intervals. The photoreduction of **1c** to the ferrous complex **1d** was monitored by the time dependence of the absorption intensity at 538 nm, which is based on the bisimidazole coordinated Fe^{2+} complex. In order to obtain a spectrum of the completely reduced ferrous **1d**/**2**/DIm vesicles, an aqueous sodium dithionate solution (25 mM, 40 µL) was added to the **1c**/**2**/DIm vesicle solution at 60 °C.

Acknowledgements

[1] a) J. Deisenhofer, O. Epp, K. Miki, R. Huber, H. Michel, *Nature* **1985**, *318*, 618–624; b) G. Feher, J. P. Allen, M. Y. Okamura, D. C. Rees, *Nature* **1989**, *339*, 111–116; c) G. McDermott, S. M. Prince, A. A. Freer, A. M. Hawthornthwaite-Lawless, M. Z. Papiz, R. J. Cogdell, N. W. Isaacs, *Nature* **1995**, *374*, 517–521; d) S. M. Prince, M. Z. Papiz, A. A. Freer, G. McDemott, A. M. Hawthornthwaite-Lawless, R. J. Codgell, N. W. Isaacs, *J. Mol. Biol.* **1997**, *268*, 412–423; e) J. M. Olson, *Photochem. Photobiol.* **1998**, *67*, 61–75.

[2] a) M. R. Wasielewski, *Chem. Rev.* **1992**, *92*, 435–461; b) J. K. M. Sanders in *The Porphyrin Handbook, Vol. 3, Inorganic, Organometallic and Coordination Chemistry* (Eds.: K. M. Kadish, K. M. Smith, R. Guilard), Academic Press, New York, **1999**, Chapter 22.

[3] Examples of covalently bound multiporphyrinic assemblies made of more than three porphyrin units: a) S. Anderson, H. L. Anderson, A. Bashall, M. McPartlin, J. K. M. Sanders, *Angew. Chem.* **1995**, *107*, 1196–1200; *Angew. Chem. Int. Ed. Engl.* **1995**, *34*, 1096–1099; b) C. C. Mak, N. Bampos, J. K. M. Sanders, *Angew. Chem.* **1998**, *110*, 3169–3172; *Angew. Chem. Int. Ed.* **1998**, *37*, 3020–3023; c) H. A. M. Biemans, A. E. Rowan, A. Verhoeven, P. Vanoppen, L. Latterini, J. Foekema, A. P. H. J. Schenning, E. W. Meijer, F. C. de Schryver, R. J. M. Nolte, *J. Am. Chem. Soc.* **1998**, *120*, 11054–11060; d) M. G. H. Vicente, M. T. Cancilla, C. B. Lebrilla, K. M. Smith, *Chem. Commun.* **1998**, 2355–2356; e) A. Nakano, A. Osuka, I. Yamazaki, T. Yamazaki, Y. Nishimura, *Angew. Chem.* **1998**, *110*, 3172–3176; *Angew. Chem. Int. Ed.* **1998**, *37*, 3023–3027; f) N. Aratani, A. Osuka, Y.-H. Kim, D.-H. Jeong, D. Kim, *Angew. Chem.* **2000**, *112*, 1517–1521; *Angew. Chem. Int. Ed.* **2000**, *39*, 1458–1462; g) J. Li, A. Ambroise, S.-I. Yang, J. R. Diers, J. Seth, C. R. Wack, D. F. Bocian, D. Holten, J. S. Lindsey, *J. Am. Chem. Soc.* **1999**, *121*, 8927–8940; h) M.-S. Choi, T. Aida, T. Yamazaki, I. Yamazaki, *Angew. Chem.* **2001**, *113*, 3294–3298; *Angew. Chem. Int. Ed.* **2001**, *40*, 3194–3198; i) S. Rucareanu, O. Mongin, A. Schuwey, N. Hoyler, A. Gossauer, *J. Org. Chem.* **2001**, *66*, 4973–4988.

[4] J. L. Sessler, B. Wang, S. L. Spring, C. T. Brown in *Comprehensive Supramolecular Chemistry, Supramolecular Reactivity and Transport: Bioorganic Systems, Vol. 4* (Eds.: J.-M. Lehn, J. L. Atwood, J. E. D. Davies, D. D. MacNicol, F. Vögtle, Pergamon), Oxford, **1996**, pp. 311–336.

[5] Examples of noncovalently bound multiporphyrinic assemblies made of more than three porphyrin units: a) A. M. Brun, S. J. Atherton, A. Harriman, V. Heitz, J.-P. Sauvage, *J. Am. Chem. Soc.* **1992**, *114*, 4632–4639; b) M. Linke, J.-C. Chambron, V. Heitz, J.-P. Sauvage, S. Encinas, F. Barigelletti, L. Flamigni, *J. Am. Chem. Soc.* **2000**, *122*, 11834–11844; c) J. L. Sessler, B. Wang, A. Harriman, *J. Am. Chem. Soc.* **1995**, *117*, 704–714; d) H. L. Anderson, *Inorg. Chem.* **1994**, *33*, 972–981; e) G. S. Wilson, H. L. Anderson, *Chem. Commun.* **1999**, 1539–1540; f) C. A. Hunter, R. K. Hyde, *Angew. Chem.* **1996**, *108*, 2064–

2067; *Angew. Chem. Int. Ed. Engl.* **1996**, *35*, 1936–1939; g) R. A. Haycock, A. Yartsev, U. Michelson, V. Sundström, C. A. Hunter, *Angew. Chem.* **2000**, *112*, 3762–3765; *Angew. Chem. Int. Ed.* **2000**, *39*, 3616–3619; h) P. Ballester, R. M. Gomila, C. A. Hunter, A. S. H. King, L. J. Twyman, *Chem. Commun.* **2003**, 38–39; i) C. M. Drain, K. C. Russel, J.-M. Lehn, *Chem. Commun.* **1996**, 337–338; j) J. Fan, A. Whiteford, B. Olenyuki, M. D. Levin, P. J. Stang, E. B. Fleischer, *J. Am. Chem. Soc.* **1999**, *121*, 2741–2752; k) A. Prodi, M. T. Indelli, C. J. Kleverlaan, F. Scandola, E. Alessio, T. Gianferrara, L. G. Marzilli, *Chem. Eur. J.* **1999**, *5*, 2668–2679; l) N. Maruo, M. Uchiyama, T. Kato, T. Arai, H. Akisada, N. Nishino, *Chem. Commun.* **1999**, 2057–2058; m) K. Ogawa, Y. Kobuke, *Angew. Chem.* **2000**, *112*, 4236–4239; *Angew. Chem. Int. Ed.* **2000**, *39*, 4070–4073; n) C. C. Mak, N. Bampos, S. L. Darling, M. Montalti, L. Prodi, J. K. M. Sanders, *J. Org. Chem.* **2001**, *66*, 4476–4486; o) M. Sakamoto, A. Ueno, H. Mihara, *Chem. Eur. J.* **2001**, *7*, 2449–2458; p) S. Yagai, T. Miyatake, H. Tamiaki, *J. Org. Chem.* **2002**, *67*, 49–58.

[6] R. Guilard, N. Senglet, Y. H. Liu, D. Sazou, E. Findsen, D. Fanre, T. D. Courieres, K. M. Kadish, *Inorg. Chem.* **1991**, *30*, 1898–1905; b) J.-H. Fuhrhop, C. Demoulin, C. Böttcher, J. Köning, U. Siggel, *J. Am. Chem. Soc.* **1992**, *114*, 4159–4165; c) J.-H. Fuhrhop, U. Bindig, U. Siggel, *J. Am. Chem. Soc.* **1993**, *115*, 11036–11037; d) E. Tsuchida, T. Komatsu, N. Toyano, S. Kumamoto, H. Nishide, *J. Chem. Soc. Chem. Commun.* **1993**, 1731–1733; e) T. Komatsu, K. Arai, H. Nishide, E. Tsuchida, *Chem. Lett.* **1993**, 1949–1952; f) T. Komatsu, E. Tsuchida, C. Böttcher, D. Donner, C. Messerschmidt, U. Siggel, W. Stocker, J. P. Rabe, J.-H. Fuhrhop, *J. Am. Chem. Soc.* **1997**, *119*, 11660–11665; g) C. Schell, H. K. Hombrecher, *Chem. Eur. J.* **1999**, *5*, 587–598; h) K. Kano, K. Fukuda, H. Wakami, R. Nishiyabu, R. F. Pasternack, *J. Am. Chem. Soc.* **2000**, *122*, 7494–7502; i) N. Nagata, S. Kugimiya, Y. Kobuke, *Chem. Commun.* **2001**, 689–690.

[7] a) T. Komatsu, K. Nakao, H. Nishide, E. Tsuchida, *J. Chem. Soc., Chem. Commun.* **1993**, 728–730; b) E. Tsuchida, T. Komatsu, K. Arai, K. Yamada, H. Nishide, C. Böttcher, J.-H. Fuhrhop, *Chem. Commun.* **1995**, 1063–1064; c) T. Komatsu, K. Yamada, E. Tsuchida, U. Siggel, C. Böttcher, J.-H. Fuhrhop, *Langmuir* **1996**, *12*, 6242–6249; d) T. Komatsu, T. Yanagimoto, E. Tsuchida, U. Siggel, J.-H. Fuhrhop, *J. Phys. Chem. B* **1998**, *102*, 6759–6765; e) T. Komatsu, T. Yanagimoto, Y. Furubayashi, J. Wu, E. Tsuchida, *Langmuir* **1999**, *15*, 4427–4433.

[8] a) E. Tsuchida, T. Komatsu, K. Arai, H. Nishide, *J. Chem. Soc., Chem. Commun.* **1993**, 730–732; b) E. Tsuchida, T. Komatsu, K. Arai, K. Yamada, H. Nishide, C. Böttcher, J.-H. Fuhrhop, *Langmuir* **1995**, *11*, 1877–1884; c) T. Komatsu, M. Moritake, A. Nakagawa, E. Tsuchida, *Chem. Eur. J.* **2002**, *8*, 5469–5480.

[9] a) E. G. McRae, M. Kasha, *J. Chem. Phys.* **1958**, *28*, 721–722; b) M. Kasha, *Radiation Res.* **1963**, *20*, 51–71.

[10] a) M. P. Byrn, C. J. Curtis, I. Goldberg, Y. Hsiou, S. I. Khan, P. A. Sawin, S. K. Tendick, C. E. Strouse, *J. Am. Chem. Soc.* **1991**, *113*, 6549–6557; b) M. P. Byrn, C. J. Curtis, Y. Hsiou, S. I. Khan, P. A. Sawin, S. K. Tendick, A. Terzis, C. E. Strouse, *J. Am. Chem. Soc.* **1993**, *115*, 9480–9497.

[11] The transition dipole moment was calculated by integrating plots of exciton coefficient divided by wavenumber, $\varepsilon(\nu)/\nu$, versus wavenumber ν and applying the equation $M^2 = 9.19 \times 10^{-3} \int [\varepsilon(\nu)/\nu] d\nu$, where M is the transition dipole moment in units of Debye.

[12] Based on the structural data reported by Strauce et al. (ref. [10]), the porphyrin core in the upper layer is supposed to locate on the +4.0, +2.7, and +4.1 Å shifts in the x, y, z directions from the center of each nearest pair in the layer below. The distances and angles from the porphyrin o to the neighbors P_{ki} in the upper layer were estimated. We then calculated all the interactions of these porphyrin pairs (total: 46 combinations), but stopped summation at a distance of some 5 nm.

[13] a) F. P. Schwarz, M. Gouterman, Z. Muljiani, D. H. Dolphin, *Bioinorg. Chem.* **1972**, *2*, 1–32; b) R. L. Brookfield, H. Ellul, A. Harriman, G. Porter, *J. Chem. Soc. Faraday Trans. 2* **1986**, *82*, 219–233; c) A. Osuka, K. Maruyama, I. Yamazaki, N. Tamai, *Chem. Phys. Lett.* **1990**, *165*, 392–396.

[14] D. M. Adams, J. Kerimo, C.-Y. Liu, A. J. Bard, P. F. Barbara, *J. Phys. Chem. B* **2000**, *104*, 6728–6736.

[15] Apparent energy transfer efficiency estimated from the steady state fluorescence intensity at 610 nm (Figure 5) was 0.61 (ref. [13b]).

[16] a) J. Lahiri, G. D. Fate, S. B. Ungashe, J. T. Groves, *J. Am. Chem. Soc.* **1996**, *118*, 2347–2358; b) C. R. Drain, *Proc. Natl. Acad. Sci. USA*, **2002**, 99, 5178–5182.

[17] a) F. A. Walker, M.-W. Lo, M. T. Ree, *J. Am. Chem. Soc.* **1976**, *98*, 5552–5560; b) R. Quinn, M. Nappa, J. S. Valentine, *J. Am. Chem. Soc.* **1982**, *104*, 2588–2595.

[18] a) J. P. Collman, R. R. Gagne, C. A. Reed, T. R. Halbert, G. Lang, W. T. Robinson, *J. Am. Chem. Soc.* **1975**, *97*, 1427–1439; b) J. R. Budge, P. E. Ellis, Jr., R. D. Jones, J. E. Linard, F. Basolo, J. E.

Baldwin, R. L. Dyer, *J. Am. Chem. Soc.* **1979**, *101*, 4760–4762; c) M. Momenteau, B. Loock, E. Bisagni, M. Rougee, *Can. J. Chem.* **1979**, *57*, 1804–1813.

[19] a) D. Mauzerall, N. L. Greenbaum, *Biochim. Biophys. Acta* **1989**, *974*, 119–140; b) N. L. Greenbaum, D. Mauzerall, *Biochim. Biophys. Acta* **1991**, *1057*, 195–207.

-62-